




12-2020

Carbon Metabolism in Cave Subaerial Biofilms

Victoria E. Frazier

University of Tennessee, Knoxville, vfrazie2@vols.utk.edu

Follow this and additional works at: https://trace.tennessee.edu/utk_gradthes

 Part of the [Bacteriology Commons](#), [Biodiversity Commons](#), [Biogeochemistry Commons](#), [Bioinformatics Commons](#), [Data Science Commons](#), [Environmental Microbiology and Microbial Ecology Commons](#), [Genomics Commons](#), [Geochemistry Commons](#), [Geology Commons](#), [Molecular Genetics Commons](#), [Speleology Commons](#), and the [Terrestrial and Aquatic Ecology Commons](#)

Recommended Citation

Frazier, Victoria E., "Carbon Metabolism in Cave Subaerial Biofilms. " Master's Thesis, University of Tennessee, 2020.

https://trace.tennessee.edu/utk_gradthes/5867

This Thesis is brought to you for free and open access by the Graduate School at TRACE: Tennessee Research and Creative Exchange. It has been accepted for inclusion in Masters Theses by an authorized administrator of TRACE: Tennessee Research and Creative Exchange. For more information, please contact trace@utk.edu.

To the Graduate Council:

I am submitting herewith a thesis written by Victoria E. Frazier entitled "Carbon Metabolism in Cave Subaerial Biofilms." I have examined the final electronic copy of this thesis for form and content and recommend that it be accepted in partial fulfillment of the requirements for the degree of Master of Science, with a major in Geology.

Annette S. Engel, Major Professor

We have read this thesis and recommend its acceptance:

Karen G. Lloyd, Anna Szykiewicz

Accepted for the Council:

Dixie L. Thompson

Vice Provost and Dean of the Graduate School

(Original signatures are on file with official student records.)

CARBON METABOLISM IN CAVE SUBAERIAL BIOFILMS

A Thesis Presented for the
Master of Science
Degree
The University of Tennessee, Knoxville

Victoria Elaine Frazier

December 2020

Copyright © 2020 by Victoria Elaine Frazier
All rights reserved.

ACKNOWLEDGEMENTS

I had so much support over the last two years during the completion of this project and others, both professionally and personally, and I am so grateful to those who stood by me and encouraged me. I'm also grateful to the Cave Conservancy Foundation, which apparently shared my curiosity about cave biofilm metabolism and provided the funding for me to be able to complete this project. Thanks to Ania Szyrkiewicz, Karen Lloyd, and Drew Steen for helping me develop ideas and learn new skills and Anthony Faiia for his work in completing stable isotope analyses and dealing with me pestering him excitedly about data. Thanks also to Audrey Paterson for her help in the lab, and Annette Engel for helping with experimental design, grant writing and editing, and generally making this project possible. I couldn't have completed this project without people who were willing to spend several cramped hours in caves with me when I asked, including Hannah Rigoni and Taryn Hicks. You both made sampling a joy, thanks so much for your help! And, of course, thank you to all those who made grad school and Knoxville a great time: Jonathan Cox, Christopher Cook, Rhianna Moore, Nick Smith, Adriana Ghiozzi, and Michael Phillips. And, finally, I don't think I could have made it through some of my more intense course loads without support from Bobby Scharping. Thanks for always being there for me, encouraging me through the rough times, and making me laugh, all from 670 miles away.

ABSTRACT

Subaerial biofilms (SABs) grow at the interface between the atmosphere and rock surfaces in terrestrial and subterranean environments around the world. Multi-colored SABs colonizing relatively dry and nutrient-limited cave surfaces are known to contain microbes putatively involved in chemolithoautotrophic processes using inorganic carbon like carbon dioxide (CO₂) or methane (CH₄). However, the importance of CO₂ and CH₄ to SAB biomass production has not been quantified, the environmental conditions influencing biomass production and diversity have not been thoroughly evaluated, and stable carbon and nitrogen isotope compositions have yet to be determined from epigenic cave SABs. The purpose of this study was two-fold: (i) to quantify the proportion of biomass in cave SABs that could be derived from chemolithoautotrophic processes using stable carbon and nitrogen isotope analysis, and (ii) to characterize and quantify taxonomic groups capable of chemolithoautotrophy using molecular techniques. Bulk stable isotope analysis of biomass carbon had $\delta^{13}\text{C}$ [delta 13-C] values between -35 and -46‰ [per mil], which were more negative than would be predicted if SAB biomass was due to heterotrophic assimilation of organic carbon having $\delta^{13}\text{C}$ values of -21 to -25‰. Using isotopic compositions of end-member compounds, two-member mixing models indicated that 31–100% of total biomass carbon could be produced via CO₂-derived carbon, and 32–66% of total biomass carbon could be due to CH₄-derived carbon incorporation. Nitrogen isotope analyses confirmed the presence of nitrifying and nitrogen-fixing microbes, which was supported by 16S rRNA gene sequence analyses that retrieved high relative abundances of putative chemolithoautotrophs belonging to the families Nitrosococcaceae, Nitrosomonadaceae, and Nitrospirales, as well as Pseudonocardiaceae. Pseudonocardiaceae are in the Actinobacteria phylum and can potentially fix CO₂. Overall microbial community composition significantly correlated with moisture content, and the relative abundances of Pseudonocardiaceae increased as moisture content decreased. Consequently, dry cave-wall habitats may select for Pseudonocardiaceae, as primary colonizers, that make the habitat conducive for other microbial groups like nitrogen cycling chemolithoautotrophs and eventually heterotrophs. Chemolithoautotrophy and nitrogen cycling in cave SABs are likely important for terrestrial cave food webs, although their contributions to providing organic carbon and nitrogen sources to nutrient-limited cave ecosystems will require additional research.

TABLE OF CONTENTS

CHAPTER ONE Introduction	1
Research Objectives and Hypotheses	3
Thesis Organization	4
CHAPTER TWO Literature Review	5
Subaerial Biofilms in Caves.....	5
Taxonomic Diversity of Cave SABs Compared to Other Habitats	5
Carbon Metabolism in Cave Microbial Communities	8
Tracing Carbon & Nitrogen Sources	9
CHAPTER THREE Materials and Methods.....	13
Site Descriptions	13
Environmental Conditions	14
Biofilm Sample Collection	16
Stable Isotope Analyses and Inorganic Carbon Measurements	17
DNA Extractions and 16S rRNA Gene Sequencing	18
16S rRNA Sequence Analysis	19
Statistical Analyses	20
CHAPTER FOUR Results.....	28
Environmental Conditions and Nutrient Sources	28
Stream level fluctuations and flooding frequency	28
Cave temperatures, relative humidity, and substrate moisture	28
CO ₂ and CH ₄ concentrations and isotopic compositions	29
Drip water and stream geochemistry	31
Drip water and stream DOC and isotope compositions.....	32
Biofilm Carbon and Nitrogen Isotope Compositions	33
Microbial Community Analysis.....	33
Biofilm diversity	33
Community composition and environmental variables	35
Correlations between taxa and SAB isotope compositions	36
CHAPTER FIVE Discussion.....	73
Prevalent Taxonomic Groups in Subaerial Biofilms from Cave Environments.....	73
Influence of Moisture on Subaerial Biofilm Diversity	76
Chemolithoautotrophic Carbon Fixation in Subaerial Biofilms	77
CHAPTER SIX Conclusions and Recommendations.....	85
List of References	87
Vita.....	100

LIST OF TABLES

Table 3.1: Descriptions of the location and biofilm morphology specific to each of six sites in caves KN14 and RN5 on 1 and 2 February 2020.	23
Table 4.1: Ambient environmental conditions at each cave SAB cave wall sampling site on the day of biofilm sampling (February 1 or 2, 2020).....	39
Table 4.2 Environmental data collected over time in drip locations and cave streams of both caves, including pH, temperature, and measurable anion concentrations.	40
Table 4.3: DIC and DOC concentrations in drip water and cave streams measured on 5/20/2020 (n=3). Alkalinity data from previous analysis (on 7/19/19) was used to validate DIC concentrations.	41
Table 4.4: Dissolved CO ₂ and CH ₄ concentrations in cave streams measured in triplicate on two dates (n = 3).	41
Table 4.5: Averaged stable carbon isotope values and standard deviations of carbonates ($\delta^{13}\text{C}_{\text{CaCO}_3}$) from each sampling site. Technical replicates (n = 3) consisted of homogenized material from the same site. Stable isotope ratios are given relative to PDB. NA denotes sites where substrate was collected but did not contain carbonate (e.g., clay for KN14-3 and RN5-1 or chert for RN5-4) and $\delta^{13}\text{C}$ could not be measured.....	42
Table 4.6: Averaged stable carbon isotope values and standard deviations (replicates n = 3) measured for DIC, CO ₂ in cave air, and DOC, all reported relative to PDB.....	43
Table 4.7: Averaged stable carbon isotope values (n = 3) and standard deviations of homogenized SAB samples ($\delta^{13}\text{C}_{\text{SAB}}$) from each site, as well as bulk stable nitrogen isotope values (n = 1). Stable isotope ratios are given relative to PDB for carbon and air-N ₂ for nitrogen. See Chapter 3 for details about the methods.	44
Table 4.8: Average alpha diversity measurements at the genus level across SAB sampling sites in both caves. Field replicate sequence counts were averaged (n = 4).	45
Table 4.9: Average relative abundances of taxa by order in each cave (KN14 and RN5). Abundances for each replicate and across cave sampling sites were averaged to summarize abundant taxa in each cave.	46
Table 4.10: Average relative abundance of genera across all sampling sites in both caves. Genera with relative abundance greater than 0.15% are shown.....	47
Table 4.11: Results of PERMANOVA models that included $\delta^{13}\text{C}$, moisture content, cave ID, temperature, and biofilm color as explanatory variables for microbial community composition across both caves. Statistical significance is indicated by bold-font for p-values below an alpha value of 0.05.	51

Table 4.12: Results of the DCA model that included predictors for SAB community composition across both caves. Statistical significance is indicated by bold-font for p-values below an alpha value of 0.05..... 51

Table 4.13: Mantel test results for Pearson's product moment correlation between SAB microbial community and (i) temperature and (ii) moisture content between caves and between sites within each cave. Statistical significance is indicated by bold-font for p-values below an alpha value of 0.05..... 51

Table 4.14: KN14 Pearson's correlation results showing the relationship between substrate moisture, carbon and nitrogen isotope composition, and taxa abundance. Statistical significance is indicated by bold-font for p-values below an alpha value of 0.05..... 52

Table 4.16: DCA model results specific to SABs within KN14, demonstrating the relationship between moisture content and microbial community composition. Statistical significance is indicated by bold-font for p-values below an alpha value of 0.05..... 53

Table 4.15: RN5 Pearson's correlation results showing the relationship between substrate moisture, carbon and nitrogen isotope composition, and taxa abundance. Statistical significance is indicated by bold-font for p-values below an alpha value of 0.05..... 53

Table 4.17: KN14 PERMANOVA model results showing the relationship between predictor variables and microbial community composition. Statistical significance is indicated by bold-font for p-values below an alpha value of 0.05..... 54

Table 4.18: RN5 PERMANOVA model results showing the relationship between predictor variables, and microbial community composition. Statistical significance is indicated by bold-font for p-values below an alpha value of 0.05..... 54

Table 4.19: DCA model specific to RN5 comparing microbial community structure to stable isotope composition and moisture content of the substrate (i.e. cave wall). Statistical significance is indicated by bold-font for p-values below an alpha value of 0.05..... 55

Table 5.1: Estimated proportions of carbon derived from CO₂ or CH₄ based on two-member mixing models between putative chemolithoautotrophic or methanotrophic biomass compared with heterotrophic biomass. Upper and lower limits are based on uncertainties of biomass δ¹³C values found in the literature. For example, uncertainty in autotrophic biomass δ¹³C values are based on variability in Rubisco fractionation factors starting from CO₂ to produced biomass, whereas the upper and lower limits of methane-derived carbon estimates are based on literature information about fractionation factors for methanotrophic metabolism and biomass production 83

LIST OF FIGURES

- Figure 3.1: Geologic map of Appalachian Valley and Ridge karst in the Knoxville, Tennessee using data from the USGS TN Geologic Map (<https://mrddata.usgs.gov/geology/state/state.php?state=TN>). Locations of cave sites used in this study are indicated by triangles. 24
- Figure 3.2: Cross-section of the RN5 cave passage showing normal water level (solid blue line) and possible frequent water level fluctuations based on clustering of biofilms within less than a meter of the water surface (light blue dotted line). Maximum flood level ~0.5 m is and frequent flooding level ~ 0.25 m are based on HOBO water level logger data from the study period (Brown dotted line, blue dotted line). Numbers denote biofilm sampling locations. 25
- Figure 3.3: Biofilm color and morphology at each sampling site. White bar lengths represent approximately 0.5 cm. Red arrows represent examples of sampled SABs. Images without red arrows depict “sheet-like” biofilms that cover the entire pictured surface. 26
- Figure 3.4: Cave SAB sampling design, showing each of six total sites within each cave and the samples collected from each site. At least one scraping (noted as dark blue or green) and three swab replicates (noted as light blue or yellow), for a minimum of four samples per site, were used for DNA analysis. 27
- Figure 4.1: Stream level fluctuations and flooding frequency in KN14 (blue) and RN5 (yellow). Change in water depth is reported relative to $t_0 = 0$ m for the measured stream surface level at the start of the study. Daily rainfall is shown in black. 56
- Figure 4.2: Flooding height and frequency in KN14 (blue) and RN5 (yellow) cave streams. 57
- Figure 4.3: Cave-wall temperature variation at SAB sampling sites at the beginning of the study and based on vertical distance from the stream base level at $t_0 = 0$ m. Light blue = KN14; Yellow = RN5. Solid lines represent the outside temperature on the sampling day for each cave, and colored dot-dash lines represent the stream temperatures. The black dotted line represents the average annual surface temperature. 58
- Figure 4.4: Cave air temperature over time from winter (February 2, 2020) to late spring (April 17, 2020), showing more variation in temperatures in the cave site KN14 (blue) than in RN5 (orange). Dotted blue lines represent the approximate time in which the data logger in KN14 recorded temperatures in the main cave stream passage, but the data logger was placed in an upper passage of the cave prior to and after this period, to establish whether cave air temperature near the stream was more variable than away from the stream. 59
- Figure 4.5: Comparison of CO₂ concentrations in cave air in February between cave locations and outside measurements. Letters denote statistically significant differences among samples despite variation in replicate measurements based on a Tukey’s HSD test (p -value < 0.05, $n=3$). 60

Figure 4.6: Comparison of CH₄ concentrations in cave air in February between cave locations and outside measurements. Letters denote the absence of statistically significant difference in CH₄ concentration among these locations based on Tukey’s HSD test (p-value > 0.05, n = 3). . 61

Figure 4.7: Dissolved inorganic carbon (DIC) carbon isotope values measured from filtered water samples of meteoric water (drips) and cave streams. δ¹³C_{DIC} values are reported relative to PDB. Letters denote significant differences among values using Tukey’s HSD test (p-value < 0.05, n = 3)..... 62

Figure 4.8: Stable carbon isotope values of rock (i.e., carbonate) substrates at each site relative to PDB (n =3)..... 62

Figure 4.9: Dissolved organic carbon (DOC) stable carbon isotope values measured in two drip water sites and the stream in both caves (relative to PDB). Letters indicate significant differences among sites based on the results of a Tukey’s HSD test (p-value < 0.05, n = 3). 63

Figure 4.10: Stable carbon isotope values for subaerial biofilms (SABs) at each sampling site for both caves. Values are relative to PDB. Letters denote statistical differences among samples determined by Tukey’s HSD test (p-value < 0.05). 63

Figure 4.11: Summary of δ¹³C values (relative to PDB) for all samples, including SAB biomass (n = 6 per cave), DOC and DIC in drip water (n = 2 per cave), CO₂ in the cave air, and rock (i.e., carbonate) substrate from each site and each cave. Data are reported in Tables 4.4 and 4.5. 64

Figure 4.12: Comparison of overall δ¹⁵N values measured from all SAB samples from each cave (n=6). δ¹⁵N values are reported relative to δ¹⁵N_{air}. 65

Figure 4.13: Initial data for δ¹⁵N values measured from all SAB samples from each cave without replication. δ¹⁵N values are reported relative to δ¹⁵N_{air}. 66

Figure 4.14: Composite evenness (Chao1, left panel) and diversity index (Shannon, center panel; Simpson, right panel) values for all SAB samples from each cave. 67

Figure 4.15: Average relative abundances of taxa at the order level for all sampling sites (1-6) in each cave (KN14 and RN5). Sequence abundances were averaged between replicates. Only orders with relative abundances greater than 1.0% are shown. 69

Figure 4.16: PCoA plot showing Bray-Curtis similarity between microbial community composition at the genus level for all replicates collected at each sampling site. Ellipses represent where 95% of the data fall..... 70

Figure 4.17: A) DCA plot showing differences in microbial community structure across all sampling sites in both caves. B) DCA plot revealing relationships among microbial community structure at the order level and changes in δ¹³C_{SAB} (p-value = 0.30) and moisture content (p-value = 0.013). Color gradient represents δ¹³C_{SAB} values. 71

Figure 4.18: DCA plots (panels A and B are the same for RN5; panels C and D are the same for KN14) showing relationships among microbial community structure, stable isotope composition, and percent moisture across both cave sites. Panels B and D show order-level correlations among taxa and overall community structure. Color gradients for each set of plots represent differences in $\delta^{13}\text{C}_{\text{SAB}}$ values. 72

Figure 5.1: Summed relative abundance of putative obligate chemolithoautotrophs at the family level, including Nitrosococcaceae, Nitromonadaceae, and Nitrospiraceae, are shown as orange bars. Relative abundances of obligate chemolithoautotrophic families summed with Pseudonocardiaceae, a potential CO_2 -fixer, are shown in yellow. Black bars represent the calculated *minimum* proportion of DIC-derived carbon needed to explain the observed $\delta^{13}\text{C}_{\text{SAB}}$ values for each SAB and grey bars show this proportion based on the $\delta^{13}\text{C}$ of cave-air CO_2 (See Table 5.1). 84

Figure 5.2: Summed relative abundance of putative methanotrophs at the family level, Methyloligellaceae, Methylospiraceae, and Methylophilaceae, are shown as blue bars. The total abundance of these groups including relative abundance of the AOB Nitrosococcaceae, Nitrosomonadaceae, and unclassified members of Rhizobiales which has the potential to oxidize or co-oxidize methane, is shown in green. Black bars represent the calculated *minimum* proportion of methane-derived carbon needed to explain the observed $\delta^{13}\text{C}_{\text{SAB}}$ values for each SAB (See Table 5.1). 84

CHAPTER ONE

INTRODUCTION

Caves are characterized by complete darkness, relatively constant temperature, high relative humidity, and low nutrient input that results in oligotrophic (nutrient-limited) ecosystem conditions (Wilkens et al., 2000). Diverse communities of microbes and troglobitic (cave obligate) and troglophilic (cave facultative) animals that live in cave ecosystems can be supported from the input of photosynthesis-derived organic matter from the surface, which drives heterotrophic metabolism (Poulson & Lavoie, 2000; Wilkens et al., 2000; Simon et al., 2003), as well as from chemolithoautotrophic microbial communities that produce their own source of organic carbon by “fixing” inorganic carbon dioxide (CO₂) (Ortiz et al., 2014). Some chemolithoautotrophs oxidize reduced inorganic chemical compounds like hydrogen sulfide (H₂S), ferrous iron, nitrite, or ammonia (Ehrich et al., 1995; Klotz et al., 2006; Amils, 2011), whereas others use methane (CH₄) and other single-carbon (C1) compounds for energy and carbon sources (Hanson & Hanson, 1996). However, the relative importance of heterotrophic and chemolithoautotrophic carbon metabolisms to cave microbial communities remains poorly understood, especially in the vadose (i.e., dry, subaerial, terrestrial) zones of epigenic cave and karst systems.

Most research concerning microbial carbon cycling in the subsurface has been done in aquatic ecosystems, such as, for example, the Nullarbor caves in Australia (Holmes et al., 2001; Tetu et al., 2013), groundwater in the Edwards Aquifer, Texas (Hutchins et al., 2016), a stream in Organ Cave, West Virginia (Simon et al., 2003), a mineral spring in southern Germany (Karwautz et al., 2017), and a karst subterranean estuary in the Yucatan peninsula, Mexico (Brankovits et al., 2017; Brankovits & Pohlman, 2020). Studies of microbial carbon cycling in karst vadose zones have mostly focused on hypogenic cave systems formed by sulfuric acid speleogenesis with elevated concentrations of dissolved and atmospheric gases that can be oxidized by chemolithoautotrophs (Vlasceanu et al., 2000; Macalady et al., 2006, 2007; Porter et al., 2009; Jones et al., 2011; Karwautz et al., 2017). In epigenic caves without elevated levels of reduced gaseous compounds, as well as basaltic lava tube caves, cave walls and sediment banks are still habitats for extensive, multi-colored subaerial biofilms (SABs) (e.g., Schabereiter-Gurtner et al., 2002, 2004; Barton et al., 2007; Barton et al., 2010; Pašić et al., 2010; Porca et al., 2012; Hathaway

et al., 2014; Ortiz et al., 2014; Riquelme et al., 2015; Lavoie et al., 2017; Gonzalez-Pimentel et al., 2018; Marques et al., 2018; Zhao et al., 2018; Luis-Vargas et al., 2019).

Microbial communities associated with SABs exist on rock and sediment surfaces across a diverse range of climates and environments (Gorbushina, 2007; Gorbushina & Broughton, 2009; Choe et al., 2018). Rock surfaces are generally considered extreme habitats due to nutrient limitation and desiccation stress (Villa et al., 2016). In general, SABs are comprised of relatively self-sufficient, complex, and symbiotic communities (Gorbushina & Broughton, 2009; Villa et al., 2016), with SABs from surface (i.e., photic) ecosystems including abundant CH₄-oxidizing (i.e., methanotrophic) (Kussmaul et al., 1998) and CO₂-fixing (i.e., photoautotrophic and chemolithoautotrophic) metabolic groups (Gorbushina, 2007; Li et al., 2016; Villa et al., 2016). Within rock surface or photic SAB communities, there is dependence on CO₂ fixed by photoautotrophic and chemolithoautotrophic organisms, nitrification and nitrogen cycling, as well as the potential importance of alternative carbon sources, such as CH₄. Nitrifying bacteria in SABs are also involved in rock weathering (Abdulla, 2009; Frey et al., 2010). A recent investigation of SAB microbial communities on castle walls in the United Kingdom by Zanardini and colleagues (2019) reveal abundant putative chemolithoautotrophs, in addition to photoautotrophic cyanobacteria, and 16S rRNA sequence representatives demonstrate a complete nitrogen cycle from the SABs, including nitrogen fixation (e.g., *Azospirillum*), ammonia oxidation (e.g., *Nitrosospira*), nitrite oxidation (e.g., *Nitrospira*), and denitrification (e.g., *Rhodobacter*).

Because cave environments cannot support photoautotrophic CO₂ fixation, cave SABs may instead rely on CO₂ fixation via chemolithoautotrophy, such as CO₂ fixation via nitrification (Ortiz et al., 2014). Microbial community composition analyses based on 16S rRNA gene sequence taxonomy of cave SABs in carbonate cave systems (e.g., Porca et al., 2012; Ortiz et al., 2014; Marques et al., 2019) and lava tubes (e.g., Hathaway et al., 2014; Riquelme et al., 2015; Lavoie et al., 2017; Gonzalez-Pimentel et al., 2018; Luis-Vargas et al., 2019) include putative chemolithoautotrophs, including ammonia-oxidizing and nitrite-oxidizing bacteria, potentially CO₂-fixing Actinobacteria, and methanotrophs. In addition, two metagenomic studies show genetic potential for chemolithoautotrophic CO₂ and CH₄ fixation in SABs (Ortiz et al., 2014; Wischart et al., 2019). Even preliminary 16S rRNA analyses of SABs from East Tennessee carbonate caves (Engel et al., 2017) reveal high proportions of putative methanotrophs of the order

Rhizobiales, putative ammonia-oxidizing chemolithoautotrophs of the families Nitrosococcaceae and Nitrosomonadaceae (Klotz et al., 2006; Prosser et al., 2014), and possible CO₂-fixers of the order Pseudonocardiales (Lynch et al., 2014). However, aside from these investigations reliant on molecular genetics, there have only been two studies that used stable isotope tracers to evaluate whether active chemolithoautotrophic metabolic processes are responsible for microbial biomass production, and both were from hypogenic caves with acidophilic SABs dominated by sulfur-oxidizing bacteria (Vlasceanu et al., 2000; Engel et al., 2001). In addition, there has been limited research to understand nutrient resources that could support SAB communities or the spatial variability of cave SAB communities across microenvironmental gradients, such as with respect to water and/or nutrient availability.

Research Objectives and Hypotheses

The main research objectives for this thesis are to (i) determine environmental drivers of spatial variation in cave SAB microbial community compositions within and between cave systems, and (ii) characterize the contribution of chemolithoautotrophic pathways to biomass production within SABs. The hypotheses tested were:

- 1) Cave SAB microbial community composition, and specifically overall diversity and dominant microorganisms, would be more similar between areas of a cave that have similar environmental conditions and expected nutrient availability.
- 2) Biofilms in areas with lower availability of organic carbon from percolating water or flooding stream water (e.g., on relatively dry surfaces) would have higher relative abundances of chemolithoautotrophs compared to SABs growing in areas actively exposed to allochthonous organic carbon input.
- 3) Bulk stable carbon isotope compositions ($\delta^{13}\text{C}$) of SAB biomass would support the presence chemolithoautotrophic functions, such as CO₂ fixation and/or CH₄ oxidation, and correspond to relative abundances of those taxonomic groups based on 16S rRNA gene sequence data.
- 4) Based on the prevalence of putative nitrifiers in cave SABs, as well as the overall potential nitrogen limitation in caves which may result in nitrogen (N₂) fixation or diazotrophy to supplement nitrogen resources, bulk stable nitrogen isotope analysis on SAB biomass are expected to show relatively low $\delta^{15}\text{N}$ values consistent with those produced via N₂ fixation and/or nitrification, as opposed to positive $\delta^{15}\text{N}$ values consistent with denitrification or assimilation of organic nitrogen.

The caves selected for this study were near Knoxville, Tennessee, and had easy access, abundant SABs, and outflowing streams with evidence of flooding during rain events. Based on previous aqueous geochemistry sampling, the cave streams also had comparable nutrient levels. Available nutrients and environmental conditions (e.g., temperature, humidity, moisture, and wet-season flooding height and frequency) were measured at each SAB sampling site. The taxonomic identities and relative abundances of SAB microbial communities were assessed from 16S rRNA gene sequences obtained from environmental DNA. 16S rRNA genes can hint to putative metabolic functions associated with certain taxa, such as CO₂ fixation or CH₄ oxidation, but 16S rRNA genes cannot give precise information about metabolic activity. Therefore, δ¹³C analyses of SABs were done to evaluate the contribution of CO₂ and/or CH₄-derived carbon to SAB biomass. Although stable isotope ratio analyses have been used to differentiate between heterotrophic and chemolithoautotrophic contributions to carbon cycling in cave and karst systems (e.g., Sarbu et al., 1996; Hutchins et al., 2016), use of δ¹³C analysis to understand the metabolism of microbial communities from SABs in epigenic carbonate cave systems has not been done previously.

Thesis Organization

This thesis is organized with four additional chapters. Chapter Two includes a literature review of the current knowledge of cave microbial communities associated with SABs and how tracing carbon sources to microbial communities can be accomplished. Chapter Three describes the methods used in this research, from sampling procedures to data analysis and statistical evaluation of the results. Chapter Four outlines the results for cave environmental conditions, stable isotope analysis, and microbial community analysis. Chapter Five includes the discussion, which is divided into three sections based on evaluations of the research hypotheses. The first section summarizes the taxonomic groups in the SABs in comparison to other studies and assesses the potential metabolisms of the most prevalent groups. The second section evaluates the importance of moisture, as an important environmental driver, on SAB diversity, and the third section of the chapter discusses the evidence for chemolithoautotrophic carbon fixation in the SABs and the implications for the different autotrophic pathways for the cave ecosystem. Finally, Chapter Six presents the main conclusions drawn from this study and a discussion of future research directions.

CHAPTER TWO LITERATURE REVIEW

Subaerial Biofilms in Caves

Subaerial biofilms (SABs) form at the interface between air and solid substrates in a wide variety of climates and conditions, including in polar, arid, tropical, and subterranean environments (Gorbushina & Broughton, 2009; Villa et al., 2016). Cave-wall SABs are abundant in caves around the world, including basaltic lava tubes and carbonate caves, where they exist as visible, multi-colored colonies on bare rock and sediment surfaces (Vlasceanu et al., 2000; Barton et al., 2007; Hathaway et al., 2014; Ortiz et al., 2014; Lavoie et al., 2017; Gonzalez-Pimentel et al., 2018; Marques et al., 2019). Cave SABs experience similar limitations to nutrient and water availability as SABs in surface, non-cave environments (Villa et al., 2016). The microbial communities in SABs in epigenic cave systems have relatively low taxonomic diversity and are often dominated by a few organisms from the phyla Actinobacteria and Proteobacteria (Ortiz et al., 2014; Tomczyk-Żak & Zielenkiewicz, 2015; Marques et al., 2019). Although cave SABs can be morphologically distinct, most notably in their pigmentation, which can be yellow, blue, pink, or white, color does not usually link to the dominance of specific taxonomic groups (Gonzalez-Pimentel et al., 2018). Cave SAB microbial community composition does vary by geographic location, substrate mineralogy, carbon input, and microenvironmental conditions within and between caves (Barton et al., 2007; Ortiz et al., 2014; Zhao et al., 2018; Marques et al., 2019). Ventilation created by airflow patterns between passages at different elevations can affect passage air and rock temperature and relative humidity, as well as alters ambient concentrations of gases (Tomczyk-Żak & Zielenkiewicz, 2015), which correspond to differences in the distribution of microbial groups (Porca et al., 2012; Ortiz et al., 2014). Growth of extensive biofilms in some caves demonstrates the apparent success of microbial communities to these conditions, but there has been limited research to understand the nutrient resources that could support the communities.

Taxonomic Diversity of Cave SABs Compared to Other Habitats

The most abundant taxa found in cave SABs include Actinobacteria, specifically from the orders Euzebyales and Pseudonocardiales, Proteobacteria, including members of the Chromatiales and Xanthomonadales, as well as Acidobacteria and Nitrospirae (e.g., Riquelme et al., 2015). These cave-wall SAB microbial communities are similar across vast geographic distances and from geologically distinct systems, including from basaltic lava tubes in the Azores Islands,

Portugal, the Canary Islands, Spain, and from Hawai'i and New Mexico, USA (Hathaway et al., 2014; Riquelme et al., 2015; Lavoie et al., 2017; Gonzalez-Pimentel et al., 2018; Luis-Vargas et al., 2019), as well as from limestone caves in China (Wu et al., 2015), USA (Barton et al., 2007), and Slovenia (Porca et al., 2012). For instance, the genus *Euzebya* has been found to dominate SABs in lava tubes and carbonate caves around the world (e.g., Hathaway et al., 2014; Riquelme et al., 2015; Yun et al., 2016; Gonzales-Pimentel et al., 2018) and the Pseudonocardiales commonly dominate SABs from lava tubes (Riquelme et al., 2015; Gonzalez-Pimentel et al., 2018), limestone caves (Schabereiter-Gurtner et al., 2004; Barton et al., 2007; Wu et al., 2015; Lavoie et al., 2017; Wischart et al., 2019; Zhu et al., 2019), and from cave paintings on sandstone (Duan et al., 2017). Even in studies that did not identify Actinobacteria beyond the level of class, Actinobacteria, in general, dominate cave-wall weathered rock samples, which indicates potential selectiveness of this environment for certain microbial groups (Yun et al., 2015).

Ammonia-oxidizing and nitrite-oxidizing bacteria, including members of the orders Nitrosococcales, Nitrosomonadales, and Nitrospirales have also been identified commonly in cave environments. At the genus level, *Nitrosococcus* is abundant across geographically and geologically distinct caves (Porca et al., 2012; Tomczyk-Zak & Zeilenkiewicz, 2015; Wu et al., 2015; Marques et al., 2019). But, recent re-classification of the genus *Nitrosococcus* from the family Chromatiales to Nitrosococcales (within the Gammaproteobacteria) in the Silva reference database now complicates interpretation of some older literature. Additional sequence analyses will be needed to confirm whether uncultured members of the order Chromatiales in cave-wall SABs from three studies, two in lava tubes and the other in limestone caves in Spain and Slovenia, are Nitrosococcales (Porca et al., 2012; Gonzalez-Pimentel et al., 2018; Luis-Vargas et al., 2019). Ammonia-oxidizing bacteria (AOB) of the family Nitrosomonadaceae have been found in Movile Cave, which is characterized by high input of CH₄, and a Slovenian limestone cave, but are not commonly reported at the family or genus level in the majority of cave SAB studies (Hutchens et al., 2003; Pašić et al., 2010; Tomczyk-Zak & Zeilenkiewicz, 2015). However, this family belongs to the order Burkholderiales, which is common in cave microbial community studies (Zhao et al., 2007; Pašić et al., 2010; Wischart et al., 2018). Potential nitrite-oxidizing bacteria of the phylum Nitrospirae are also frequently identified in lava tube and carbonate cave microbial communities (Hathaway et al., 2014; Ortiz et al., 2014; Lavoie et al., 2017; Thompson et al., 2019).

Microbial community composition of cave-wall SABs also somewhat resemble those from SABs in non-cave environments, although the body of literature discussing microbial community structure of SABs on stone surfaces and monuments has largely been separate from that of cave-wall biofilms, with rare citations between the cave SAB and surface SAB literature. Of course, a major environmental difference between cave SABs and those found on the surface is the presence of sunlight, which results in surface SABs containing a large proportion of phototrophic prokaryotes and eukaryotes (Gorbushina et al., 2007; Choe et al., 2018). These phototrophic organisms provide the primary source of carbon via CO₂ fixation to heterotrophic members of the community, including heterotrophic bacteria and fungi (Villa et al., 2016). However, despite differences in community composition, surface and cave SABs share challenges associated with growth on solid surfaces with limited nutrient availability. These conditions likely produce functionally similar communities among the surface and cave environments (Zanardini et al., 2019). Desiccation resistance and the ability to manufacture organic carbon and nitrogen from inorganic nutrient sources via photoautotrophy, chemolithoautotrophy, methanotrophy, or diazotrophy appear to be the primary functions of SAB communities, regardless of the presence of light (Villa et al., 2016; Zanardini et al., 2019). Photic SABs also are colonized by chemolithoautotrophs, including nitrifiers and methanotrophs, as well as nitrogen-fixing organisms similar to cave SABs (Kusmaul et al., 1998; Mansch & Bock, 1998; Villa et al., 2018; Zanardini et al., 2019).

Other extreme environments that could be considered analogous to both photic and cave SABs include rocky soils from arid to cold climates. For instance, members of the family Pseudonocardiaceae are not commonly reported in photic SAB microbial communities, but this family is abundant in desert soils and cave SABs. Lavoie et al. (2017) found higher proportions of Pseudonocardiaceae in cave SABs compared to overlying surface desert soils. This group can fix atmospheric CO₂ and metabolize C1 compounds to supplement limited organic carbon resources (Lynch et al., 2014; Mohammadipanah & Wink 2016; Ji et al., 2017). Other members of this family, including *Pseudonocardia dioxanivorans*, are also nitrogen-fixers, which could enable them to supplement limited nitrogen resources (Mahendra & Alvarez-Cohen, 2005).

The dominance of certain Actinobacteria, ammonia-oxidizers, and nitrifiers in cave environments may distinguish cave SABs from SABs in other environments. Although caves are

characterized by relatively stable temperature and high humidity, most caves are nutrient-limited, so successful microbial groups would need to make the most of inadequate resources or be able to use alternative sources of nutrients. Therefore, the existence of so-called endemic or cave-adapted microbial groups has been long debated in the cave literature (Lavoie et al., 2017; Thompson et al., 2019), particularly when considering the most likely mechanisms for caves to become colonized by microbes, such as through meteoric water and soil percolation through fractures in the overlying epikarst or from flooding cave streams (Yun et al., 2016; Lavoie et al., 2017; Zhao et al., 2018; Thompson et al., 2019). However, more research is needed to demonstrate if and how the cave-wall environment selects for specific taxonomic and functional microbial groups from source inocula that may be comprised of many more functionally diverse microbes from the surface or other proximal environments.

Carbon Metabolism in Cave Microbial Communities

In carbon-limited cave environments, some microbes can utilize inorganic carbon sources (i.e., CO₂, bicarbonate, CH₄, etc.) via chemolithoautotrophy and supplement organic carbon availability. Cave microbial communities can contain abundant taxa putatively involved in methanotrophy (e.g., Methyloligellaceae) (Zhao et al., 2018; Wischart et al., 2019), diazotrophy (Marques et al., 2019), and chemolithoautotrophic processes such as nitrification or ammonia oxidation (e.g., by *Nitrosococcus* spp., *Nitrosomonas* spp., Nitrospirae, and Nitrospinae) (Ortiz et al., 2014; Gonzalez-Pimentel et al., 2018; Marques et al., 2019; Wischart et al., 2019; Zhu et al., 2019). Although the inference of metabolic function from taxonomic identity is not always reliable (e.g., based on 16S rRNA gene sequence similarity), certain functions, like methanotrophy and chemolithoautotrophic ammonia oxidation, are conserved within known phylogenetic groups (e.g., Klotz et al., 2006). Therefore, the taxonomy of these organisms is a relatively good indicator of their metabolic potential. Other studies show the relative abundances of various taxonomic groups and pathways associated with methanotrophic or chemolithoautotrophic functions via analysis of 16S rRNA gene sequences (Hathaway et al., 2014; Ortiz et al., 2014; Gonzalez-Pimentel et al., 2018; Zhao et al., 2018; Marques et al., 2019; Wischart et al., 2019), metagenomics (Ortiz et al., 2014; Wischart et al., 2019), or by using quantitative PCR of genes for specific functions, such as for the particulate methane monooxygenase (pMMO) enzyme pathway (Zhao et al., 2018). For instance, in Kartchner Caverns, Arizona, metabolic pathways for the chemolithoautotrophic CO₂ fixation are overrepresented in cave communities compared to surface soil communities, which

suggests that there is a reliance on chemolithoautotrophy in the cave compared to heterotrophic metabolism of photosynthetically-fixed organic carbon from the surface (Ortiz et al., 2014).

Cave microbial communities consisting of methanotrophs have also been implicated in net CH₄ removal from cave air from various caves around the world (Webster et al., 2016; Waring et al., 2017; Zhao et al., 2018). Net removal of atmospheric CH₄ from caves is based on two observations: (i) frequently measured sub-atmospheric CH₄ levels in caves and (ii) CH₄ detected entering a cave at entrances or from fractures but that could not be measured at some distance from an input location within cave passages (Webster et al., 2016; Waring et al., 2017). A recent study from cave sediments in Manao-Pee Cave, Thailand, determined that CH₄ oxidation may contribute up to 20.5% of energy metabolism within the cave microbial ecosystem (Zhao et al., 2018). However, despite numerous studies that consider the possibility of chemolithoautotrophy in cave SABs based on putative taxonomic function and genetic potential (Schabereiter-Gurtner et al., 2004; Barton et al., 2007; Porca et al., 2012; Ortiz et al., 2014; Tomczyk-Żak & Zielenkiewicz 2015; Gonzalez-Pimentel et al., 2018; Zhao et al., 2018; Marques et al., 2019; Wischart et al., 2019), these molecular methods cannot discriminate between living, dormant, or dead organisms, and do not demonstrate active metabolic functions.

Tracing Carbon & Nitrogen Sources

Carbon stable isotope ratio ($\delta^{13}\text{C}$) analysis is a useful tool for tracing sources of carbon in ecosystems. Due to the distinctive carbon isotope ratios of biomass produced through chemolithoautotrophy (Preuß et al., 1989), $\delta^{13}\text{C}$ analysis has been used in aquatic cave ecosystems to determine chemolithoautotrophic carbon fixation and the transfer of fixed carbon within cave food webs (Vlasceanu et al., 2000; Engel et al., 2001; Hutchens et al., 2003; Simon et al., 2003; Opsahl & Chanton, 2006; Porter et al., 2009; Hutchins et al., 2016; Karwautz et al., 2017; Brankovits et al., 2017; Brankovits & Pohlman, 2020). For instance, bulk carbon isotope analysis of caddis fly and chironomid larvae in surface streams has also shown evidence for the importance of CH₄-derived carbon to aquatic food webs, even in photosynthetic ecosystems (Bell et al., 2014; Sampson et al., 2019). In addition, $\delta^{13}\text{C}$ analysis can show recycling of isotopically light (i.e., low $\delta^{13}\text{C}$ values) carbon within biofilms (Staal et al., 2007). Although multiple studies have successfully applied bulk $\delta^{13}\text{C}$ analysis and stable carbon isotope tracing to the investigations of carbon metabolism in aquatic karst biofilms and microbial mats (e.g., Vlasceanu et al., 2000; Simon et al., 2003; Hutchins et al., 2016), there have been limited studies using these methods for

cave-wall SABs (Vlasceanu et al., 2000; Engel et al., 2001; Karwautz et al., 2017). These former investigations were from hypogenic caves and of unusual cave-wall biofilms with extensive mucous-rich biomass (referred to as snottites) dominated by acidophilic sulfur-oxidizing or other bacteria. However, cave SABs common to epigenic carbonate caves and lava tubes tend to have considerably less biomass, typically form isolated colonies or groups of colonies that are only millimeters in diameter and only hundreds of microns thick. This restrictive size may explain earlier inabilities to obtain enough material for isotopic analyses.

Bulk stable carbon isotope ratios of microbial biomass are determined by (i) the isotopic composition of carbon that is being assimilated and (ii) fractionation factors of the irreversible enzymatic pathways involved in metabolism of that original carbon source. The two carbon isotopes that are measured for these analyses are ^{12}C and ^{13}C , and discrimination for the lighter isotope (^{12}C) versus the heavier isotope (^{13}C) during chemolithoautotrophic processes will result in biomass and organic carbon that is isotopically lighter than the isotopic composition of the initial inorganic sources (e.g., CO_2) (Vieth & Wilkes, 2010). Chemolithoautotrophic pathways can have some of the largest fractionation effects (Preuß et al., 1989). Conversely, the carbon isotope composition of biomass produced from heterotrophy will be the nearly the same as the original carbon source isotope composition (i.e., organic carbon) (Palmer et al., 2001). Differences in isotopic composition are expressed in delta (δ) notation, which is the ratio of $^{13}\text{C}/^{12}\text{C}$ of a sample compared to a standard. This value for the ratio, $\delta^{13}\text{C}$, is reported in per mil (‰).

To differentiate between inorganic and organic carbon sources, the $\delta^{13}\text{C}$ values of each potential endmember source must be measured, and the fractionation effect associated with each metabolic pathway must be known. Hypothesized carbon sources to cave SABs include (i) allochthonous dissolved organic carbon (DOC) from the surface and originally photosynthetically-produced organic matter, (ii) dissolved inorganic carbon (DIC) that could be as bicarbonate, originating from the dissolution of carbonate bedrock and delivered through percolating meteoric water or flooding stream water, (iii) atmospheric and dissolved CO_2 , or (iv) atmospheric or dissolved CH_4 . For instance, if a cave SAB was composed of predominately heterotrophs that were consuming photosynthetically-derived organic carbon, which can have $\delta^{13}\text{C}$ values generally from -5 to -35‰ (Vieth & Wilkes, 2010), then the predominately heterotrophic biomass would likely have a $\delta^{13}\text{C}$ value between -5 and -35‰.

The Calvin-Benson-Bassham (CBB) Cycle is responsible for the reduction of CO₂ to glucose in most chemolithoautotrophs via the enzyme ribulose-1,5-bisphosphate carboxylase (Rubisco), but other pathways used by microbes perform similar enzymatic functions, such as the reductive pentose-phosphate, reductive acetyl-coA, reductive-TCA cycle pathways, as well as the 3-hydroxypropionate/4-hydroxybutyrate (3-HP/4-HB) cycle, dicarboxylate/4-hydroxybutyrate (DC/4-HB) cycle, and the 3-hydroxypropionate (3-HP) bicycle (Preuß et al., 1989; Hügler & Sievert 2011). Biomass produced by Rubisco typically results in $\delta^{13}\text{C}$ values about -20 to -35‰ lower (i.e., more negative) than the original inorganic carbon source isotopic composition (Preuß et al., 1989). Biogenic CH₄ is isotopically lighter than CO₂ ($\delta^{13}\text{C}_{\text{CH}_4}$ values of -55 to -85‰), and methanotrophic “fixation” of CH₄ produces microbial biomass with $\delta^{13}\text{C}$ values of -85‰ to -110‰ (Vieth & Wilkes, 2010). Thus, the presence of CO₂- or CH₄-derived carbon from chemolithoautotrophy would likely result in cave SAB biomass $\delta^{13}\text{C}$ values ($\delta^{13}\text{C}_{\text{SAB}}$) that are lower than -35‰. However, it is also possible that $\delta^{13}\text{C}_{\text{SAB}}$ values for microbial biomass derived from CO₂ or CH₄ fixation could be even lower, depending on initial $\delta^{13}\text{C}$ values of DIC ($\delta^{13}\text{C}_{\text{DIC}}$) and $\delta^{13}\text{C}$ values of CH₄ ($\delta^{13}\text{C}_{\text{CH}_4}$), as well as fractionation factors of each enzymatic pathway.

Genomic analysis of 16S rRNA gene sequences obtained from microbial biomass cannot indicate whether putative pathways are active or important to community function, even though relatively conserved functions associated with certain taxonomic groups could provide information about putative function. Therefore, for this thesis research, microbial community composition analyses from 16S rRNA sequences used to determine the presence of taxa putatively associated with certain functions were paired with $\delta^{13}\text{C}$ analysis of cave SABs and endmember carbon sources to determine whether the putative metabolic chemolithoautotrophic activities likely explain the isotopic compositions of cave SAB biomass.

Furthermore, since microbial nitrogen cycling pathways, such as nitrification, are tied to both carbon and nitrogen isotope compositions of microbial biomass, bulk $\delta^{15}\text{N}$ measurements were also used to provide information about nitrogen cycling within the potentially nutrient-limited cave SABs. The primary microbial processes that fractionate nitrogen isotopes include fixation of atmospheric N₂ via the reduction of N₂ to ammonia, nitrification via the oxidation of ammonia to nitrite and then to nitrate, assimilation of nitrogen sources, and denitrification via the reduction of nitrate to nitrous oxide (N₂O) and finally N₂ gas (Casciotti & Buchwald, 2012). By

converting nitrate to N₂ gas, denitrification enriches the remaining nitrate in ¹⁵N isotopes by +13 to +40‰, thereby resulting in positive δ¹⁵N_{NO₃} values (Barford et al., 1999; Waser et al., 1998; Ryabenko, 2013). Preferential uptake of isotopically light nitrate by microbes also fractionates nitrogen isotopes by ~ 6‰ when nitrate is not limiting, which produces higher δ¹⁵N_{NO₃} values in the nitrate pool and lower bulk δ¹⁵N values for microbial biomass (Waser et al., 1998; Ryabenko, 2013). A similar process occurs during the uptake of ammonia, but the fractionation between ammonia and biomass is more dramatic and has been measured at -16.1 to -23.8‰ in *E. coli* experiments (Vo et al., 2013). Nitrification fractionates nitrogen isotopes between reactant (ammonia) and product (nitrate) by -12 to -29‰ and can produce soil nitrate with δ¹⁵N values between -10.4 and -5.8‰, such as in hardwood forest flood leachate (Spoelstra et al., 2007). The uptake of isotopically light nitrate or ammonia by microbes, and the fractionation associated with uptake, can then result in lower δ¹⁵N values for bulk microbial biomass compared to the original nitrogen isotope composition (Spoelstra et al., 2007).

Nitrogen fixation by free-living diazotrophs involves preferential uptake of N₂ enriched in the lighter ¹⁴N isotope. As the standard for a measurement of stable nitrogen isotope composition, atmospheric N₂ has a δ¹⁵N value of ~0‰ and incorporation of fixed nitrogen into microbial biomass results in biomass with lower δ¹⁵N values (Dojani et al., 2007). Free-living diazotrophs fractionate nitrogen isotopes by about -2.5‰ between the reactant (N₂) and product (ammonia) (Craine et al., 2015). In this study, bulk δ¹⁵N values were measured to explore potential nitrogen cycling pathways utilized by cave SABs, specifically the presence of nitrogen fixation and/or nitrification within these biofilms, as indicated by the prevalence of AOB found in previous 16S rRNA sequencing studies. However, interpretations of bulk nitrogen isotope compositions are difficult to perform because the microbial processes that affect biomass and inorganic or organic nitrogen δ¹⁵N values are not well constrained and knowing the availability of multiple nitrogen sources and their δ¹⁵N values are analytically challenging.

CHAPTER THREE MATERIALS AND METHODS

Site Descriptions

The two study caves (KN14 and RN5) are separated by 65 kilometers in the Appalachian Valley and Ridge (AVR) Province of Eastern Tennessee, one in Knox County (KN) and the other in Roane County (RN). The specific cave names are withheld to keep the locations private, but the naming with county abbreviation and cave number is linked to the Tennessee Cave Survey (TCS) scheme, from which access can be requested at <http://www.subworks.com/tcs/>. Despite the distance between the caves, they are found in stratigraphically adjacent and mineralogically similar lower Ordovician formations (Figure 3.1), formed by the abundant thrust faulting in the AVR Province that created each valley and ridge being comprised of repeating geologic units. Generally, the soluble carbonate units make up the valleys and erosion-resistant siliciclastic units make up the ridges in the AVR Province (Figure 3.1). According to geologic maps of the area, KN14 formed in the Kingsport Formation and RN5 formed in the overlying Mascot Dolomite Formation, which are described as being dolomitic with chert nodules (Hardeman et al., 1966).

The main passages of both caves contain perennially outflowing streams. The origin of the outflowing stream in KN14 is a spring within the cave, but the origin of the stream in RN5 is unknown. The elevations of KN14 and RN5 cave entrances are approximately 299 m and 274 m above sea level, respectively. Both cave passages are at the foot of a bluff. Based on the change in elevation from the cave entrances to the tops of each bluff measured using elevation profiles in Google Earth Pro, the thickness of bedrock and soil overlying RN5 and KN14 are approximately 52 m and 18 m, respectively. Although RN5 runs more than 200 m horizontally into the side of this bluff, the main room in KN14 is very close, no more than 30 m, from the side of the bluff. In addition, the area above the main room in KN14 is steep, rocky, and more sparsely forested, but the area directly above RN5 is relatively flat, based on elevation profiles, and heavily forested.

Some fresh clay deposition was present in KN14 within a meter of stream base level, which is indicative of potential flooding. In RN5, a thin layer of soft sediment covers much of the rock surface in the main passage. This sediment layer is up to 3 mm thick, comprised of very fine-grained carbonate silt, and is consistent with descriptions of carbonate silt produced on rock surfaces via weathering of the underlying carbonate bedrock (Hajna, 2003). Seepage in this thin sediment layer was associated with microbial growth that followed distinct flow paths on the cave

walls (Figure 3.2). No debris (e.g., branches, leaves, or garbage) was observed in either cave, indicating that there has not been a large or recent flood event. Possible frequent flooding levels in RN5 were suggested by deposition of a dark clay, which was distinct from the light-colored carbonate sediment, on the cave wall and within a half meter of the base-level stream surface. This sediment had a distinct collection of colonies (Figure 3.2). There were multiple areas in both caves where water drips or seeps into the cave passage, and many wet areas were associated with SABs (Table 3.1).

Environmental Conditions

The two cave study sites were chosen because of their ease of access, presence of perennial outflowing streams, and abundant SABs. Six biofilm sampling sites were chosen in each cave (Table 3.1), including SABs near stream level and SABs from upper, drier passages. A total of three sampling trips were conducted over the study period. The first sampling trips occurred on 1 and 2 February 2020, when both cave sites were visited. The major tasks accomplished during this initial trip were: (i) deployment of stream water level and temperature/humidity data loggers; (ii) measurement of ambient environmental data, including temperature, moisture, CO₂ and CH₄ concentrations in cave air and outside, and vertical distance of each site from stream level; (iii) measurement of pH, temperature, and major ion analysis of drip water and streams; (iv) collection of gas and water from drip areas and streams, as well as carbonate samples from each site, for $\delta^{13}\text{C}$ analysis of DIC, bedrock CaCO₃, and atmospheric CO₂; and (v) collection of SAB biomass using swab and scraping methods. Subsequent sampling trips were done to collect additional drip water and stream water for nutrient analysis, as well as to monitor temperature at each sampling site.

Stream level variation and flooding frequency in both cave streams were determined with HOB0® U20L water depth (i.e., stage) data loggers (Onset Computer Corporation, Bourne, MA, USA) deployed from February to May, which was part of the winter-wet season and into drier-spring season. The data loggers were placed in PVC housing to keep from being removed during potential storm events. Local barometric pressure obtained from the weather station at McGhee Tyson Airport (KTYS, GHCND:USW00013891) in Knoxville, TN, and the data were downloaded via the Iowa State University- Iowa Environmental Mesonet (https://mesonet.agron.iastate.edu/request/download.phtml?network=TN_ASOS#) and used to calculate water depth in meters from absolute pressure, according to manufacturer instructions (Onset Computer Corporation, Bourne, MA, USA). Water level accuracy is from 1.0 to 2.0 cm with $\pm 0.3\%$ pressure error at a stable

temperature. Continuous monitoring of temperature and relative humidity (RH) at a single location in each cave was done from February to May by using weatherproof HOBO® U23 Pro V2 temperature/RH dataloggers (Onset Computer Corporation). Surface (i.e., outside) temperature and RH were measured with a data logger placed outside in Knoxville for the duration of the study period. Accuracy for temperature and RH is less than $\pm 3.5\%$ and 2.5% , respectively, with a resolution of 0.05% . Data were acquired from the data loggers using a HOBO® Optic USB Base station and compatible coupler interfaced with a computer.

Cave air was collected immediately after entering an area where sampling would take place, and before other members of the team entered the area, to prevent human breath contamination. Gas samples were collected in triplicate from cave air into evacuated 60 mL serum vials with butyl rubber caps and aluminum crimp-seals, and dissolved CO₂ and CH₄ concentrations were measured in triplicate for each cave stream after headspace equilibration in 60 mL serum bottles. Measurements for CO₂ and CH₄ were done using a SRI 8610C gas chromatograph (GC) (SRI Instruments, Torrance, CA, USA) with a thermal conductivity detector and flame ionization detector with methanizer, respectively, and standard curves for CO₂ and CH₄ concentrations. Dissolved gas concentrations were calculated based on the volume of water collected and Henry's Law constant for each gas. Determination of the $\delta^{13}\text{C}$ of CO₂ was done in triplicate using Labco Exetainer® (Lampeter, Wales, United Kingdom) 12 mL glass vials inside and outside the cave. Vials were flushed three times with ambient air prior to filling with cave air.

Ambient environmental conditions were collected at each site prior to biofilm sampling, including substrate moisture, air, water and cave-wall temperature, and air RH. Although moisture was a potentially important nutrient source and was readily evident as water beaded up on the rock or on SABs, sufficient moisture could not be collected. However, moisture content of the cave-wall substrate was measured with an AccuMASTER model 7445 Duo Pro Pin & Pinless Moisture Meter (Calculated Industries, Carson City, NV, USA), with the electromagnetic pad sensor and a reported accuracy of $\pm 3\%$. Substrate temperature at each site was measured using a model 1022D Dual Laser Digital Infrared Thermometer (Etekcity Corporation, Anaheim, CA, USA), with $\pm 2\%$ or 2°C accuracy. These measurements were done over the four months, for a total of three time points for both caves.

Additional environmental data included bedrock carbonate rock samples at each biofilm sampling site and water. Collection of water for major ion concentrations was done by using sterile 10 mL HSW Norm-Ject syringes (Henke-Sass, Wolf, Germany) from the stream and from two active drip water locations in each cave. Drip locations were chosen, where possible, from SAB sampling locations. Depending on drip rates, several active drips had to be sampled within the same area at the same time, specifically along a single fracture, to obtain enough volume. Drip rates were not quantified, but the presence or absence of dripping was noted during each visit (Table 3.1). Drip sites 1 or 2 in KN14 were periodically dry after a few weeks without rain, but RN5 drip sites were active throughout the study period. All water samples were filtered to 0.2 μm using Whatman filters into clean Nalgene HDPE bottles. Water samples for cation analysis were preserved with trace metal grade nitric acid to pH 2. All samples were stored at 4°C prior to analyses.

Major ions, including chloride, nitrate, sulfate, sodium, potassium, and ammonium, for example, were measured using a Dionex Integriion High Pressure Ion Chromatograph (HPIC) (Thermo Scientific, USA) within 48 hours of collection. Standard curves of known concentrations of each analyte were used, with method detection limits based on the lower limit of each standard curve. Instrument error for each analyte was quantified by replicate injection of samples, and errors for analytes which could be measured above detection limit are listed with the following detection limits: Detection limits for measured anions were 1 \pm 0.01 mg/L for chloride, 1 \pm 0.01 mg/L for nitrate, 1 mg/L for nitrite, 1.5 \pm 0.02 mg/L for sulfate, 1 mg/L for bromide, and 1.5 mg/L for phosphate. Detection limits for measured cations were 2.5 \pm 0.3 mg/L for calcium, 1.25 \pm 0.14 mg/L for magnesium, 1 \pm 0.15 mg/L for sodium, 2.5 \pm 0.01 mg/L for potassium, and 1.25 mg/L for ammonium. Alkalinity data were obtained by titration with 0.1N H₂SO₄ during a previous geochemical analysis of the cave streams (obtained 11 and 28 July 2019), and were compared to the DIC concentrations obtained during $\delta^{13}\text{C}$ analysis in this study.

Biofilm Sample Collection

Samples for DNA and carbon and nitrogen analyses were collected from six areas of each cave (Table 3.1). Biofilm sampling sites 1 to 4 in RN5 are illustrated in Figure 3.2. Because biomass for different SAB areas and colonies varied (Figure 3.3), and was insufficient for all analytical needs, biomass was collected using two different methods, which resulted in a nested

experimental design for sample collection and the intended purpose of each sample (Figure 3.4). The first method for DNA analyses only used BD BBL CultureSwab sterile media-free rayon-tipped swabs to obtain biomass (Thermo Fisher Scientific, Waltham, MA, USA). Three swabs were used for each site. The second method for DNA analysis, lyophilization, and isotope analysis involved scraping biofilms into 1.5 mL Eppendorf tubes with a sterile inoculating loop. All biofilm material was stored at -80°C prior to DNA extraction and lyophilization, which was done using a Labconoco freeze dry system. Each sampling method resulted in sufficient biomass to perform DNA extractions from the six sites in both caves and to obtain $\delta^{13}\text{C}$ and $\delta^{15}\text{N}$ data from all scrapings, but duplicate extractions of scraped material from some sites was impossible due to low biomass.

Stable Isotope Analyses and Inorganic Carbon Measurements

Carbon and nitrogen isotope compositions were measured separately using a Thermo Finnigan Delta+XL mass spectrometer and Thermo Scientific GasBench II gas chromatograph for carbonates, dissolved inorganic carbon (DIC), and dissolved organic carbon (DOC), and a Costech EA gas chromatograph for biomass organic carbon (GC-IRMS) at the University of Tennessee Stable Isotope Laboratory. Each of the measurements are described separately.

Water samples for the $\delta^{13}\text{C}$ measurement of DIC and DOC were collected in 12 mL Exetainer vials that had been muffled to remove any organic carbon contamination, evacuated and flushed with helium, and contained 10 drops of H_3PO_4 to acidify samples and remove inorganic carbon upon injection of filtered water into the closed vials. Samples were stored at 4°C and allowed to return to room temperature before analysis. DIC concentrations and $\delta^{13}\text{C}$ were measured from CO_2 in the headspace of each acidified vial. Following the removal of DIC via acidification and subsequent measurement of DIC $\delta^{13}\text{C}$ from CO_2 in the vial headspace, DOC was also measured from these vials by addition of potassium persulfate, which oxidizes organic carbon to CO_2 . The CO_2 in the headspace after initial acidification ($\delta^{13}\text{C}_{\text{DIC}}$) and oxidation ($\delta^{13}\text{C}_{\text{DOC}}$) are measured at each respective step by GC-IRMS and reported relative to the Pee Dee Belemnite (PDB) standard (Lang et al., 2011). Blanks were run for the vials, H_3PO_4 , and potassium persulfate oxidizing reagent. $\delta^{13}\text{C}$ of CO_2 ($\delta^{13}\text{C}_{\text{CO}_2}$) from cave air and outside air was measured directly from sealed Exetainer vials filled at ambient pressure. Lab air served as the blank. Additionally, solid carbonate samples were homogenized using an agate mortar and pestle, then acidified with

phosphoric acid to release CO₂, which was measured for δ¹³C with GC-IRMS (Paul & Skrzypek, 2007).

For δ¹³C analysis of SAB biomass, inorganic carbon (i.e., carbonate) was removed from the lyophilized SAB material by acidification with 0.2 N HCl and air-drying overnight. Unacidified lyophilized material was also used for δ¹⁵N analysis of SAB material. δ¹⁵N values are compared to atmospheric nitrogen (N₂) as the standard. The instrument standard deviation for δ¹⁵N was 0.3‰.

The instrument standard deviation for δ¹³C analysis of SAB biomass was 0.1‰. Standards used for δ¹³C analysis of SAB biomass and DOC were acetate (acetCOST) and UT729, calibrated against the international standards USGS40 and USGS41. Standard error among three technical replicates, which consisted of three subsets of homogenized material from the one original sample, was 0.5‰ for δ¹³C_{SAB}. Carbonate standards were ANUM1 and CALSED, which were calibrated to LSVEC and NBS19 international standards. The standard error between three technical replicates, which consisted of three subsets of homogenized material from the one original sample, was 0.06‰ for δ¹³C of carbonate samples. In-house standards used for δ¹³C analysis of cave air CO₂ were ANUM1 and CALSED, which were calibrated to the international standards LSVEC and NBS 19. The standard error of δ¹³C_{CO2} between triplicate vials collected at each site was 0.4‰.

δ¹³C analysis of CH₄ (δ¹³C_{CH4}) from cave and outside air, which was collected in muffled 12 mL Exetainer vials filled to ambient pressure, was performed at the University of California–Davis Stable Isotope Facility by first concentrating CH₄ using a Thermo Scientific Precon concentration unit, followed by stable carbon isotope ratio measurement using a Thermo Scientific Delta V Plus isotope ratio mass spectrometer. In-house standards were UCDM1, UCDM2, Beecher, AH024079, and 043332T. The standard error of δ¹³C_{CH4} between triplicate vials collected at each site was 0.4‰ and instrument standard deviation among reference materials was 0.14‰.

DNA Extractions and 16S rRNA Gene Sequencing

Extraction of nucleic acids was performed on swabs and biofilm scrapings from each location using DNeasy PowerSoil DNA Isolation kits, following manufacturer instructions (Qiagen, Hilden, Germany), but modified to ensure lysis of Actinobacteria and other Gram-positive bacteria. Specifically, as recommended in kit protocol, an incubation step at 70°C for 10 minutes was added to the protocol prior to the bead beating step. The concentrations of extracted DNA were estimated by using a NanoDrop 2000c UV/Vis spectrophotometer (Thermo Fisher

Scientific) that measured the absorbance ratios at both 260/280 nm and 260/230 nm. The success of DNA extractions was also verified using agarose gels and gel electrophoresis.

Homogenized sample extractions were used to sequence the V4 region of the 16S rRNA gene using Illumina MiSeq sequencing technology (Molecular Research LP, Shallowater, TX). Briefly, the primers used were 515F and 806R, a barcode was included on the forward primer, and amplification was performed using a Qiagen HotStart Taq Plus Master Mix kit (Thermo Fisher Scientific) for 30 cycles of denaturing at 94°C for 30 sec, annealing at 53°C for 40 sec, and elongation of 72°C for 1 min. Barcoded samples were pooled and purified using Ampure XP beads prior to Illumina sequencing, according to manufacturer's instructions. Raw sequence files for each sample were submitted to the NCBI Sequence Read Archive under the BioProject PRJNA649551 (<http://www.ncbi.nlm.nih.gov/bioproject/PRJNA649551>), under the BioSample accession numbers SAMN15679595 - SAMN15679649.

16S rRNA Sequence Analysis

Following unbinning of paired-end raw sequence files and removal of primers and linker sequences using MRDNA FASTqProcessor software (MRDNA, Shallowater, TX), sequence processing and taxonomic identification was performed using MOTHUR v.1.44.1, according to the standard operating procedure for MiSeq technology (Schloss et al., 2009; Kozich et al., 2013; Schloss, 2020). Briefly, paired end sequences were aligned and combined based on quality scores associated with each base pair using the *make.contigs* command, followed by removal of sequences of the wrong length (greater than 275 bp) and sequences with ambiguous bases. The remaining sequences were aligned to the SILVA v.138 database (Quast et al., 2013; Yilmaz et al., 2014) and sequences with poor alignment were removed. Detection and removal of chimera were also done in MOTHUR using the *vsearch* command, and sequences identified as Eukarya, Archaea, mitochondria, or otherwise unidentified sequences were also removed.

Sequences were clustered at 97% sequence identity into operational taxonomic units (OTUs) and taxonomic identity was assigned to each OTU based on the SILVA v.138 reference database. This cutoff was used because strains belonging to the same species have been frequently shown to have more than 97% 16S rRNA sequence similarity (Konstantinidis & Tiedje, 2005). Microbial community composition across all samples were analyzed using the *phyloseq* package in R. Because putative functions associated with certain taxa can give valuable information about the functional potential of the community, functional information associated with the taxonomic

identities of abundant OTUs were investigated (Kozich et al., 2013). A literature review was performed on taxonomic groups and functional information obtained from descriptions of cultured representatives are discussed. Alpha diversity at the genus level across all samples and between caves was quantified using the *phyloseq* package function *estimate_richness*. Specifically, Chao1, Shannon, and Simpson diversity indices were applied to the dataset.

Statistical Analyses

Environmental variables were confirmed to be drawn from a normal distribution using the Shapiro-Wilk normality test and were z-score transformed for comparability within the models. No other data transformations were required. A Levene's test to determine data homogeneity of variance in R was done prior to all Tukey's Honest Significant Difference (HSD) post-hoc tests performed to determine significant differences between samples for environmental data. For comparisons between two groups, Welch's two-sample t-tests were used. Microbial data based on presence/absence of sequences from MOTHUR were used in the R package *phyloseq* (McMurdie & Holmes, 2013). Because the relevant research questions focus on the putative function of certain taxa, analyses were performed from the genus to phylum level, and sequence counts for OTUs with identical taxonomic assignments at the genus level were combined. Taxonomic identities, environmental data from the day of biofilm sampling, and sequence counts were imported into R as a *phyloseq* object for analysis using *phyloseq* and *vegan* packages.

For statistical tests comparing microbial community composition between caves, sequence count data were averaged for replicate swabs and scrapings at each site to avoid inflation of degrees of freedom when comparing microbial communities between caves. For analyses of differences among sites within each cave, biological replicates accounted for variation at each site. To account for different sequencing depths between samples and replicates, all data analyzed using multivariate statistics were rarefied to the lowest sequencing depth prior to analysis using the *phyloseq* function *rarefy_even_depth*. Averaged sequencing counts between field replicates yielded between 129,770 and 272,251 reads, with an average of 187,021 reads across all sample sites, and 129,770 reads was used as the lowest sequencing depth for rarefaction. To explore patterns in microbial community structure among cave SABs, Bray-Curtis similarity between caves and sites within caves was measured and represented as principal coordinate analysis (PCoA) plots.

Related to the overarching hypotheses for this research, permutational multivariate analysis of variance (PERMANOVA) tests were performed to investigate the following sub-hypotheses:

- (i) Microbial community composition is driven by microenvironmental community variation more than geographic distance and communities will, therefore, be more similar between environmentally similar sites from both caves. To test this hypothesis, community composition was compared between caves.
- (ii) Differences in microbial community composition within caves are driven by microenvironmental conditions that may differ between sampling sites, primarily substrate (i.e., cave wall) temperature and moisture. To test this hypothesis, microbial communities were compared based on moisture content and temperature at each site within caves on the day of SAB collection.
- (iii) Carbon isotope composition of cave SABs is influenced by microbial community composition, namely the presence of certain taxonomic groups that have the capability to fix CH₄ or CO₂. To test this hypothesis, microbial community compositions were compared based on the measured $\delta^{13}\text{C}$ values from each site within the two caves.
- (iv) Based on findings from previous studies, microbial community composition does not differ significantly by biofilm color, specifically white, yellow, and pink. To test this hypothesis, microbial community composition of cave SABs were compared based on biofilm color within and across both caves.

PERMANOVA tests were used to test hypotheses that would determine whether variation in microbial community composition between and within caves could be explained by variations in environmental conditions, $\delta^{13}\text{C}$ value, or biofilm color. Because some of the SABs did not directly correspond to drip locations, the only quantitative data at each SAB sampling site were substrate temperature and moisture content. Prior to performing PERMANOVA tests, the *betadisper* function in *vegan* was used to test for equal dispersion of groups that were to be compared, between (i) caves, (ii) temperature and moisture, (iii) carbon isotope compositions, and (iv) cave SAB color. Equal dispersion was found within caves (p-value = 0.333), within sites (p-value = 0.154), within environmental variable groups (moisture p-value = 0.09) and between biofilms of different color for all samples and within caves (p-value = 0.150). Therefore, assumption of equal dispersion is met for performing PERMANOVA.

Due to the nested design of the study (Figure 3.4), the vegan function *adonis* in R was used by setting *strata* at the level of cave ID. This was to account for error that could result from differences in community composition that cannot be easily measured, such as evolutionary history of the cave or flooding disturbance frequency throughout the lifetime of a SAB. Accounting for a nested random effect in the model discounts some error that could be created by distance and enables the model to show if remaining patterns in community composition are sustained across the caves. In addition, although biofilm color is included to describe predictors of community composition in cave SABs based on results from the literature that suggests community composition correlates to color, this has not been thoroughly tested. Therefore, the inclusion of color here is to test correlations among community composition and stable isotope composition or environmental variables.

Correspondence analysis was used to illustrate patterns in microbial community composition and their correlation to changes in moisture content and carbon isotope composition. Due to arch effects produced through canonical correspondence analysis (CCA) (Paliy & Shankar, 2016), detrended correspondence analysis (DCA) was used to show correlations between environmental variables, using the *bioenv* function, and microbial community structure, and to test for significance in these correlations. To compare environmental variables within DCA models, values were z-score transformed, as indicated in the corresponding data tables. In addition, the top 20 taxa across both caves and within each cave were selected using the *taxa_sums* function in the *phyloseq* package and plotted using DCA to investigate which taxa were affected by environmental variables (i.e., moisture).

Mantel tests were also performed using the *mantel* function from the *vegan* R package (Oksanen et al., 2019). The Pearson's product moment correlation method was applied to the correlation of Bray-Curtis dissimilarity matrices of rarefied genus-level bacterial abundance and Euclidian distance matrices of environmental data to test the hypothesis that microbial community composition is correlated to temperature and moisture content.

To quantify the correlation between taxa and environmental variables, Pearson's product moment correlation coefficients were found between the top 20 most abundant families within each cave and moisture content, as well as the SAB's $\delta^{13}\text{C}$ value. The top 20 most abundant families across all sites comprised 79% of the overall 16S rRNA sequences in KN14 and 69% in

RN5. Families that showed significant Pearson's product moment correlation (i.e., p-value > 0.05) to either of these variables were determined.

Table 3.1: Descriptions of the location and biofilm morphology specific to each of six sites in caves KN14 and RN5 on 1 and 2 February 2020.

Cave ID	Site ID	Site Description	Drip?	Biofilm Description
KN14	1	Low-hanging rock with wet surface and slow, active sheet flow across a flowstone speleothem	Yes, but periodically dry	Scattered pink/white colonies, some small blue colonies
	2	Low-hanging rock with wet surface; occasional water flowing down rock surface and dripping over biofilms	Yes, but periodically dry	Yellow-blue encrustation/sheet biofilm on lower sides of rock; nodules of precipitated calcite located on upper side of rock
	3	Clay bank next to breakdown pile where stream sinks and exits room	No	Pink and white isolated to merged colonies
	4	Rock layer with active drip and soda straw formation (speleothem)	Sampled drip #1; periodically dry	Yellow, large isolated colonies that formed sheet near drip point
	5	Ceiling of main room, flat sloped rocks on either side of a fracture with active dripping	Sampled drip #2	White to pink with sheet morphology, no isolated colonies
	6	Rock in upper passage, wet surface	No	White, isolated to coalescing colonies
RN5	1	Clay layer over limestone within 0.3 m from stream surface at base flow	No; stream	Pink to white, raised isolated colonies, and gray to blue flat isolated colonies
	2	Carbonate mud deposited over limestone	No	Large, isolated yellow colonies
	3	Carbonate mud deposited over limestone	Yes	Large area with scattered, small white to yellow colonies, following dripline
	4	Chert nodule	Yes	White to yellow scattered, small colonies
	5	Flat limestone low-hanging ceiling near a vertical fracture with several drip points	Sample drip #1	White to yellow scattered, small colonies
	6	Carbonate mud on ceiling in upper passage	No	Isolated yellow colonies

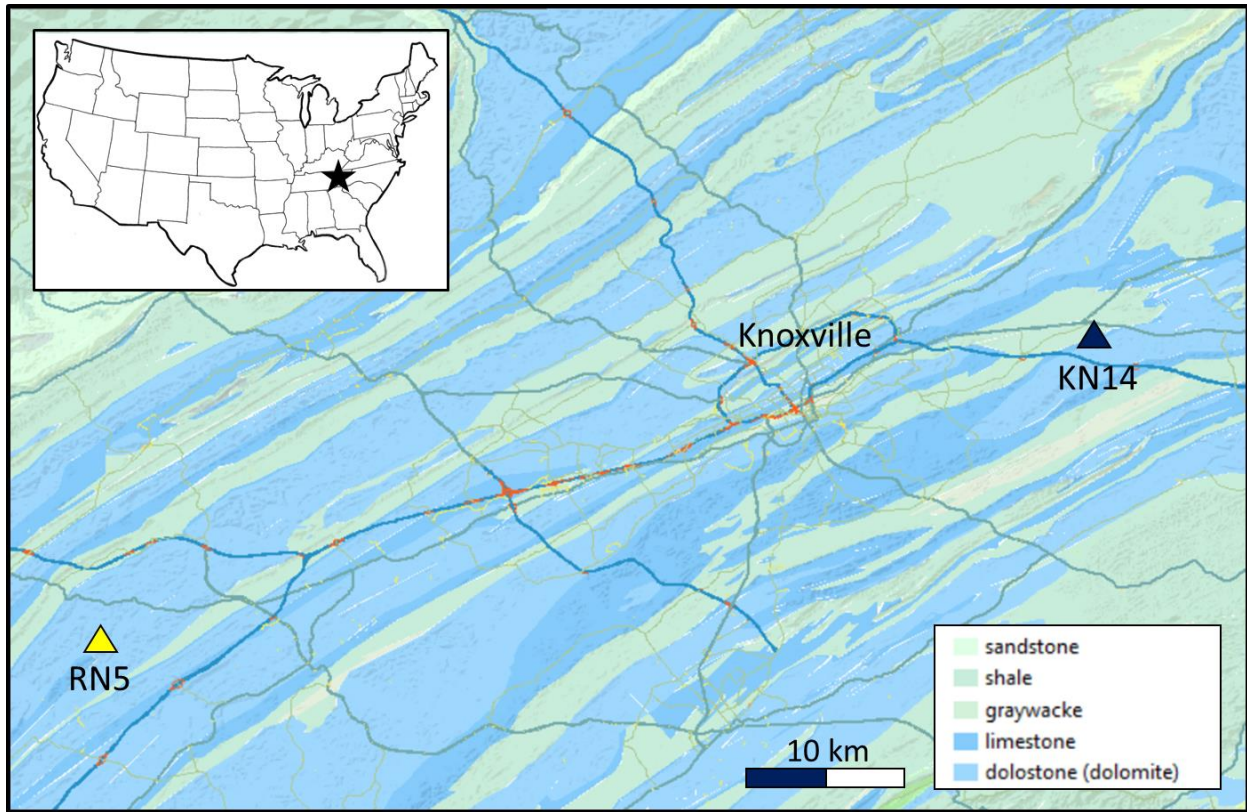


Figure 3.1: Geologic map of Appalachian Valley and Ridge karst in the Knoxville, Tennessee using data from the USGS TN Geologic Map (<https://mrdata.usgs.gov/geology/state/state.php?state=TN>). Locations of cave sites used in this study are indicated by triangles.

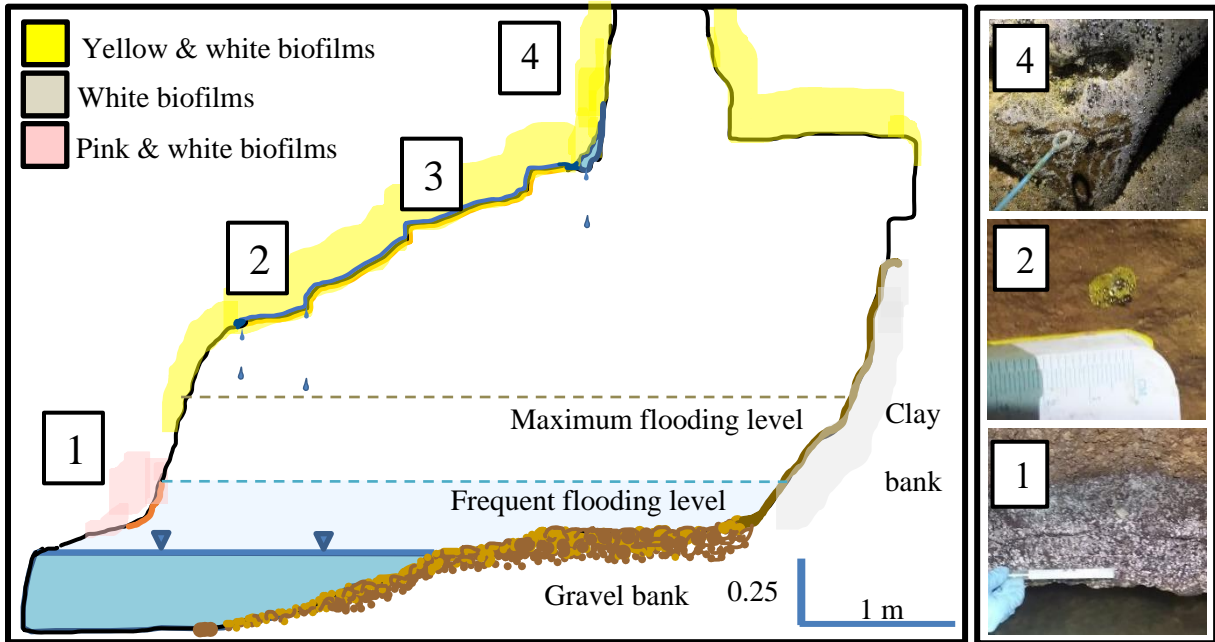


Figure 3.2: Cross-section of the RN5 cave passage showing normal water level (solid blue line) and possible frequent water level fluctuations based on clustering of biofilms within less than a meter of the water surface (light blue dotted line). Maximum flood level ~0.5 m and frequent flooding level ~ 0.25 m are based on HOBO water level logger data from the study period (Brown dotted line, blue dotted line). Numbers denote biofilm sampling locations.

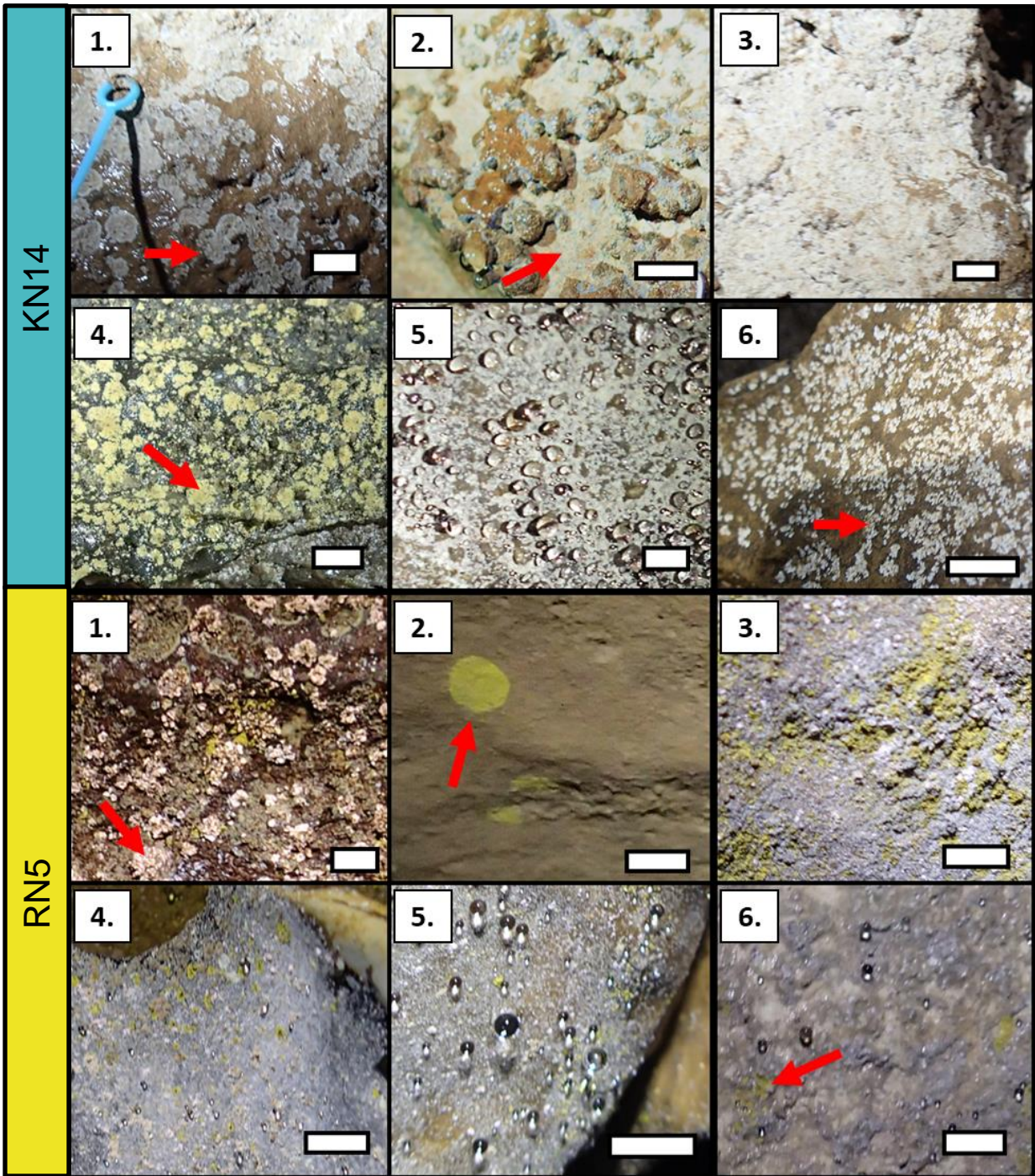


Figure 3.3: Biofilm color and morphology at each sampling site. White bar lengths represent approximately 0.5 cm. Red arrows represent examples of sampled SABs. Images without red arrows depict “sheet-like” biofilms that cover the entire pictured surface.

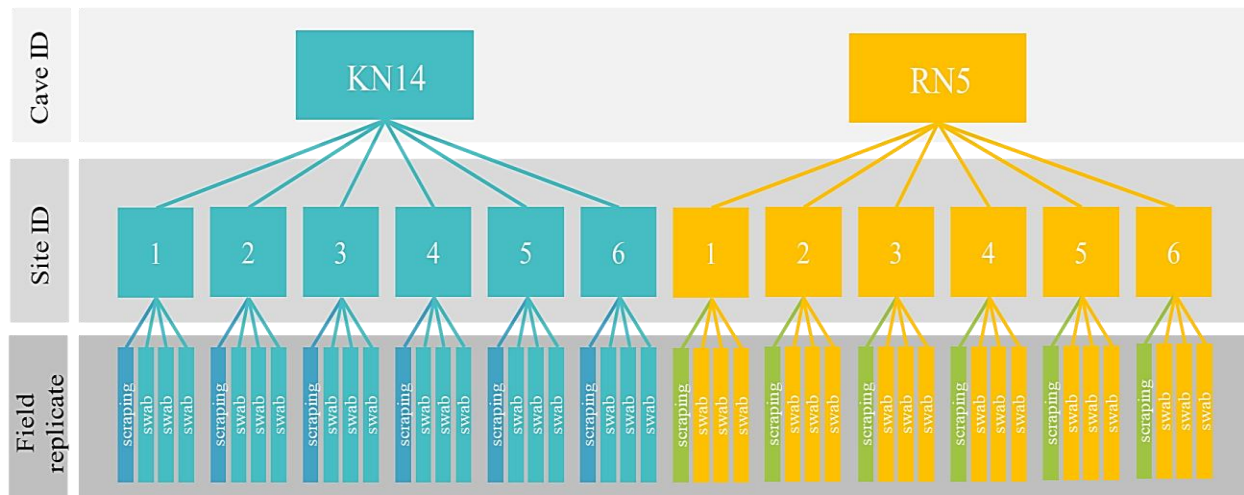


Figure 3.4: Cave SAB sampling design, showing each of six total sites within each cave and the samples collected from each site. At least one scraping (noted as dark blue or green) and three swab replicates (noted as light blue or yellow), for a minimum of four samples per site, were used for DNA analysis, whereas scraping samples only were used for $\delta^{13}\text{C}$ analysis.

CHAPTER FOUR RESULTS

Environmental Conditions and Nutrient Sources

Stream level fluctuations and flooding frequency

Vertical distances from the stream level to SAB sampling sites were measured at the time of collection and data logger deployment. This level was set as the “base stream level” (Figure 4.1). Vertical distances from the stream to SAB sites are listed on Table 4.1. The stream levels were continuously logged for 81 days, from 2 February to 19 April 2020 (Figure 4.2). Water level infrequently dropped, by at most 2.3 cm, below base stream level in KN14, and at most by 12 cm in RN5. Timings of stream level fluctuations were similar between both caves, with peak flooding occurring within a day of heavy local rainfall (Figure 4.1). Changes in base stream level that exceeded +10 cm occurred for 94% and 28% of this time in KN14 and RN5, respectively. Changes of more than +20 cm occurred for 74% (KN14) and 7% (RN5) of this time. Fluctuations of more than 0.5 m were common in KN14, where levels rose higher than +0.5 m for 23% of the study period, but rare occurrences in RN5, representing less than 1% of the study period. Flooding frequency at different water level heights for both caves are shown in Figure 4.2.

The maximum changes in water levels were +2.4 m and +0.59 m for KN14 and RN5, respectively (Figure 4.1). The lowest sampled SAB sites in KN14 (i.e., sites 1, 2, and 3) were located 0.9, 0.95, and 1.05 m above base stream level, respectively, and the frequency of flooding exceeding the height of these three sites was 5.1% of the study period, which corresponded to approximately 4 days that SABs would have been flooded. KN14 site 5 was located 1.5 m from stream base level and was exposed briefly to stream water for up to 28 hours during the study period (i.e., flooding frequency at +1.5 m = 1.3%). In contrast, the lowest RN5 SAB site (site 1) had colonies between 10 and 20 cm from the stream surface. This site was exposed to stream water for a minimum of 5 and a maximum of 22 days. All other sites in RN5 were located above the maximum flooding height and, therefore, had no exposure to stream water during the study period.

Cave temperatures, relative humidity, and substrate moisture

Cave air temperatures increased with greater vertical distances above both stream base levels, which has implications for SAB development (Figure 4.3). During the study period, the

average local surface temperatures was 14.2 °C (ranging from -3.07 to 26.72 °C). At the KN14 datalogger location, cave air temperature varied and closely followed fluctuations in surface temperatures (Figure 4.4), with an average of 11.46 °C. To evaluate whether cave air temperatures were more stable away from the stream, the data logger in KN14 was relocated to about 0.5 m from the stream level for about one month after the start of the study and in hopes the water level would not rise above the logging location (these data are shown between the dotted lines on Figure 4.4, ending 19 March 2020). Cave air temperature near the stream was more variable and lower temperatures corresponded to localized pulses in water height that followed rainfall events. At the RN5 data logger location, however, cave air temperature was stable and varied within the accuracy of the instrument, from 14.29 to 14.43 °C (Figure 4.4).

Proximity to stream level, flooding history, and thermal gradients within cave passages have the potential to affect substrate moisture content and passage ventilation, which have important implications for SAB development and gas exchange. After the data loggers equilibrated to the cave temperature (about 1 day), RH values were 100% for both caves during the study. The percent moisture of the cave walls ranged from 19–84% in KN14 and 63–100% in RN5 (Table 4.1), and SAB sites proximal to the stream or active drips had higher moisture content. Differences in moisture content between the caves were statistically significant (Welch's two-sample t-test, p-value = 0.02), with no sites at KN14 being completely saturated (i.e., 100% moisture content) and more sites in KN14 having lower moisture content overall, even though KN14 had more frequent passage flooding.

CO₂ and CH₄ concentrations and isotopic compositions

Lower moisture content on the walls, despite 100% RH, could be due to greater ventilation and exchange of air of different temperatures between the cave passages and surface, which could also be reflected in cave air gas concentrations, specifically CO₂. Although both caves had significantly higher CO₂ concentrations compared to outside air (Tukey's HSD tests for KN14 vs outside, p-value = 0.002; RN5 vs outside, p-value < 0.001), which suggested a buildup of CO₂ inside the caves, cave air CO₂ concentrations were also significantly higher in RN5 than KN14 (Tukey's HSD test p-value = 0.005), which implies KN14 may be more ventilated (Figure 4.5). The air temperature data also support that KN14 has higher ventilation capacity and frequency compared to RN5 (Spötl et al., 2005) (Figure 4.4).

Although other studies report net depletion of CH₄ in cave air (Waring et al., 2017), CH₄ concentrations measured in this study did not differ significantly from atmospheric levels (Figure 4.6). CH₄ was measured at 1.89 (±0.16) ppmv outside the caves, which is consistent with average ground-level, modern-day atmospheric CH₄ concentrations from the literature (Webster et al., 2015), although the $\delta^{13}\text{C}_{\text{CH}_4}$ value for outside air was $-44.6 \pm 0.3\text{‰}$ (Table 4.6), which was higher than measured for air in other studies at $\sim -47\text{‰}$ (Quay et al., 1999; Dlugokencky et al., 2011). Cave air CH₄ in KN14 was similar to outside atmospheric levels at 1.94 (±0.16) ppmv, with $\delta^{13}\text{C}_{\text{CH}_4}$ values being $-43.4 \pm 0.1\text{‰}$. Cave air in RN5 was lower than atmospheric levels at 1.65 (±0.18) ppmv with $\delta^{13}\text{C}_{\text{CH}_4}$ values being $-42.9 \pm 0.4\text{‰}$. The in-cave gas concentrations, as well as between caves and outside air, were not statistically significant (Figure 4.6; Tukey's HSD test, p-value > 0.05), and the isotope compositions were also not significantly different between the two caves using Tukey's HSD test (p-value = 0.267), but were significantly different between to outside air and caves (p-value = 0.007 for KN14, p-value < 0.001 for RN5). However, at the resolution of sampling in this study, CH₄ concentrations in the cave were nearly indistinguishable from outside the cave atmospheric levels, and assessment of net production or depletion of CH₄ in cave air, which has been measured from other caves (e.g., Waring et al., 2017), as well as determination of potential source(s) of CH₄ to the systems are not possible without additional sampling.

Elevated CO₂ concentrations in caves, relative to atmospheric CO₂ levels, have been attributed to CO₂ production through respiration in overlying soil and within caves (Spötl et al., 2005; Matthey et al., 2016). If caves are not well-ventilated, then isotopically light CO₂ accumulates (Spötl et al., 2005). CO₂ concentrations and isotopic compositions from KN14 and RN5 cave air were measured to determine the extent of ventilation and potential effect of respiration on $\delta^{13}\text{C}_{\text{CO}_2}$ values (Table 4.6, Figure 4.5). Average $\delta^{13}\text{C}_{\text{CO}_2}$ values for KN14 and RN5 were -14.4‰ and -19.4‰ , respectively, whereas the average measured outside air $\delta^{13}\text{C}_{\text{CO}_2}$ value was -9.7‰ (Table 4.6). Tukey's HSD tests showed statistically significant differences in $\delta^{13}\text{C}_{\text{CO}_2}$ values between both caves (p-value < 0.001) and between each cave and outside CO₂ (p-value < 0.001). Higher CO₂ concentrations and more negative $\delta^{13}\text{C}_{\text{CO}_2}$ values for RN5 indicate less ventilation, which is also matched by stable air temperatures for RN5 (Figure 4.4). However, because cave ventilation is influenced by temperature differences, it is possible that, at other times of the year (e.g., in the

summer when no gas exchange might occur, *sensu lato* Spötl et al., 2005), CO₂ concentrations and isotopic compositions could vary.

Drip water and stream geochemistry

Major ion concentrations, dissolved gases (CO₂ and CH₄), DIC, and DOC were measured from two drip sites and the stream water from each cave, listed in Table 4.1 and Table 4.2. Ammonium, nitrite, bromide, and phosphate were below detection limit in all samples. These aqueous concentration data were used to evaluate potential nutrient availability and variability through time, as well as potential sources for the nutrients for SABs (e.g., natural, from geological and biogeochemical sources, or from anthropogenic activity).

Of all the measured ions, nitrate can serve as an important nutrient source. At KN14, drip water nitrate concentrations were similar through time but changed when rates slowed; nitrate concentration increased from ~2 mg/L to 6.9 mg/L at one site during a period of lower flow compared to earlier sampling times (Table 4.2). Nitrate concentrations in RN5 were lower than KN14 and did not vary significantly through time (Table 4.2). Nitrate concentrations above 3 mg/L as N or 13.3 mg/L as NO₃⁻ are consistent with literature values indicating probable contamination from anthropogenic sources, such as human waste or fertilizers (Power & Schepers, 1989), such that nearby septic tank effluent could be responsible for higher cave stream nitrate concentrations.

The DIC concentrations include dissolved CO₂, bicarbonate (HCO₃⁻), carbonate (CO₃²⁻), and carbonic acid (H₂CO₃) species. Alkalinity measures the sum of titratable bases, which is dominated by bicarbonate in karst waters; consequently, DIC and alkalinity values should be comparable (Table 4.3). Dissolved CO₂ concentrations were similar through time and demonstrated that only a small fraction of the DIC was as dissolved CO₂ at the measured pH values (Table 4.4). DIC concentrations for KN14 were slightly higher than in RN5 where DIC concentrations in drips were higher than in the cave stream (Table 4.3). $\delta^{13}\text{C}_{\text{DIC}}$ values in both caves ranged from -15.4 to -12.2‰ with a standard error of 1.1‰ between the means of sample sites and both caves (Table 4.6, Figure 4.7). Analysis of variance (ANOVA) and a Tukey's HSD post-hoc test showed no significant differences in $\delta^{13}\text{C}_{\text{DIC}}$ values between the caves (p-value > 0.05), but there was significant variation between sites within caves (Figure 4.7). For biofilms exposed to meteoric water at drip points or to the cave stream, DIC could be one of the primary sources of inorganic carbon to chemolithoautotrophs (See Chapter 2).

Differences in $\delta^{13}\text{C}_{\text{DIC}}$ values could be attributed to differences in the carbonate bedrock $\delta^{13}\text{C}$ composition. Both caves formed in geologically similar dolomitic rock, and the $\delta^{13}\text{C}$ values of carbonate rock samples for all but two sampling sites ranged from -0.54 to -2.0‰ (Table 4.5, Figure 4.8), which is consistent with other values for marine carbonates that range from -4 to +4‰ relative to PDB (Clayton & Degens, 1959). Two carbonate substrate samples from KN14 sites 1 and 4, both speleothems, had $\delta^{13}\text{C}$ values of -9.0 ± 0.32 (n = 3) and -8.9 ± 0.03 ‰ (n = 3), respectively, which are consistent with literature values for freshwater-precipitated secondary carbonates (Clayton & Degens, 1959).

Dissolved CH_4 values ranged from 0.14–0.22 $\mu\text{g/L}$ in both cave streams over two sampling dates, which corresponds to 8.7–13.7 nmol/L CH_4 (Table 4.4). Dissolved CH_4 concentrations from the two cave streams were not significantly different from each other, but both streams had concentrations that were higher than would be expected if dissolved CH_4 was in equilibrium with atmospheric CH_4 , which would be approximately 2.8 nmol/L (Table 4.4).

Drip water and stream DOC and isotope compositions

KN14 drip water had elevated DOC concentrations compared to drip water at RN5 (Table 4.3), which were more consistent with literature reports of oligotrophic conditions at 2 mg C/L DOC or less (Kaplan & Newbold, 2000). But, KN14 drip water DOC concentrations were still below what has been reported for the rare maximum concentrations of 5.0 mg C/L for limestone aquifers (Kaplan & Newbold, 2000). Considering that there is more epikarst (i.e., overburden) at RN5 than KN14, which would affect the time water takes to move through the epikarst, as well as processes like organic matter sorption to minerals and/or DOC consumption by microbes (Kaplan & Newbold, 2000), this may explain why RN5 had lower drip water DOC concentrations (Pabich et al., 2001). However, DOC concentrations are only one parameter to consider; measurements of DOC quality (i.e., biodegradability) like fluorescence are needed to understand how distance travelled through the epikarst may affect the nature of the DOC, as well as to evaluate the quality of DOC between the drip water and cave stream water (Fellman et al., 2008).

The $\delta^{13}\text{C}$ of DOC could also be used to understand the source and nature of DOC. The $\delta^{13}\text{C}_{\text{DOC}}$ values for all water samples ranged from -25.7 to -20.8‰ with a standard error of 2.1‰ between the means of sample sites across both caves (Table 4.6 and Figure 4.9). Comparison of overall $\delta^{13}\text{C}_{\text{DOC}}$ values using ANOVA and a Tukey's HSD post-hoc test revealed statistically

significant differences between caves (p-value = 0.003). Average $\delta^{13}\text{C}_{\text{DOC}}$ values in RN5 were more negative, at $-25.2 \pm 1.02\text{‰}$ (n = 3), compared to values from KN14, at $-21.4 \pm 0.56\text{‰}$ (n = 3). No statistically significant difference was found between sampling sites in cave RN5, but there was some variation in $\delta^{13}\text{C}_{\text{DOC}}$ values between sampling sites in KN14 (Figure 4.9).

Biofilm Carbon and Nitrogen Isotope Compositions

Average $\delta^{13}\text{C}_{\text{SAB}}$ values from each site for both caves ranged from $-35.3 \pm 1.1\text{‰}$ to $-46.7 \pm 0.2\text{‰}$, with 63% of the values falling below -40‰ (Table 4.7 and Figure 4.10). The lowest value recorded for all data was at RN5 site 4 ($-46.7 \pm 0.2\text{‰}$) compared to the minimum value for KN14 ($-42.6 \pm 0.2\text{‰}$). There were no statistically significant differences between $\delta^{13}\text{C}_{\text{SAB}}$ values in the two caves using a Welch's two sample t-test assuming unequal variance (p-value > 0.05). However, a Tukey's HSD post-hoc test revealed statistically similar $\delta^{13}\text{C}_{\text{SAB}}$ values between samples accounting for variation among replicates; these designations are shown in Figure 4.10. The $\delta^{13}\text{C}$ values for bedrock, DIC, DOC, and CO_2 and CH_4 from the cave air were compared to evaluate potential inorganic and organic sources for SAB communities and to determine if microbial groups in SABs produced a distinctive carbon isotope signature indicative of chemolithoautotrophy, and $\delta^{13}\text{C}_{\text{SAB}}$ values were lower than any of the other measured carbon sources (Figure 4.11).

Although the $\delta^{15}\text{N}$ values of various nitrogen-containing compounds could not be measured from the cave air, rock, or water for this study, and the $\delta^{15}\text{N}$ values of unacidified SAB biomass ($\delta^{15}\text{N}_{\text{SAB}}$) were not replicated due to low nitrogen content and insufficient material, measurements were done to evaluate if there would be potential differences in nitrogen metabolism among the SAB microbial communities. $\delta^{15}\text{N}_{\text{SAB}}$ values ranged from -6.3 to $+1.0\text{‰}$ in KN14 and -11.9 to -4.2‰ in RN5 (Table 4.7 and Figure 4.13). There were statistically significant overall differences in $\delta^{15}\text{N}_{\text{SAB}}$ values between the two caves, with generally more negative values measured in RN5, relative to atmospheric nitrogen (Welch's two-sample t-test assuming unequal variance, p-value = 0.011) (Figure 4.12). Average $\delta^{15}\text{N}_{\text{SAB}}$ values across sampling sites within each cave were $-2.4 \pm 3.1\text{‰}$ in KN14 and $-7.8 \pm 2.8\text{‰}$ in RN5 (Table 4.7 and Figure 4.12).

Microbial Community Analysis

Biofilm diversity

Alpha diversity measurements for each SAB site were determined at the genus level using Chao1, Shannon, and Simpson indices (Figure 4.14). Although Chao1 indices are used as a

measurement of richness, or the number of different genera present in the biofilm, the Shannon's index considered both richness (the number of genera) and evenness (the relative abundance of each genus). Simpson's index is considered a measure of the dominance of certain groups on a scale of 0 (no dominance) to 1 (complete dominance). Values for Shannon's diversity index across all KN14 SAB sites ranged from 2.73 (site 1) to 3.69 (site 5), and across all RN5 sites from 3.23 (site 1) to 4.09 (site 6). Simpson's index of diversity in KN14 ranged from 0.72 (site 1) to 0.91 (site 5) and from 0.85 (site 1) to 0.95 (site 2) in RN5 (Table 4.8). Comparison of alpha diversity between the two caves, as measured by Shannon and Simpson metrics, showed lower overall diversity in KN14 compared to RN5 (Welch's two sample t-test, p-value < 0.001). Chao1 indices showed higher mean genera richness in KN14 compared to RN5 (Figure 4.14). But, because the Chao1 index values ranged from 635 to 745 in KN14 and 565 to 767 in RN5 (Table 4.7), the differences were not statistically significant (Welch's two-sample t-test, p-value = 0.2111). These results demonstrate that SABs in KN14 had lower evenness due to the dominance of a few groups and lower overall population diversity (Kim et al., 2017).

Based on the average rarefied abundances of each bacterial order (Table 4.9 and Figure 4.15), SABs from KN14 were dominated by Pseudonocardiales, followed by Rhizobiales, Steroidobacteriales, and Burkholderiales, which matched what the alpha diversity analyses suggested with relatively high Simpson's indices. The overall SAB community compositions in RN5 had nearly equal abundances of Pseudonocardiales, Nitrosococcales, and Euzebyales (Table 4.8), with other abundant taxa including Burkholderiales, Rhizobiales, and Nitrospirales. Among the Pseudonocardiales, the genus *Crossiella* was abundant in both caves, and an unnamed genus within the Nitrosococcales (wb1-P19) and the genus *Euzebya* were also prevalent in both caves (Table 4.10). *Nitrospira* spp. were ubiquitous in low abundances across all sites in both caves, and an unclassified genus belonging to the Rhizobiales family Methyloligellaceae was the most abundant putative methylotroph across both caves (Table 4.10).

Despite the overall similarity in bacterial groups at the order levels, PERMANOVA analyses indicated that the community compositions in both caves at the genus level were significantly different, with 84.1% of the variance in the data explained by differences inherent to each cave ($R^2 = 0.841$, p-value = 0.005). This is represented graphically as a PCoA of all the SAB samples (Figure 4.16). Significant differences were also found between sites within each cave

based on the PERMANOVA (KN14 p-value < 0.001; RN5 p-value < 0.001). Collectively, these results suggest that SAB communities from the same cave were more similar to each other than between SABs in the other cave, but that SAB communities also significantly differed among sampling sites in both caves.

Community composition and environmental variables

Because moisture content and temperature differed between the two caves, covariation between these variables, as well as biofilm color and carbon isotope composition, with community composition were investigated using various statistical analyses, as outlined in Chapter 3. According to PERMANOVA, temperature and biofilm color could not explain differences in SAB community composition, but moisture content could (p-value = 0.011) (Table 4.11). However, DCA of all SAB communities across both caves did not confirm significance among $\delta^{13}\text{C}$ values and community composition, despite a significant relationship indicated in the PERMANOVA test (p-value = 0.270). The DCA suggested a strong relationship between community composition and moisture content (Table 4.12 and Figure 4.16), although this was also supported by a Mantel test suggesting temperature and community composition correlated (p-value < 0.05; Table 4.12). Upon further analysis, Mantel tests using a moisture dissimilarity matrix revealed a significant correlation between community composition and moisture in KN14 but not RN5, and that temperature was not a significant predictor of community composition across sites in either cave (p-value > 0.05). Pearson's product moment correlations using the relative abundances of the top 20 most abundant orders (Table 4.14 and Table 4.15 for KN14 and RN5, respectively) suggested there were significant negative correlations between moisture and relative abundances for Azospirillales, Steroidobacteriales, Pseudonocardiales, Sphingomonadales, and Rhizobiales (i.e., as moisture increased, relative abundances of taxa decreased), but positive correlations for Burkholderiales and Nitrosococcales (i.e., as moisture increased, relative abundances of taxa increased).

PERMANOVA and DCA were used to evaluate community composition and other variables separately within KN14 (Table 4.16 and Table 4.17) and for RN5 (Table 4.18, Table 4.19, and Figure 4.18). Although covariate interactions among each of these variables were evident, significant interactions were noted for KN14 between $\delta^{13}\text{C}$ value and biofilm color (p-value = 0.003), moisture (p-value = 0.038), and temperature (p-value = 0.044), as well as between

biofilm color and temperature (p-value = 0.001) and temperature and moisture (p-value = 0.001) (Table 4.17 and Table 4.16). For RN5, there were significant interactions between community composition and $\delta^{13}\text{C}$ values, percent moisture, and biofilm color, as well as between percent moisture and biofilm color. The DCA model for RN5 showed statistically significant correlations among microbial community composition and moisture content and $\delta^{13}\text{C}$ value (Table 4.18 and Table 4.19), but only moisture, not $\delta^{13}\text{C}$ value, was found to significantly correlate to microbial community composition in KN14 (Table 4.16 and Table 4.17). According to DCA, SAB carbon isotope compositions in RN5 explained 56.1% of variance and moisture content explained 28.8% (Table 4.19 and Figure 4.18), while moisture content explained 73.6% of the variance in microbial community composition for KN14 (Table 4.16 and Figure 4.18).

For KN14, SAB color (i.e., white or yellow) could explain 34.3% of the total variance within communities using PERMANOVA tests, although color covaried with percent moisture (30.3%). When both biofilm color and moisture content were included in the same model, color only accounted for 17.4% of variance. Collectively, these results support past research that specific taxa have distinct colony colors (Lavoie et al., 2017), and contrast other research that found no significant difference in community composition based on biofilm color (Hathaway et al., 2014). Although interactions among these variables likely complicate their interpretation, it is possible that community composition and color may be significantly linked to moisture content.

Correlations between taxa and SAB isotope compositions

Bulk $\delta^{13}\text{C}_{\text{SAB}}$ values significantly correlated to community composition in RN5 but not in KN14. Negative correlations between the relative abundances of specific taxa and $\delta^{13}\text{C}_{\text{SAB}}$ values (i.e., taxon abundance increases with lower $\delta^{13}\text{C}$ values) could indicate that those taxa may be responsible for generating those carbon isotope signatures, for example, via chemolithoautotrophic carbon fixation (Table 4.14 and Table 4.15) (See Chapter 5). In KN14, negative correlations between taxon abundance and $\delta^{13}\text{C}$ values were found for Blastocatellia family 11-24_fa, Hyphomicrobiaceae, Rhizobiaceae, and Reyraneliaceae. These taxa were more abundant in SABs with lower $\delta^{13}\text{C}_{\text{SAB}}$ values, and their abundances significantly correlated with changes in $\delta^{13}\text{C}_{\text{SAB}}$ values (Table 4.14 and Table 4.15). Of these families, the 11-24_fa and Rhizobiaceae also correlated positively with moisture content. Nitrosococcaceae also negatively correlated with $\delta^{13}\text{C}_{\text{SAB}}$ values, but this was not statistically significant, possibly due to covariance with moisture.

For RN5, taxa that negatively correlated to $\delta^{13}\text{C}_{\text{SAB}}$ values included Euzebyaceae, Nitrosomonadaceae, unclassified Rhizobiales, Beijerinckiaceae, and Anaerolineaceae. Nitrosomonadaceae also positively correlated to moisture content. For instance, Nitrosococcaceae dominated several SABs, ranging from 5.5 to 22% relative abundances for RN5 sites. Nitrosomonadaceae ranged from 0.43 and 2.3% of all bacterial 16S rRNA sequences in this study across both caves and also have conserved putative function as chemolithoautotrophic ammonia oxidizers (Alfreider et al., 2018). Although these families both correlated significantly with moisture content, and *Nitrosomonas* abundance correlated significantly with carbon isotope composition in RN5 only, the relationship between the more abundant Nitrosococcaceae and $\delta^{13}\text{C}_{\text{SAB}}$ values was not statistically significant (Table 4.11). In addition, Pseudonocardiaceae also positively correlated with $\delta^{13}\text{C}_{\text{SAB}}$ values in RN5 but not in KN14 (Table 4.11 and Table 4.12). However, due to significant covariance of this family with moisture, covariate interactions between the two variables may complicate interpretation of these results.

Several families negatively correlated to bulk $\delta^{15}\text{N}_{\text{SAB}}$ values, including Beijerinckiaceae, Inquilinaceae (order Azospirillales), Xanthomonadaceae, and Rhizobiales incertae sedis (Table 4.14 and Table 4.15). At the family level, Beijerinckiaceae are associated with aerobic N_2 fixation and some members can also perform methylotrophy and methanotrophy (Marín & Arahal, 2014). Close relatives to unclassified Beijerinckiaceae and unclassified members of Rhizobiaceae and Hyphomicrobiaceae had low relative abundances but were ubiquitous in all samples and negatively correlated to $\delta^{15}\text{N}_{\text{SAB}}$ values (KN14 $r = -0.8$, RN5 $r = -0.4$), although the Rhizobiaceae and Hyphomicrobiaceae also negatively correlated with $\delta^{13}\text{C}_{\text{SAB}}$ values. The Hyphomicrobiaceae identified in this study were mainly comprised of close relatives to the genus *Hyphomicrobium*, which are generally aerobic chemoorganoheterotrophs that grow in oligotrophic conditions and on C1 compounds, including methanol (Oren et al., 2014). The families Xanthomonadaceae and Rhizobiaceae, and members of the Azospirillales, contain taxa that are known to be free-living diazotrophs (Steenhoudt, & Vanderleyden, 2000; Desgarences et al., 2014).

In reality, the presence of any observable correlation between microbial community composition and $\delta^{13}\text{C}$ depends on (i) proportionality between the amount of isotopically light carbon derived from the metabolism of certain groups and their abundance in a SAB, and (ii) the abundance of 16S rRNA sequences that accurately reflect the activity and contribution of taxa to

community metabolism. Because these assumptions may not be true, interpretation of correlations are presented here with caution.

Table 4.1: Ambient environmental conditions at each cave SAB cave wall sampling site on the day of biofilm sampling (February 1 or 2, 2020).

Cave ID	Site ID	Vertical dist. from stream (m)	Temp (°C)	% Moisture (pad)
KN14	1	0.9	9.7	44.8
	2	0.95	9.9	19.9
	3	1.05	9.8	55.5
	4	2.15	10.5	19.0
	5	1.5	10.1	73.9
	6	2.35	11.2	84.0
RN5	1	0.2	13.8	100
	2	0.98	14.0	62.6
	3	0.98	13.9	72.9
	4	1.23	14.0	89.7
	5	1.85	13.8	99.9
	6	5.0+	13.0	88.7

Table 4.2 Environmental data collected over time in drip locations and cave streams of both caves, including pH, temperature, and measurable anion concentrations.

Date	Analyte	KN14			RN5		
		drip 1	drip 2	stream	drip 1	drip 2	stream
2/2/2020	pH	8.06	8.23	7.34	8.06	NA ¹	7.26
	Temp. (°C)	10.6	10.8	13.4	15.7	NA	14.4
	Cl ⁻ (mg/L)	0.64	0.58	3.94	1.20	0.91	2.35
	SO ₄ ²⁻ (mg/L)	5.09	4.74	4.19	1.85	5.69	1.52
	NO ₃ ⁻ (mg/L)	1.30	2.07	6.18	1.10	1.89	4.33
	Na ⁺ (mg/L)	3.98	2.36	5.38	2.43	4.14	3.08
	K ⁺ (mg/L)	1.36	0.19	0.95	0.05	BDL ²	0.32
	Mg ²⁺ (mg/L)	16.23	13.12	18.66	21.28	22.99	16.51
	Ca ²⁺ (mg/L)	47.03	49.70	48.56	30.04	36.29	31.61
3/19/2020	Analyte	drip 1	drip 2	stream	drip 1	drip 2	stream
	pH	7.89	7.64	7.23	7.65	8.04	7.05
	Temp. (°C)	13.5	13.9	13.9	14.0	14.3	14.4
	Cl ⁻ (mg/L)	0.54	0.51	3.93	1.19	0.67	2.02
	SO ₄ ²⁻ (mg/L)	4.46	4.42	4.02	1.02	3.83	1.46
	NO ₃ ⁻ (mg/L)	1.22	1.74	5.42	0.64	0.73	3.29
	Na ⁺ (mg/L)	2.15	1.23	2.42	1.33	1.20	3.17
	K ⁺ (mg/L)	1.29	0.21	0.88	0.05	BDL	0.25
	Mg ²⁺ (mg/L)	16.78	14.63	18.58	21.78	22.25	14.18
	Ca ²⁺ (mg/L)	50.96	54.33	47.94	31.67	35.79	27.51
5/16/2020	Analyte	drip 1	drip 2	stream	drip 1	drip 2	stream
	pH	7.71	7.83	7.31	8.02	8.37	7.23
	Temp. (°C)	14.4	14.6	14.9	14.7	15.0	14.5
	Cl ⁻ (mg/L)	0.78	0.75	3.97	1.39	1.17	2.40
	SO ₄ ²⁻ (mg/L)	6.74	4.91	4.54	1.50	4.12	2.07
	NO ₃ ⁻ (mg/L)	1.40	6.86	5.68	0.97	2.06	4.22
	Na ⁺ (mg/L)	3.49	2.07	5.19	4.33	3.20	4.66
	K ⁺ (mg/L)	0.53	1.38	0.96	0.12	BDL	0.41
	Ca ²⁺ (mg/L)	53.65	43.31	45.89	28.55	29.36	33.92

¹ BDL = below detection limit

Table 4.3: DIC and DOC concentrations in drip water and cave streams measured on 5/20/2020 (n = 3). Alkalinity data from previous analysis (on 19 June 2019) was used to validate DIC concentrations.

Water source ID	Associated SAB site ID	DIC (mg CO₃/L)	Alkalinity (mg CO₃/L)	DOC (mg C/L)
KN14 drip 1	KN14 site 4	256.5	-	4.75
KN14 drip 2	KN14 site 5	254.0	-	4.66
KN14 stream	KN14 sites 1–3	260.1	255.2	3.71
RN5 drip 1	RN5 site 5	218.4	-	1.34
RN5 drip 2	RN5 site 6	222.3	-	2.72
RN5 stream	RN5 site 1	196.2	192.6	2.32

Table 4.4: Dissolved CO₂ and CH₄ concentrations in cave streams measured in triplicate on two dates (n = 3).

Water source ID	Date	Associated SAB site ID	Dissolved CO₂ (mg/L)	Dissolved CH₄ (µg/L)
KN14 stream	02/02/2020	KN14 1–3	6.05	0.22
	03/19/2020	KN14 1–3	8.18	0.14
RN5 stream	02/02/2020	RN5 site 1	5.47	0.17
	03/19/2020	RN5 site 1	8.84	0.14

Table 4.5: Averaged $\delta^{13}\text{C}$ values and standard deviations of carbonates ($\delta^{13}\text{C}_{\text{CaCO}_3}$) from each sampling site. Technical replicates ($n = 3$) consisted of homogenized material from the same site. $\delta^{13}\text{C}_{\text{CaCO}_3}$ values are given relative to the PDB standard. NA denotes sites where substrate was collected but did not contain carbonate (e.g., clay for KN14–3 and RN5–1 or chert for RN5–4) and $\delta^{13}\text{C}_{\text{CaCO}_3}$ could not be measured.

SAB site ID	$\delta^{13}\text{C}_{\text{CaCO}_3}$
KN14 1	-9.03 ± 0.32
KN14 2	-0.59 ± 0.07
KN14 3	NA
KN14 4	-8.88 ± 0.03
KN14 5	-0.70 ± 0.03
KN14 6	-1.21 ± 0.01
RN5 1	NA
RN5 2	-1.51 ± 0.03
RN5 3	-1.58 ± 0.04
RN5 4	NA
RN5 5	-1.99 ± 0.03
RN5 6	-1.88 ± 0.02

Table 4.6: Averaged $\delta^{13}\text{C}$ values and standard deviations (replicates $n = 3$) measured for DIC, CO_2 , and CH_4 in cave air, and DOC, all reported as per mil (‰) relative to the PDB standard.

Water collection site	$\delta^{13}\text{C}_{\text{DIC}}$	$\delta^{13}\text{C}_{\text{CO}_2}$	$\delta^{13}\text{C}_{\text{CH}_4}$	$\delta^{13}\text{C}_{\text{DOC}}$
KN14 drip 1	-13.03 ± 0.02	-	-	-22.50 ± 0.73
KN14 drip 2	-15.24 ± 0.004	-	-	-20.75 ± 0.91
KN14 stream	-14.16 ± 0.16	-	-	-21.19 ± 0.59
Cave air KN14	-	-14.00 ± 0.40	-43.44 ± 0.05	-
Outside air KN14	-	-10.07 ± 0.36	-44.34 ± 0.24	-
RN5 drip 1	-13.95 ± 0.03	-	-	-24.92 ± 0.66
RN5 drip 2	-14.20 ± 0.04	-	-	-25.66 ± 0.24
RN5 stream	-15.63 ± 0.04	-	-	-24.87 ± 0.40
Cave air RN5	-	-19.40 ± 0.39	-42.93 ± 0.42	-
Outside air RN5	-	-9.34 ± 0.34	-44.81 ± 0.17	-

Table 4.7: Averaged bulk $\delta^{13}\text{C}$ values ($n = 3$) and standard deviations of homogenized SAB samples ($\delta^{13}\text{C}_{\text{SAB}}$) from each site, as well as bulk $\delta^{15}\text{N}$ values ($n = 1$). $\delta^{13}\text{C}$ and $\delta^{15}\text{N}$ values are given relative to PDB and air- N_2 , respectively. See Chapter 3 for details about the methods.

SAB site ID	$\delta^{13}\text{C}_{\text{SAB}}$	$\delta^{15}\text{N}_{\text{SAB}}$
KN14 1	-42.45 ± 0.58	-1.02
KN14 2	-40.56 ± 0.19	-5.98
KN14 3	-41.83 ± 0.35	+0.22
KN14 4	-38.30 ± 1.18	-2.55
KN14 5	-42.65 ± 0.16	-6.25
KN14 6	-35.31 ± 1.08	+1.01
RN5 1	-44.89 ± 0.50	-4.19
RN5 2	-38.07 ± 0.43	-6.09
RN5 3	-44.85 ± 0.51	-9.50
RN5 4	-46.70 ± 0.17	-8.53
RN5 5	-42.68 ± 0.57	-6.32
RN5 6	-36.10 ± 0.31	-11.88

Table 4.8: Average alpha diversity measurements at the genus level across SAB sampling sites in both caves. Field replicate sequence counts were averaged (n = 4).

Cave ID	KN14						RN5					
Site	1	2	3	4	5	6	1	2	3	4	5	6
Chao1	745.7	680.9	682.4	723.2	635.0	778.8	733.0	587.8	571.2	565.1	627.1	767.2
Shannon	2.73	3.09	2.84	2.83	3.69	3.29	3.23	4.06	3.85	3.70	3.94	4.09
Simpson	0.72	0.81	0.75	0.73	0.91	0.82	0.85	0.95	0.93	0.93	0.94	0.94

Table 4.9: Average relative abundances of taxa by order in each cave (KN14 and RN5). Abundances for each replicate and across cave sampling sites were averaged to summarize abundant taxa in each cave.

KN14 Order	Avg. % Abundance	RN5 Order	Avg. % Abundance
Pseudonocardiales	44.21	Pseudonocardiales	13.71
Rhizobiales	6.80	Nitrosococcales	13.55
Steroidobacterales	4.23	Euzebyales	13.08
Burkholderiales	3.63	Burkholderiales	5.59
SBR1031	3.51	Bacteria_unclassified	4.40
11-24	3.04	Rhizobiales	4.12
Solirubrobacterales	2.36	Nitrospirales	3.13
Nitrospirales	2.19	Gammaproteobacteria_unclassified	2.74
Gemmatales	2.00	Gemmatales	2.02
Azospirillales	1.97	Alphaproteobacteria_unclassified	1.66
Xanthomonadales	1.61	11-24	1.63
Bacteria_unclassified	1.57	bacteriap25_or	1.60
Sphingomonadales	1.44	PLTA13	1.46
Gemmatimonadales	1.30	Chitinophagales	1.32
Alphaproteobacteria_unclassified	1.10	Pirellulales	1.22
Steroidobacterales	1.04	Steroidobacterales	0.97

Table 4.10: Average relative abundance of genera across all sampling sites in both caves. Genera with relative abundance greater than 0.15% are shown.

Genus	KN14.1.avg	KN14.2.avg	KN14.3.avg	KN14.4.avg	KN14.5.avg	KN14.6.avg	RN5.1.avg	RN5.2.avg	RN5.3.avg	RN5.4.avg	RN5.5.avg	RN5.6.avg
<i>Crossiella</i>	52.34	42.10	49.05	51.15	27.08	41.00	1.00	16.81	15.42	14.49	14.95	17.89
wb1-P19	0.08	0.07	0.09	0.08	0.07	0.15	21.30	5.93	13.50	12.02	14.07	14.26
<i>Euzebya</i>	0.21	0.20	0.20	0.24	0.16	0.16	30.73	0.00	0.01	15.61	0.00	0.44
Bacteria_unclassified	1.10	1.09	1.51	0.62	1.95	3.09	2.17	4.01	5.23	4.30	6.98	3.67
<i>Nitrospira</i>	1.89	0.84	2.43	1.13	2.66	4.28	3.78	6.04	2.54	1.32	3.48	1.67
Euzebyaceae_unclassified	0.00	0.00	0.00	0.00	0.00	0.00	4.90	0.26	13.81	8.21	3.23	1.39
11-24_ge	5.99	0.33	4.80	0.27	5.29	1.58	1.31	3.63	1.17	1.24	1.29	1.21
<i>Steroidobacter</i>	1.95	5.32	2.45	2.79	6.34	3.55	0.71	1.19	0.86	0.51	0.10	2.13
A4b_ge	4.11	0.91	5.41	0.36	4.56	5.34	0.67	1.30	0.56	0.35	0.23	0.68
Gammaproteobacteria_unclassified	1.08	0.25	0.18	0.52	0.96	0.34	0.67	0.97	1.77	2.39	7.34	3.30
uncultured	1.22	0.91	1.91	0.53	2.45	2.02	0.67	2.81	1.03	1.24	1.26	1.95
Alphaproteobacteria_unclassified	0.29	0.65	0.75	0.37	3.71	0.81	1.79	3.13	1.33	1.47	1.20	1.09
Comamonadaceae_unclassified	2.49	0.62	1.81	0.33	2.43	1.45	0.94	0.71	0.44	0.40	0.45	0.74
<i>Inquilinus</i>	0.06	6.40	0.06	5.19	0.06	0.04	0.04	0.21	0.00	0.04	0.00	0.43
PLTA13_ge	0.18	0.76	0.42	0.83	0.83	0.27	1.25	1.31	1.61	2.17	1.66	0.89
uncultured	1.43	1.87	0.93	1.08	1.27	2.35	0.28	0.06	0.47	0.39	0.31	0.85
bacteriap25_ge	0.13	0.40	0.31	0.14	0.29	0.20	0.29	1.58	2.47	1.39	2.61	1.23
NB1-j_ge	0.52	0.09	2.45	0.09	0.73	0.78	1.11	1.41	0.68	0.61	0.82	0.52
uncultured	0.20	1.92	0.33	1.46	0.64	1.01	0.40	0.33	0.81	0.43	0.78	0.83
SWB02	0.40	0.61	1.26	0.19	1.35	0.69	1.17	1.32	0.57	0.41	0.20	0.80
Methyloligellaceae_ge	0.26	0.26	0.27	0.98	0.82	0.30	0.16	0.42	0.55	0.92	0.38	3.10
<i>Luteimonas</i>	0.69	3.30	0.19	3.05	0.69	0.12	0.04	0.00	0.05	0.02	0.01	0.03
Xanthobacteraceae_unclassified	0.15	2.05	0.03	2.75	0.29	0.23	0.06	1.44	0.15	0.20	0.07	0.48
Burkholderiales_unclassified	0.23	0.28	0.15	0.23	0.73	0.46	0.74	1.22	1.03	0.79	1.03	0.94
<i>Terrimonas</i>	0.14	1.33	0.06	0.55	0.11	0.24	0.85	1.60	0.78	0.66	0.81	0.56
B1-7BS_ge	0.00	0.00	0.07	0.00	0.00	0.00	0.25	1.30	1.52	0.96	2.84	0.57
uncultured	0.07	0.15	0.13	0.23	0.28	0.14	0.16	2.44	0.67	0.74	0.72	0.93
<i>Hyphomicrobium</i>	0.83	0.46	0.73	0.60	0.93	0.38	0.17	1.33	0.27	0.39	0.30	0.24
<i>Sphingomonas</i>	0.38	3.09	0.25	0.64	0.63	0.44	0.27	0.01	0.06	0.01	0.03	0.71
uncultured_ge	0.32	1.02	0.18	0.80	0.89	1.15	0.02	0.14	0.10	0.18	0.29	1.15
MND1	0.50	0.35	0.21	0.17	0.29	0.85	0.40	0.25	0.68	0.68	1.25	0.38
RB41	0.32	1.06	0.13	0.38	0.59	0.72	0.66	0.26	0.08	0.05	0.27	1.40
<i>Haliangium</i>	0.29	0.63	0.19	0.46	0.53	0.40	0.34	0.35	0.52	0.72	0.67	0.63

Table 4.10 continued

Genus	KN14 .1.avg	KN14 .2.avg	KN14 .3.avg	KN14 .4.avg	KN14 .5.avg	KN14 .6.avg	RN5. 1.avg	RN5. 2.avg	RN5. 3.avg	RN5. 4.avg	RN5. 5.avg	RN5. 6.avg
Vicinamibacter- aceae_ge	0.46	0.59	0.37	0.27	0.48	1.21	0.36	0.85	0.43	0.38	0.19	0.62
Blastocatell- aceae _unclassified	0.87	0.28	0.18	0.24	0.98	0.74	0.22	0.49	0.21	0.24	0.28	1.05
<i>Pedomicrobium</i>	0.57	0.45	1.03	0.42	1.28	0.52	0.11	0.52	0.13	0.13	0.12	0.40
67-14_ge	0.12	0.34	0.05	0.93	2.26	0.23	0.03	0.06	0.06	0.07	0.06	1.36
<i>Nordella</i>	0.28	0.79	0.41	0.60	1.13	0.45	0.19	0.25	0.32	0.30	0.16	0.53
OM190_ge	0.15	0.25	0.36	0.15	0.34	0.40	0.74	0.45	0.62	0.58	0.75	0.47
uncultured	1.02	0.05	1.56	0.10	1.36	0.05	0.21	0.04	0.10	0.16	0.08	0.22
Hyphomicrobia- ceae_unclass- ified	0.35	0.56	0.33	0.26	0.67	0.33	0.14	0.98	0.15	0.20	0.16	0.79
Rhizobiaceae _unclassified	1.38	0.32	0.37	0.20	1.66	0.55	0.07	0.09	0.03	0.05	0.01	0.09
IMCC26256_ge	0.02	0.15	0.03	0.51	0.08	0.05	0.15	0.87	1.20	0.93	0.21	0.61
uncultured	0.53	0.14	0.54	0.13	0.23	0.32	0.27	0.54	0.64	0.39	0.45	0.60
Subgroup_2_ge	0.06	0.00	0.03	0.01	0.05	0.11	0.19	3.14	0.61	0.16	0.39	0.02
TRA3-20_ge	0.26	0.18	0.41	0.10	0.17	0.60	0.88	0.32	0.54	0.29	0.69	0.14
Gemmataceae _unclassified	0.23	0.15	0.46	0.13	0.42	0.36	0.18	0.61	0.38	0.21	0.48	0.70
uncultured	0.03	0.09	0.03	2.30	1.55	0.10	0.01	0.00	0.00	0.00	0.00	0.00
CCM11a_ge	0.23	0.22	0.24	0.07	0.17	0.26	0.26	0.96	0.38	0.31	0.55	0.38
<i>Pirellula</i>	0.27	0.09	0.65	0.05	0.30	0.23	0.28	1.18	0.32	0.20	0.16	0.26
<i>Pseudonocardia</i>	0.74	0.27	0.56	0.28	0.26	0.36	0.03	0.08	0.23	0.17	0.06	0.79
uncultured_ge	0.13	0.18	0.30	0.10	0.35	0.24	0.18	0.65	0.32	0.19	0.31	0.60
<i>Gaiella</i>	0.36	0.35	0.17	0.38	0.18	0.36	0.05	0.34	0.16	0.23	0.11	0.81
Latescibacter- ota_ge	0.06	0.01	0.33	0.04	0.18	0.49	0.28	0.18	0.55	0.35	0.74	0.24
Gemmati- monadaceae_ _unclassified	0.14	0.31	0.19	0.16	0.29	1.03	0.12	0.12	0.08	0.09	0.18	0.49
<i>Conexibacter</i>	0.06	0.94	0.05	0.48	1.00	0.21	0.01	0.00	0.09	0.11	0.12	0.12
Subgroup_17_ _ge	0.16	0.08	0.16	0.03	0.20	0.32	0.19	0.32	0.47	0.65	0.43	0.11
<i>Panacagri- monas</i>	0.58	0.97	0.30	0.23	0.30	0.41	0.09	0.08	0.01	0.01	0.01	0.02
Sphingomonad- aceae_ _unclassified	0.64	0.38	0.15	0.45	0.18	0.13	0.40	0.13	0.18	0.11	0.07	0.17
Planctomycet- ota _unclassified	0.02	0.02	0.03	0.05	0.14	0.04	0.20	0.69	0.46	0.35	0.75	0.25
Subgroup_10	0.27	0.42	0.17	0.25	0.62	0.31	0.14	0.02	0.22	0.17	0.11	0.28
Steroidobacter- aceae_ _unclassified	0.04	1.33	0.04	1.19	0.08	0.04	0.02	0.01	0.01	0.00	0.00	0.02
<i>Parcubacteria</i> _unclassified	0.08	0.01	0.11	0.02	0.07	0.04	0.19	0.12	0.26	1.20	0.62	0.07
uncultured	0.08	0.13	0.38	0.03	0.13	0.03	0.51	0.36	0.24	0.43	0.39	0.05

Table 4.10 continued

Genus	KN14 .1.avg	KN14 .2.avg	KN14 .3.avg	KN14 .4.avg	KN14 .5.avg	KN14 .6.avg	RN5. 1.avg	RN5. 2.avg	RN5. 3.avg	RN5. 4.avg	RN5. 5.avg	RN5. 6.avg
SM1A02	0.06	0.04	0.11	0.03	0.06	0.09	0.20	1.39	0.21	0.17	0.20	0.15
RBG-13-54-9_ge	0.01	0.05	0.01	0.08	0.05	0.09	0.10	0.23	0.75	0.34	0.75	0.23
Actinobacteria_unclassified	0.10	0.06	0.08	0.23	0.06	0.11	0.10	0.02	0.36	0.32	0.22	0.89
uncultured_ge	0.67	0.13	0.34	0.06	0.45	0.34	0.15	0.09	0.07	0.03	0.06	0.08
mle1-7	0.04	0.24	0.09	0.08	0.14	0.04	0.29	0.54	0.34	0.30	0.24	0.08
Pla4_lineage_ge	0.05	0.03	0.06	0.02	0.07	0.05	0.22	0.19	0.44	0.41	0.57	0.21
Subgroup_22_ge	0.05	0.02	0.06	0.02	0.20	0.10	0.16	0.18	0.38	0.19	0.73	0.20
Pirellulaceae_unclassified	0.08	0.16	0.09	0.10	0.15	0.22	0.10	0.34	0.20	0.13	0.24	0.45
uncultured_ge	0.07	0.16	0.13	0.14	0.14	0.40	0.16	0.08	0.19	0.09	0.21	0.49
Rokubacteriales_ge	0.05	0.07	0.07	0.03	0.15	0.15	0.16	0.50	0.23	0.16	0.32	0.32
Subgroup_7_ge	0.15	0.31	0.03	0.31	0.22	0.38	0.05	0.17	0.05	0.04	0.06	0.39
Rhizobiales_unclassified	0.09	0.09	0.04	0.06	0.12	0.18	0.39	0.10	0.40	0.35	0.15	0.20
Chloroflexi_unclassified	0.06	0.01	0.22	0.03	0.25	0.08	0.09	0.47	0.33	0.23	0.18	0.21
A0839_ge	0.02	0.03	0.18	0.04	0.13	0.03	0.27	0.44	0.42	0.26	0.18	0.06
Solirubrobacter	0.02	0.47	0.01	1.00	0.08	0.17	0.01	0.00	0.00	0.00	0.00	0.22
MB-A2-108_ge	0.08	0.09	0.09	0.32	0.04	0.31	0.01	0.04	0.08	0.10	0.54	0.28
IS-44	0.19	0.20	0.18	0.09	0.37	0.45	0.33	0.05	0.02	0.02	0.06	0.00
uncultured_ge	0.05	0.04	0.18	0.04	0.07	0.05	0.39	0.39	0.10	0.46	0.13	0.08
SC-I-84_ge	0.07	0.29	0.05	0.32	0.20	0.45	0.04	0.06	0.09	0.03	0.11	0.22
Acidibacter	0.10	0.22	0.29	0.16	0.30	0.10	0.08	0.04	0.07	0.11	0.08	0.22
Pedosphaeraceae_unclassified	0.13	0.12	0.14	0.06	0.13	0.17	0.20	0.08	0.21	0.11	0.27	0.12
Dongia	0.08	0.05	0.28	0.06	0.11	0.19	0.10	0.26	0.11	0.17	0.02	0.29
uncultured_ge	0.03	0.11	0.07	0.08	0.13	0.01	0.21	0.34	0.18	0.21	0.27	0.11
Omnitrophales_ge	0.01	0.01	0.05	0.01	0.01	0.04	0.12	0.05	0.54	0.27	0.59	0.03
JG30-KF-CM45_ge	0.14	0.37	0.12	0.27	0.37	0.11	0.03	0.07	0.03	0.04	0.01	0.13
MBNT15_ge	0.07	0.09	0.11	0.03	0.22	0.03	0.27	0.31	0.14	0.11	0.16	0.16
AKYG587	0.01	0.04	0.13	0.11	0.09	0.02	0.17	0.57	0.07	0.02	0.05	0.42
Bacteroidia_unclassified	0.04	0.12	0.04	0.12	0.10	0.14	0.21	0.13	0.18	0.16	0.29	0.11
uncultured_ge	0.00	0.00	0.00	0.00	0.00	0.00	0.09	1.33	0.03	0.01	0.12	0.02
WD2101_soil_group_ge	0.08	0.21	0.03	0.07	0.04	0.07	0.12	0.47	0.19	0.01	0.05	0.26
Obscuribacteraceae_ge	0.00	0.01	0.03	0.01	0.02	0.01	0.15	0.73	0.21	0.18	0.17	0.06
KD4-96_ge	0.17	0.13	0.12	0.16	0.16	0.48	0.02	0.02	0.06	0.07	0.04	0.15
JGI_0001001-H03	0.08	0.04	0.02	0.06	0.03	0.16	0.29	0.01	0.18	0.16	0.26	0.28
Gemmata	0.30	0.14	0.15	0.07	0.14	0.20	0.06	0.25	0.01	0.03	0.02	0.15

Table 4.10 continued

Genus	KN14 .1.avg	KN14 .2.avg	KN14 .3.avg	KN14 .4.avg	KN14 .5.avg	KN14 .6.avg	RN5. 1.avg	RN5. 2.avg	RN5. 3.avg	RN5. 4.avg	RN5. 5.avg	RN5. 6.avg
<i>Acidobacteriae_unclassified</i>	0.02	0.01	0.03	0.01	0.09	0.02	0.04	0.79	0.08	0.04	0.09	0.13
<i>Dadabacteriales_ge</i>	0.00	0.00	0.01	0.00	0.00	0.00	0.18	0.57	0.21	0.13	0.27	0.01
<i>Beijerinckiaceae_unclassified</i>	0.06	0.13	0.02	0.09	0.18	0.05	0.03	0.03	0.23	0.42	0.08	0.09
<i>Rhodanobacteraceae_unclassified</i>	0.08	0.01	0.71	0.01	0.18	0.06	0.13	0.01	0.04	0.07	0.09	0.03
<i>Candidatus_Omnitrophus</i>	0.04	0.01	0.07	0.01	0.04	0.04	0.10	0.15	0.20	0.21	0.52	0.09
<i>KF-JG30-C25_ge</i>	0.00	0.01	0.00	0.00	0.02	0.36	0.02	0.10	0.20	0.35	0.27	0.03
<i>Pajaroellobacter</i>	0.08	0.04	0.09	0.03	0.53	0.05	0.04	0.06	0.09	0.13	0.09	0.10
<i>SJA-28_ge</i>	0.00	0.01	0.00	0.02	0.05	0.01	0.04	0.07	0.59	0.27	0.18	0.07
<i>Reyranella</i>	0.11	0.21	0.28	0.08	0.16	0.03	0.05	0.11	0.05	0.08	0.05	0.09
<i>Pla3_lineage_ge</i>	0.02	0.02	0.04	0.01	0.08	0.08	0.14	0.40	0.14	0.10	0.16	0.12
<i>Ellin6067</i>	0.10	0.05	0.06	0.04	0.18	0.11	0.11	0.15	0.10	0.16	0.11	0.10
<i>Phycisphaerae_unclassified</i>	0.00	0.00	0.00	0.01	0.02	0.01	0.10	0.67	0.11	0.05	0.15	0.10
<i>Bryobacter</i>	0.08	0.08	0.11	0.05	0.09	0.16	0.16	0.09	0.12	0.06	0.05	0.17
<i>Pedosphaeraeaceae_ge</i>	0.05	0.09	0.25	0.05	0.07	0.14	0.13	0.08	0.13	0.04	0.09	0.09

Table 4.11: Results of PERMANOVA models that included $\delta^{13}\text{C}$, moisture content, cave ID, temperature, and biofilm color as explanatory variables for microbial community composition across both caves. Statistical significance is indicated by bold-font for p-values below an alpha value of 0.05.

Predictor Variable (z-score transformed)	F.Model	R ²	p-value
$\delta^{13}\text{C}_{\text{SAB}}$	4.768	0.161	0.014
% moisture	9.330	0.315	0.039
Cave ID	6.355	0.060	0.856
Temperature	0.560	0.019	0.853
Biofilm color	4.098	0.276	0.356

Table 4.12: Results of the DCA model that included predictors for SAB community composition across both caves. Statistical significance is indicated by bold-font for p-values below an alpha value of 0.05.

Both Caves Variables	DCA1	DCA2	R ²	p-value
$\delta^{13}\text{C}_{\text{SAB}}$	-0.952	0.305	0.256	0.268
Moisture content	0.985	0.174	0.638	0.001

Table 4.13: Mantel test results for Pearson's's product moment correlation between SAB microbial community and (i) temperature and (ii) moisture content between caves and between sites within each cave. Statistical significance is indicated by bold-font for p-values below an alpha value of 0.05.

Predictor Variable	Microbial Community	Mantel statistic r	p-value
Temperature	Between caves	0.7278	0.001
Temperature	Within RN5	-0.1641	0.561
Temperature	Within KN14	-0.4365	0.976
% Moisture	Between caves	0.4522	0.004
% Moisture	Within RN5	0.2429	0.210
% Moisture	Within KN14	0.5536	0.032

Table 4.14: KN14 Pearson’s correlation results showing the relationship between substrate moisture, $\delta^{13}\text{C}$ and $\delta^{15}\text{N}$, and taxa abundance. Statistical significance is indicated by bold-font for p-values below an alpha value of 0.05.

KN14 Family	percent moisture correlation	r	p-value	$\delta^{13}\text{C}$ correlation	r	p-value	$\delta^{15}\text{N}$ correlation	r	p-value
Pseudonocardiaceae	–	-0.42	0.027	NA	0.11	0.576	+	0.55	0.003
(Blastocatellia) 11-24_fa	+	0.49	0.009	–	-0.67	0	NA	0.14	0.498
(Aerolineae) A4b	+	0.8	0	NA	-0.15	0.459	+	0.43	0.025
Comamonadaceae	+	0.67	0	NA	-0.32	0.109	NA	0.23	0.239
Nitrospiraceae	+	0.73	0	NA	0.28	0.163	+	0.41	0.035
Steroidobacteraceae	NA	-0.11	0.588	NA	-0.08	0.71	–	-0.6	0.001
Hyphomicrobiaceae	NA	0.35	0.078	–	-0.56	0.003	NA	-0.32	0.101
Gemmataceae	+	0.69	0	NA	-0.13	0.522	NA	0.15	0.459
Nitrosomonadaceae	+	0.53	0.004	NA	0.36	0.068	NA	0.09	0.663
Sphingomonadaceae	–	-0.57	0.002	NA	-0.07	0.737	–	-0.56	0.003
Reyranellaceae	NA	0.33	0.089	–	-0.72	0	NA	0.02	0.915
Xanthomonadaceae	–	-0.8	0	NA	0.1	0.621	–	-0.5	0.008
Xanthobacteraceae	–	-0.72	0	NA	0.17	0.39	NA	-0.29	0.137
NB1-j_fa	+	0.43	0.026	NA	-0.23	0.244	+	0.52	0.006
Gemmatimonadaceae	NA	-0.24	0.22	+	0.54	0.004	NA	-0.24	0.235
Solirubrobacteraceae	NA	-0.26	0.189	NA	0	0.994	–	-0.6	0.001
Inquilinaceae	–	-0.71	0	NA	0.15	0.44	–	-0.48	0.038
Beijerinckiaceae	NA	-0.03	0.876	NA	-0.24	0.231	–	-0.8	0.001
Rhizobiaceae	+	0.41	0.031	–	-0.47	0.014	NA	-0.28	0.154

Table 4.15: RN5 Pearson’s correlation results showing the relationship between substrate moisture, $\delta^{13}\text{C}$ and $\delta^{15}\text{N}$, and taxa abundance. Statistical significance is indicated by bold-font for p-values below an alpha value of 0.05.

RN5 Family	percent moisture correlation	r	p-value	$\delta^{13}\text{C}$ correlation	r	p-value	$\delta^{15}\text{N}$ correlation	r	p-value
Pseudonocardiaceae	–	-0.39	0.041	+	0.42	0.027	–	-0.54	0.003
Euzebyaceae	NA	0.36	0.059	–	-0.66	0.001	+	0.4	0.037
(Aerolinae) A4b	–	-0.68	0.001	+	0.5	0.007	NA	0.16	0.418
Steroidobacteraceae	NA	-0.31	0.109	+	0.58	0.001	–	-0.75	0.009
Hyphomicrobiaceae	–	-0.58	0.001	+	0.61	0.001	NA	-0.04	0.838
Gammaproteobacteria unclassified	–	0.48	0.01	NA	0.09	0.665	NA	-0.07	0.727
Gemmataceae	–	-0.51	0.006	+	0.75	0.001	NA	-0.2	0.297
Nitrosomonadaceae	+	0.37	0.051	–	-0.46	0.015	+	0.43	0.0216
Blastocatellaceae	NA	0.09	0.646	+	0.65	0.001	–	-0.49	0.008
Pirellulaceae	–	-0.67	0.001	+	0.57	0.001	NA	-0.16	0.423
Xanthobacteraceae	–	-0.67	0.001	+	0.6	0.001	NA	-0.04	0.837
Chitinophagaceae	–	-0.42	0.026	+	0.46	0.015	NA	0.06	0.771
Methyloligellaceae	NA	0	0.982	+	0.6	0.001	–	-0.78	0.001
Nitrosococcaceae	+	0.64	0.001	–	-0.36	0.059	NA	0.22	0.269
Anaerolineaceae	NA	0.14	0.464	–	-0.47	0.012	NA	-0.18	0.365
Rhizobiales unclassified	NA	0.09	0.645	–	-0.49	0.008	NA	-0.05	0.789
Beijerinckiaceae	NA	-0.12	0.556	–	-0.47	0.011	–	-0.4	0.037
Nitrospiraceae	NA	-0.28	0.152	NA	0.21	0.293	+	0.48	0.01
Rhizobiales Incertae Sedis	NA	0.05	0.817	NA	0.37	0.055	–	-0.85	0.001

Table 4.16: DCA model results specific to SABs within KN14, demonstrating the relationship between moisture content, $\delta^{13}\text{C}$, and microbial community composition. Statistical significance is indicated by bold-font for p-values below an alpha value of 0.05.

KN14 Variable	DCA1	DCA2	R ²	p-value
$\delta^{13}\text{C}_{\text{SAB}}$	0.976	-0.219	0.075	0.382
Moisture content	-0.949	0.315	0.736	0.001
Temperature	0.122	0.993	0.044	0.550

Table 4.17: KN14 PERMANOVA model results showing the relationship between predictor variables and microbial community composition. Statistical significance is indicated by bold-font for p-values below an alpha value of 0.05.

KN14 Predictor Variable	F.Model	R ² (total = 1)	p-value
$\delta^{13}\text{C}_{\text{SAB}}$	3.248	0.115	0.016
Moisture content	10.87	0.303	0.001
Temperature	1.783	0.067	0.131
Biofilm color	13.03	0.343	0.001
Total between site IDs	11.62	0.734	0.001

Table 4.18: RN5 PERMANOVA model results showing the relationship between predictor variables, and microbial community composition. Statistical significance is indicated by bold-font for p-values below an alpha value of 0.05.

RN5 Predictor Variable	F.Model	R ² (total = 1)	p-value
$\delta^{13}\text{C}$ of SABs	5.602	0.178	0.002
% moisture	4.861	0.158	0.003
Temperature	2.768	0.096	0.019
Biofilm color	8.241	0.397	0.001
Total between site IDs	9.123	0.675	0.001

Table 4.19: DCA model specific to RN5 comparing microbial community structure to $\delta^{13}\text{C}$ and moisture content of the substrate (i.e. cave wall). Statistical significance is indicated by bold-font for p-values below an alpha value of 0.05.

RN5 variable	DCA1	DCA2	R²	p-value
$\delta^{13}\text{C}$ value of SAB	-0.865	0.501	0.5606	0.001
% moisture	0.675	0.739	0.2875	0.011

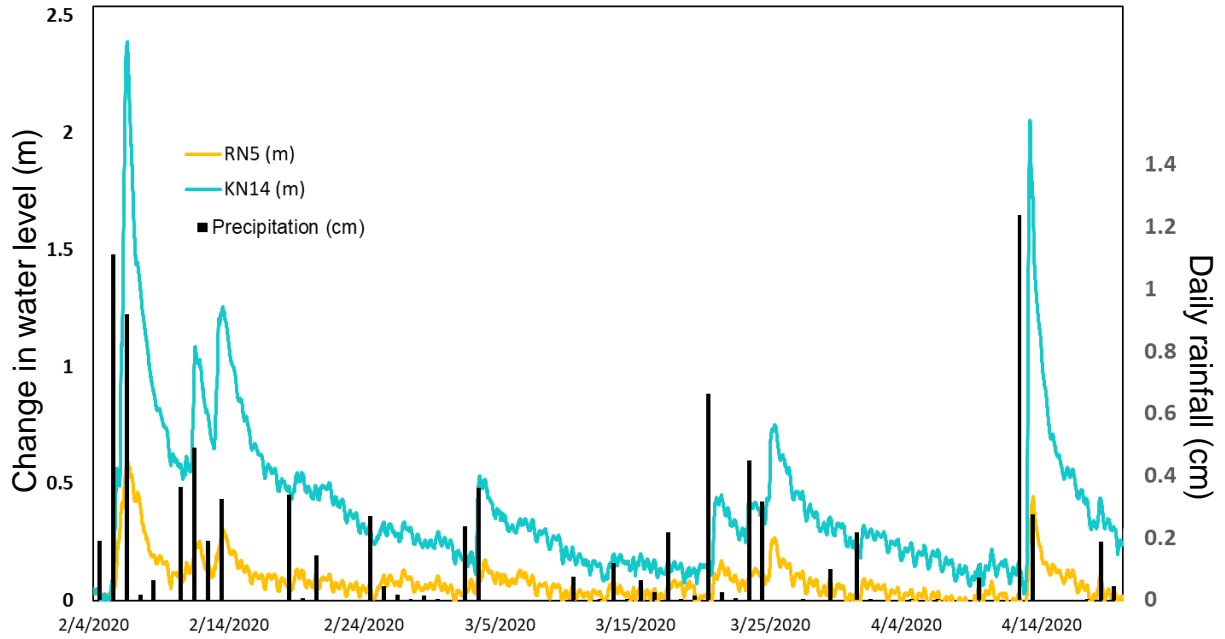


Figure 4.1: Stream level fluctuations and flooding frequency in KN14 (blue) and RN5 (yellow). Change in water depth is reported relative to $t_0 = 0$ m for the measured stream surface level at the start of the study. Daily rainfall is shown in black.

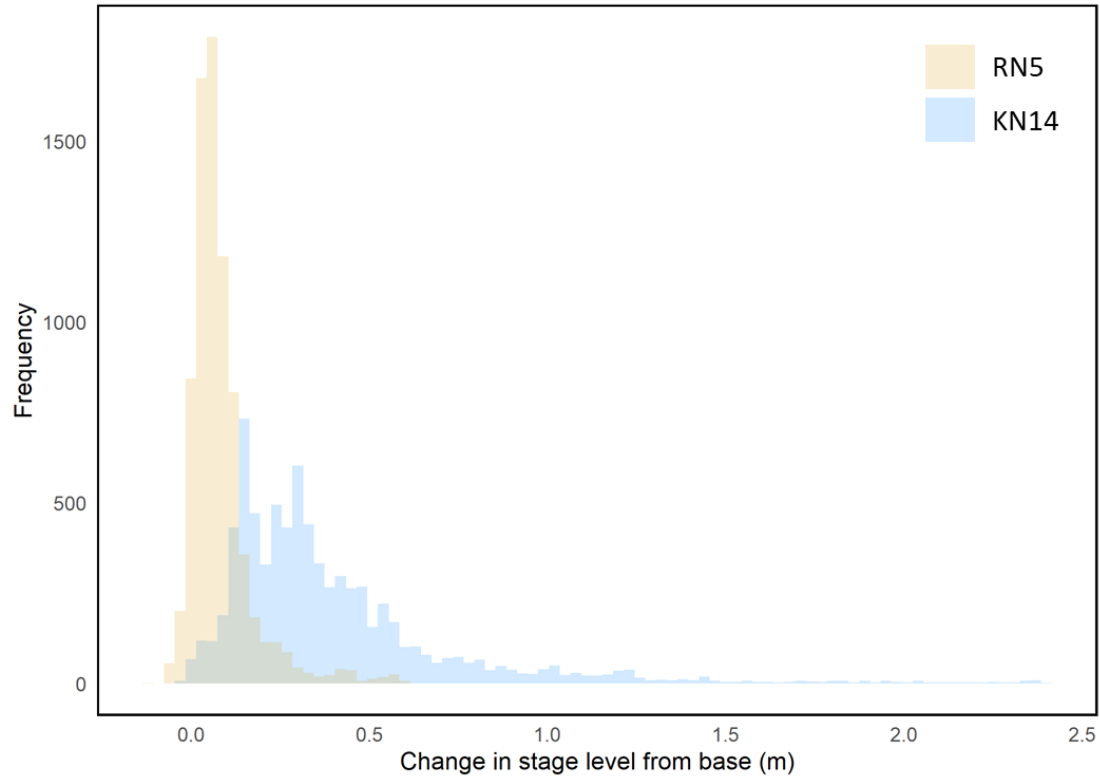


Figure 4.2: Flooding height and frequency in KN14 (blue) and RN5 (yellow) cave

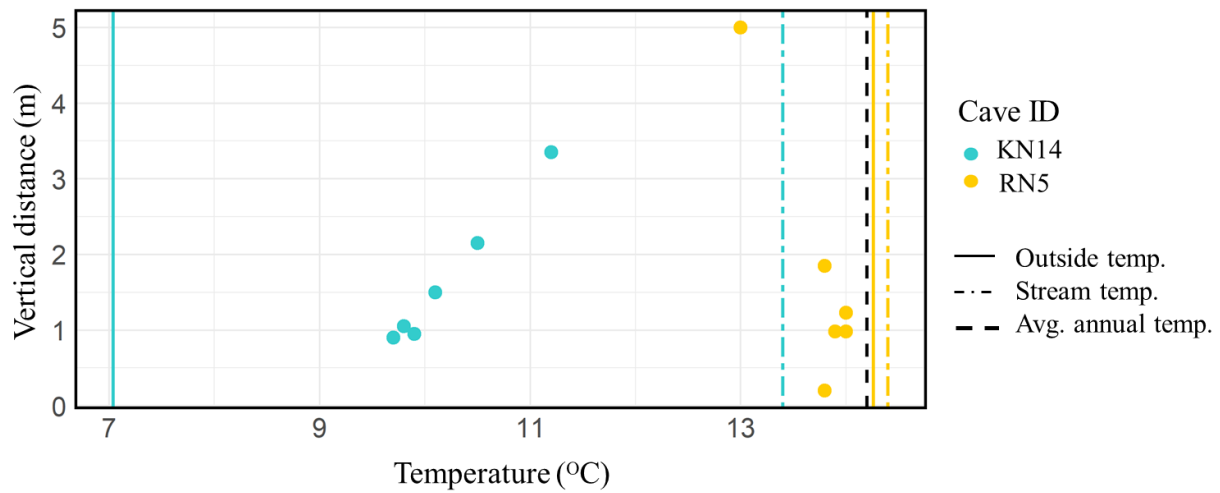


Figure 4.3: Cave-wall temperature variation at SAB sampling sites at the beginning of the study and based on vertical distance from the stream base level at $t_0 = 0$ m. Light blue = KN14; Yellow = RN5. Solid lines represent the outside temperature on the sampling day for each cave, and colored dot-dash lines represent the stream temperatures. The black dotted line represents the average annual surface temperature.

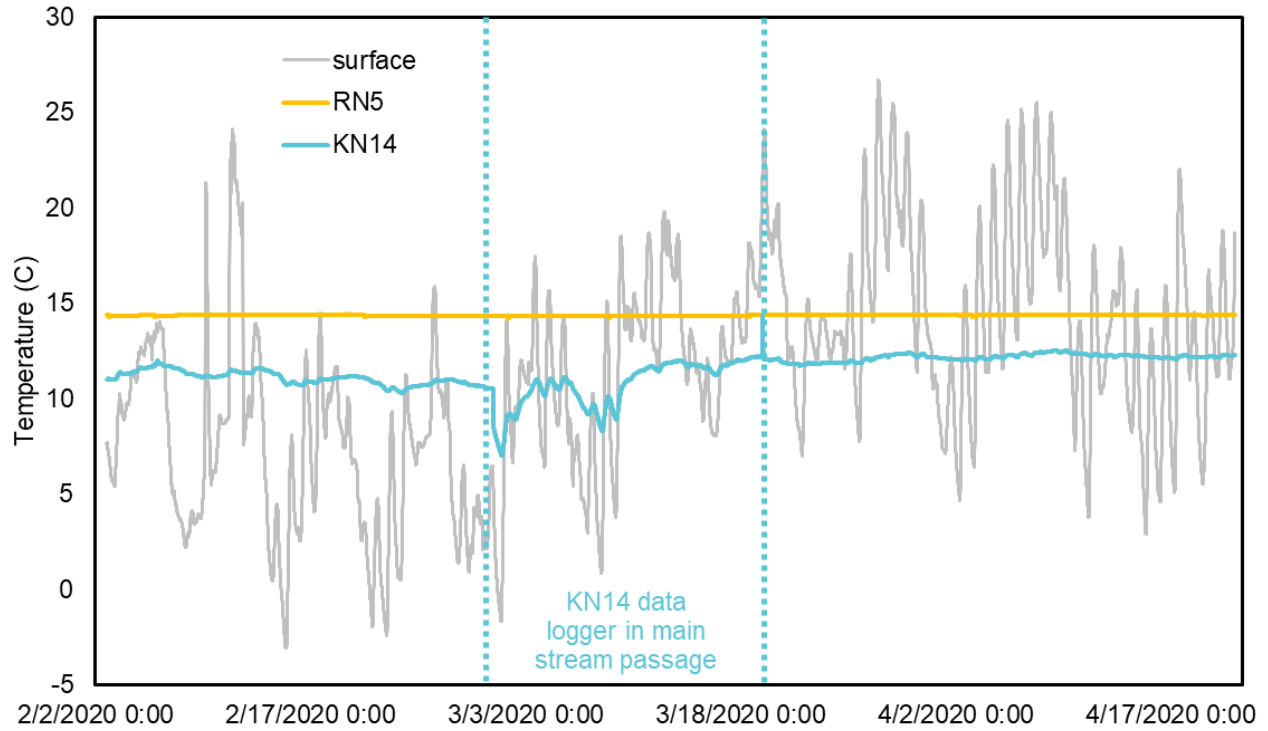


Figure 4.4: Cave air temperature over time from winter (February 2, 2020) to late spring (April 17, 2020), showing more variation in temperatures in the cave site KN14 (blue) than in RN5 (orange). Dotted blue lines represent the approximate time in which the data logger in KN14 recorded temperatures in the main cave stream passage, but the data logger was placed in an upper passage of the cave prior to and after this period, to establish whether cave air temperature near the stream was more variable than away from the stream.

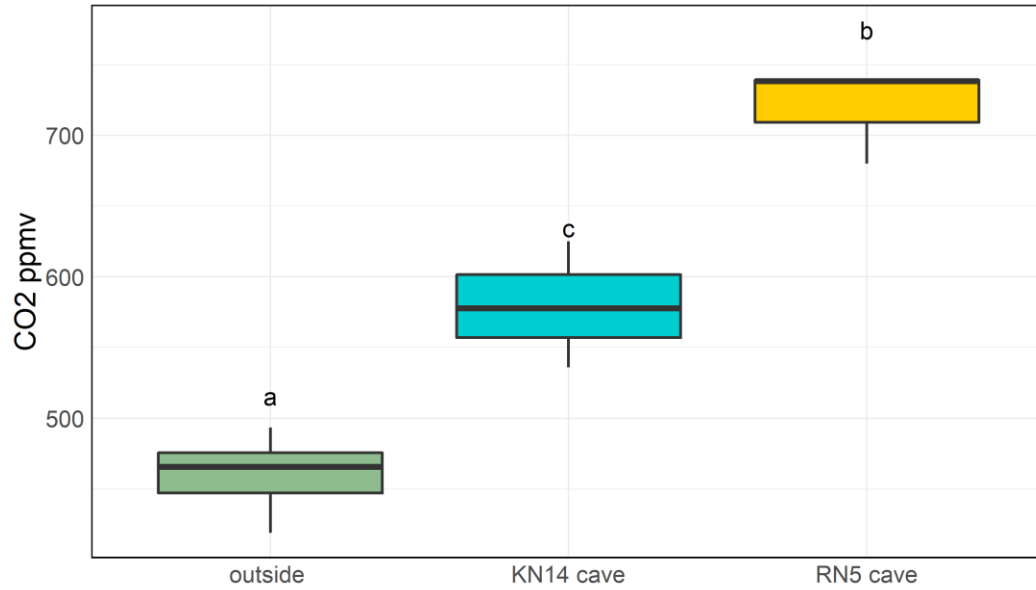


Figure 4.5: Comparison of CO₂ concentrations in cave air in February between cave locations and outside measurements. Letters denote statistically significant differences among samples despite variation in replicate measurements based on a Tukey's HSD test (p-value < 0.05, n = 3).

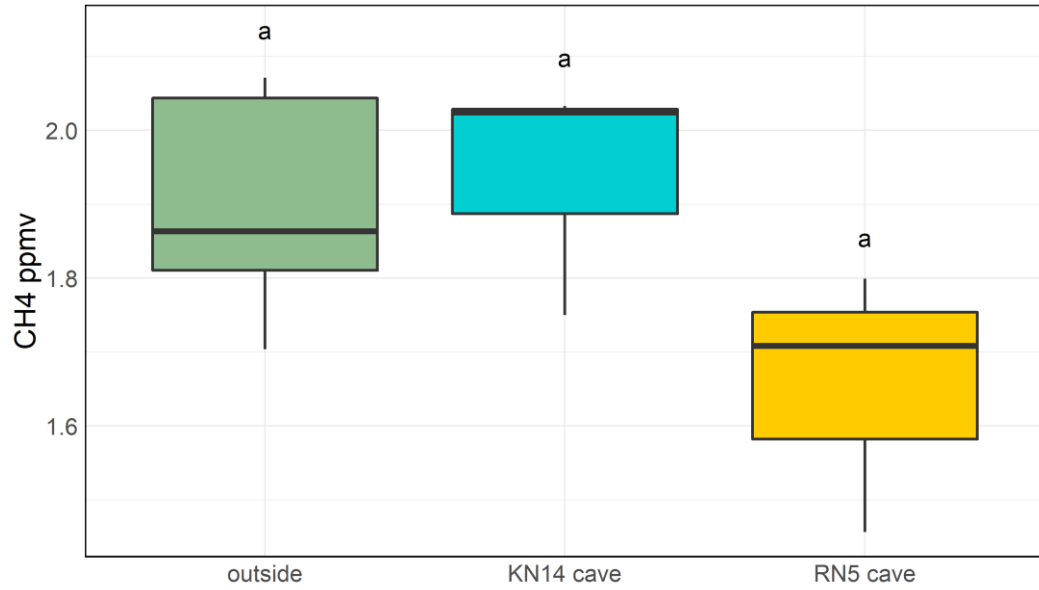


Figure 4.6: Comparison of CH₄ concentrations in cave air in February between cave locations and outside measurements. Letters denote the absence of statistically significant difference in CH₄ concentration among these locations based on Tukey's HSD test (p-value > 0.05, n = 3).

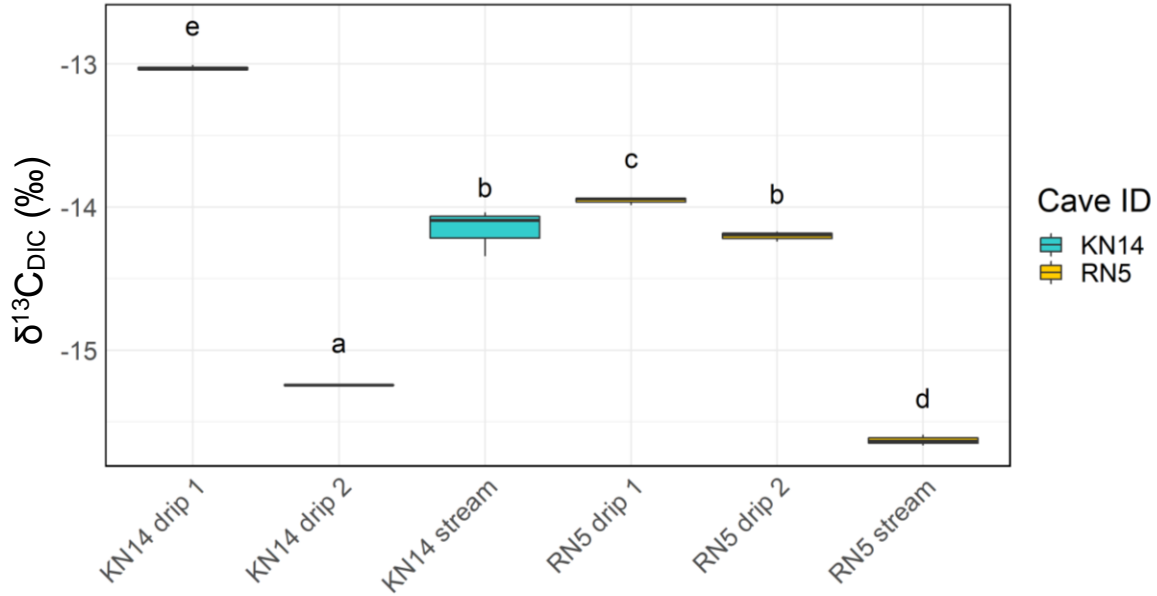


Figure 4.7: $\delta^{13}\text{C}$ of dissolved inorganic carbon (DIC) measured from filtered water samples of meteoric water (drips) and cave streams. $\delta^{13}\text{C}_{\text{DIC}}$ values are reported relative to PDB. Letters denote significant differences among values using Tukey's HSD test (p-value < 0.05, n = 3).

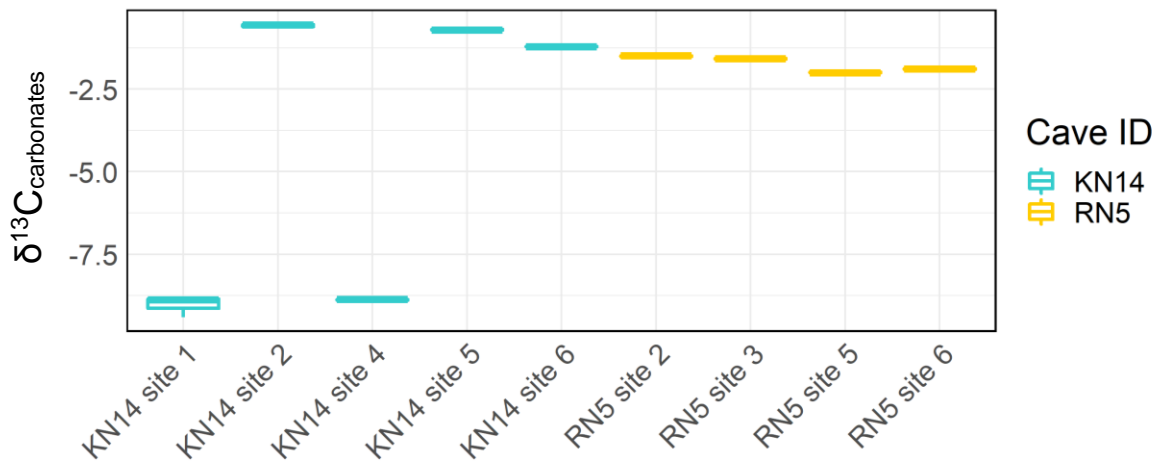


Figure 4.8: $\delta^{13}\text{C}$ values of rock (i.e., carbonate) substrates at each site relative to PDB (n = 3).

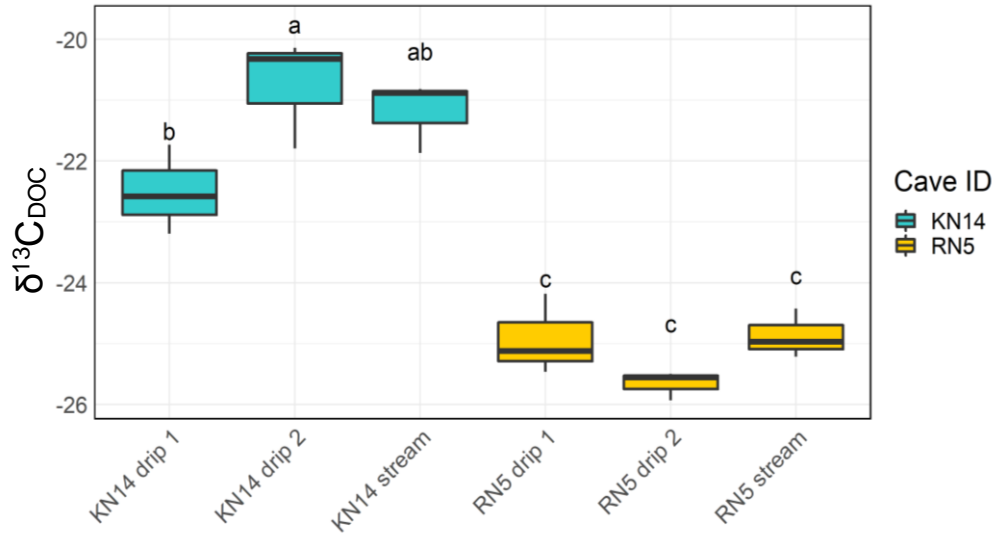


Figure 4.9: $\delta^{13}C$ of dissolved organic carbon (DOC) measured in two drip water sites and the stream in both caves (relative to PDB). Letters indicate significant differences among sites based on the results of a Tukey's HSD test (p -value < 0.05, $n = 3$).

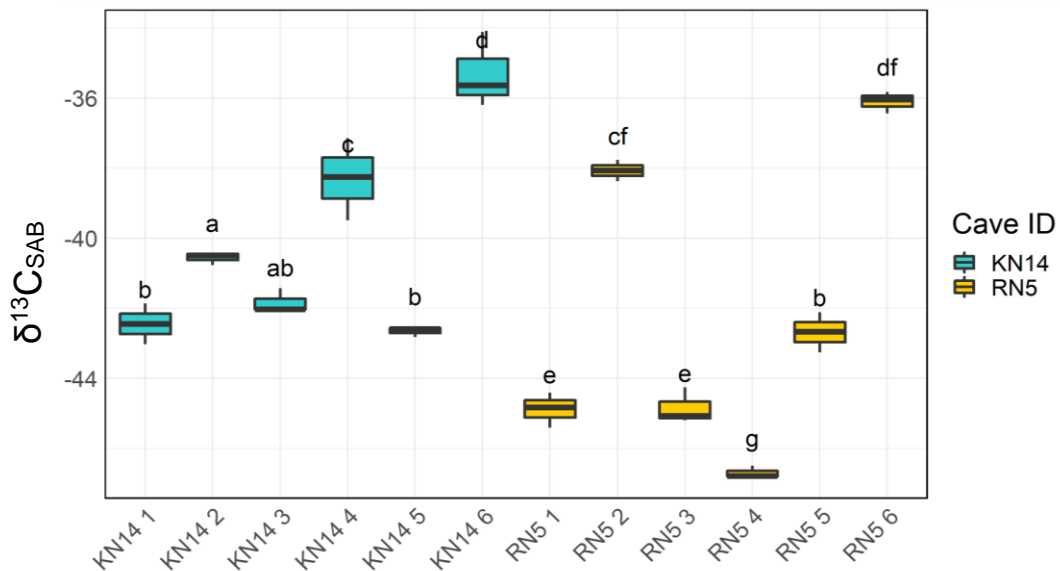


Figure 4.10: $\delta^{13}C$ values of subaerial biofilms (SABs) at each sampling site for both caves. $\delta^{13}C$ values are relative to the PDB standard. Letters denote statistical differences among samples determined by Tukey's HSD test (p -value < 0.05).

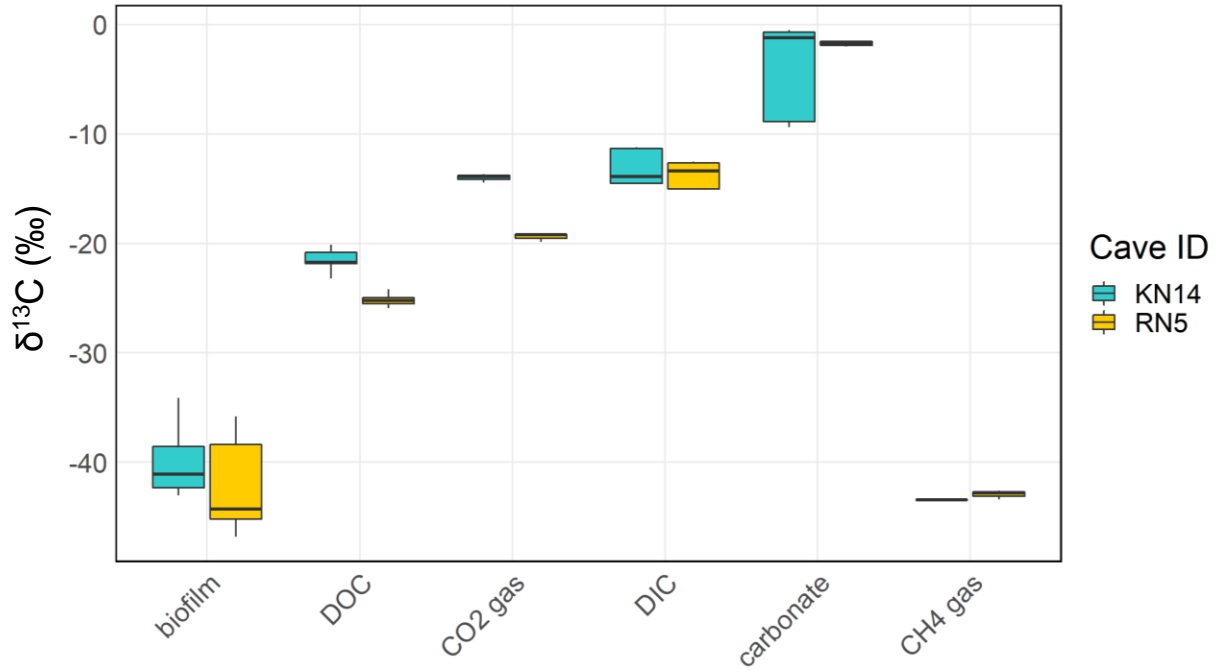


Figure 4.11: Summary of $\delta^{13}\text{C}$ values (relative to PDB) for all samples, including SAB biomass ($n = 6$ per cave), DOC and DIC in drip water ($n = 2$ per cave), CO₂ and CH₄ in the cave air, and rock (i.e., carbonate) substrate from each site and each cave. Data are reported in Tables 4.5 and 4.6.

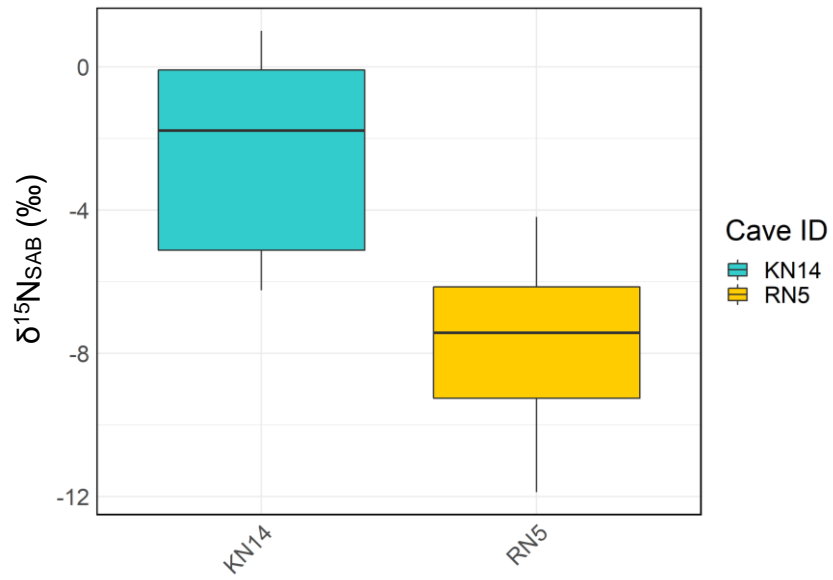


Figure 4.12: Comparison of bulk $\delta^{15}\text{N}$ values measured from all SAB samples from each cave ($n = 6$). $\delta^{15}\text{N}$ values are reported relative to air- N_2 .

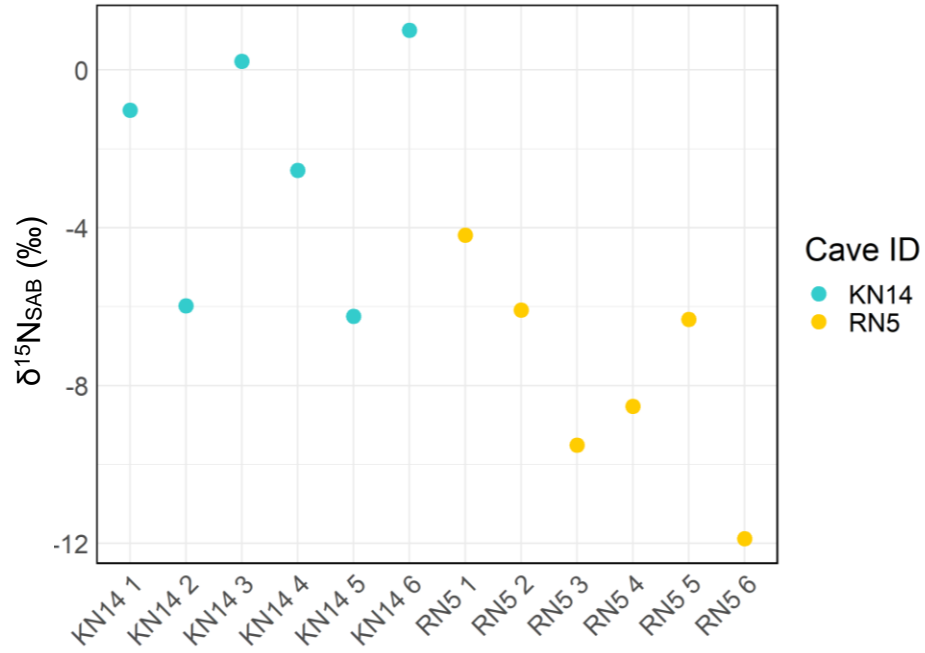


Figure 4.13: $\delta^{15}\text{N}$ values measured from all SAB samples from each cave without replication. $\delta^{15}\text{N}$ values are reported relative to air- N_2 .

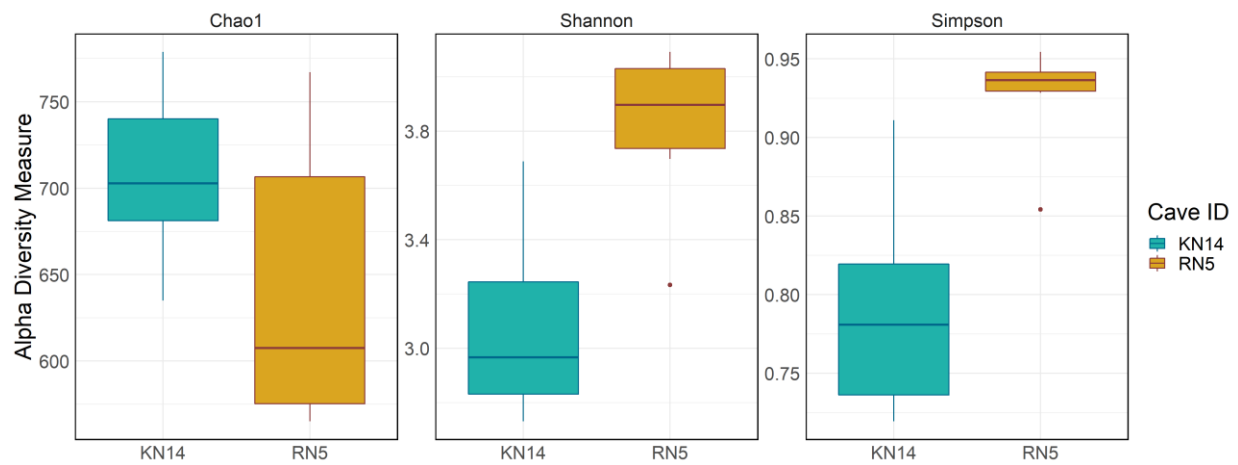


Figure 4.14: Composite evenness (Chao1, left panel) and diversity index (Shannon, center panel; Simpson, right panel) values for all SAB samples from each cave.

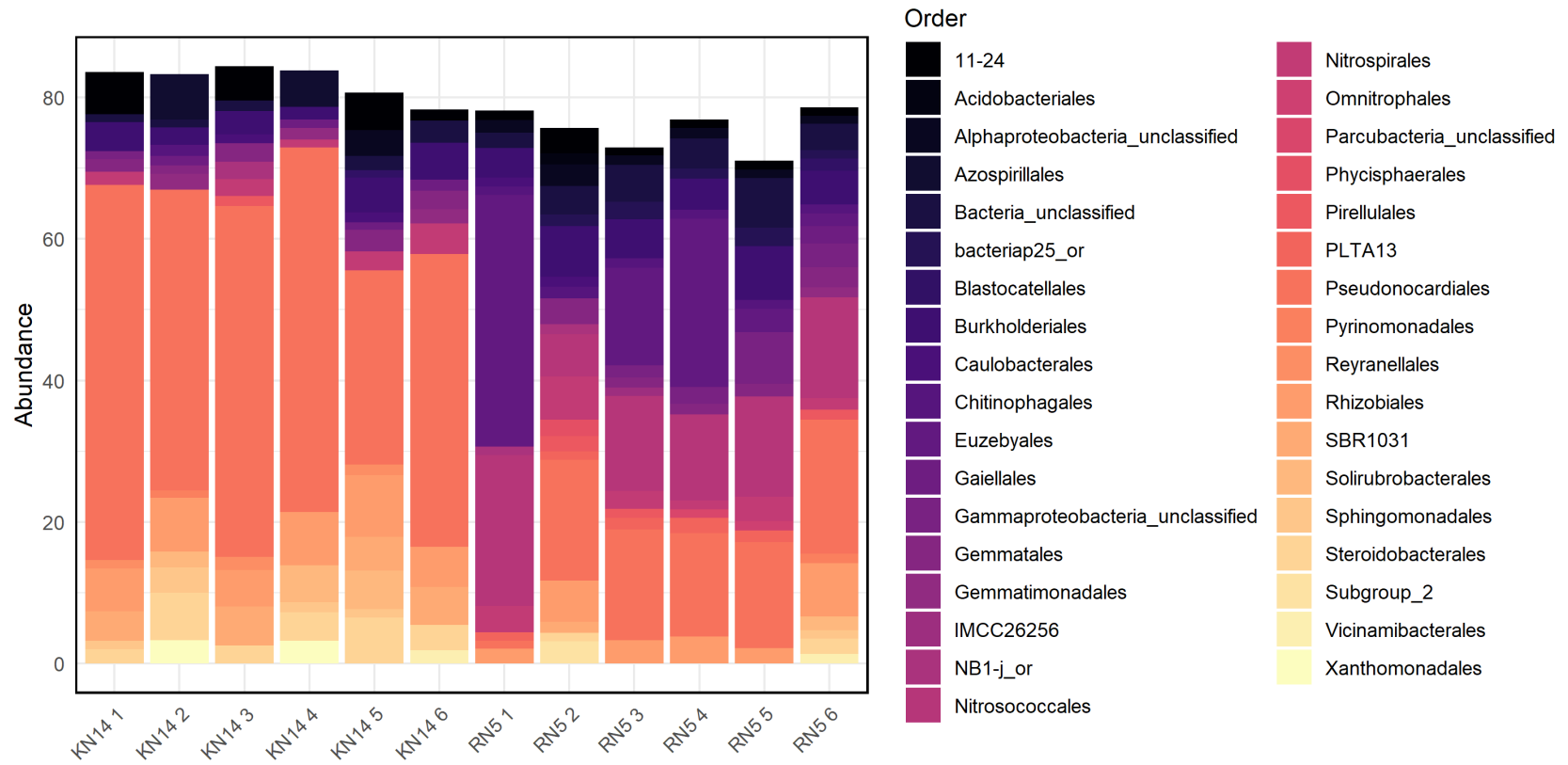


Figure 4.15: Average relative abundances of taxa at the order level for all sampling sites (1–6) in each cave (KN14 and RN5). Sequence abundances were averaged between replicates. Only orders with relative abundances greater than 1.0% are shown.

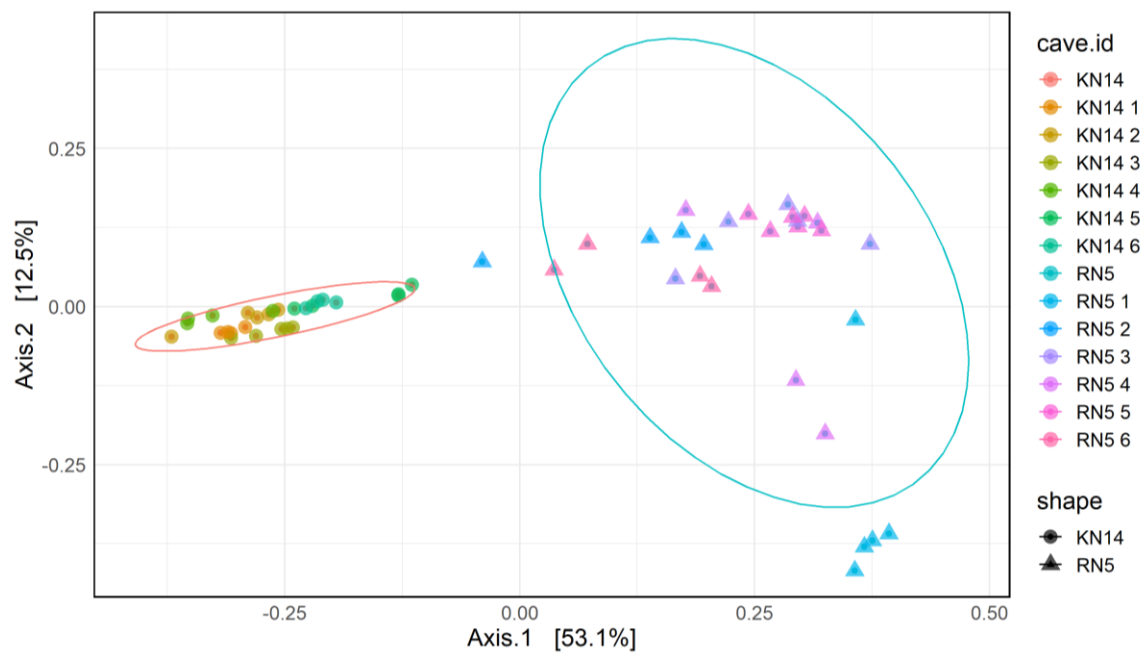


Figure 4.16: PCoA plot showing Bray-Curtis similarity between microbial community composition at the genus level for all replicates collected at each sampling site. Ellipses represent where 95% of the data fall.

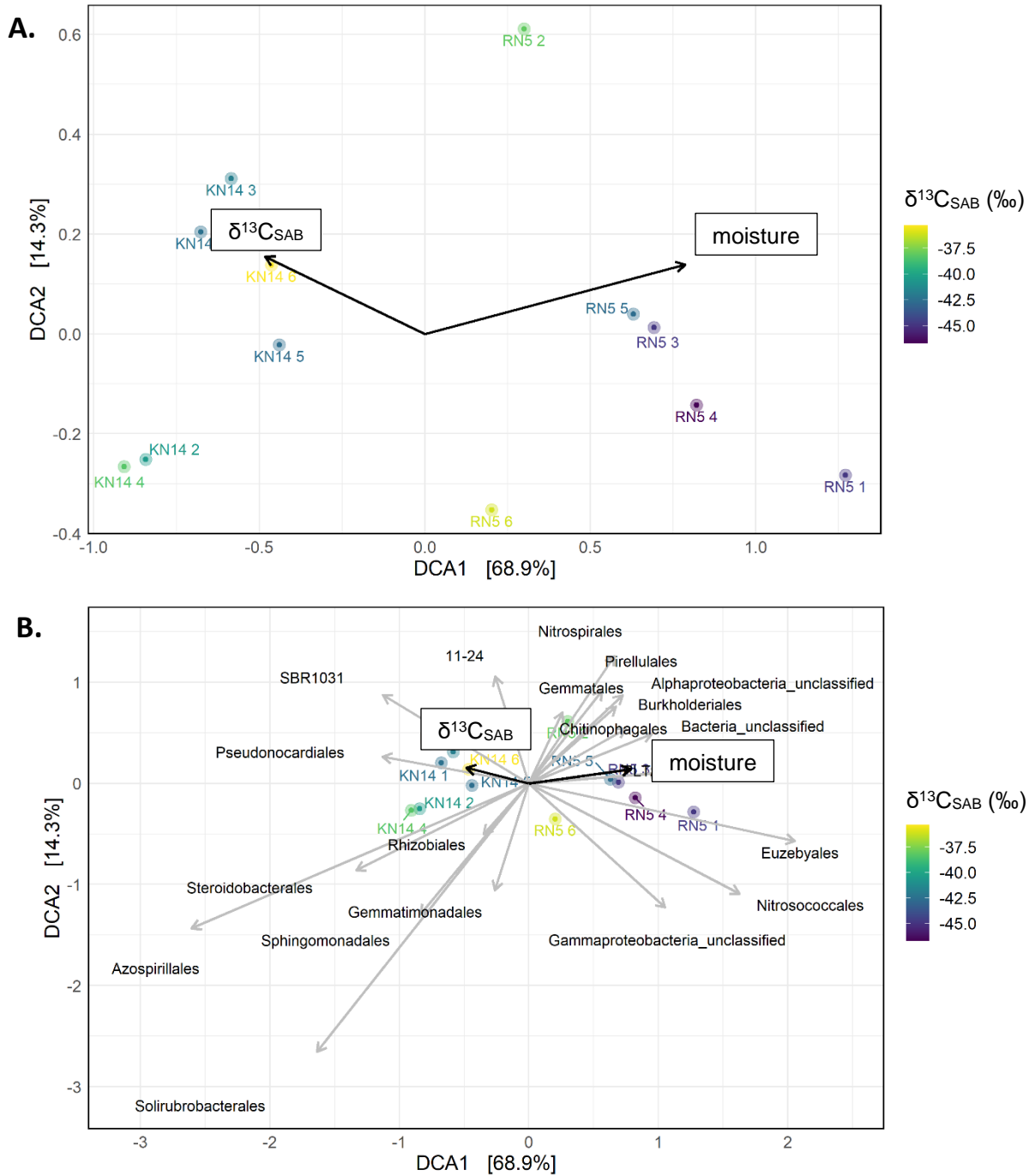


Figure 4.17: A) DCA plot showing differences in microbial community structure across all sampling sites in both caves. B) DCA plot revealing relationships among microbial community structure at the order level and changes in $\delta^{13}\text{C}_{\text{SAB}}$ (p-value = 0.30) and moisture content (p-value = 0.013). Color gradient represents $\delta^{13}\text{C}_{\text{SAB}}$ values.

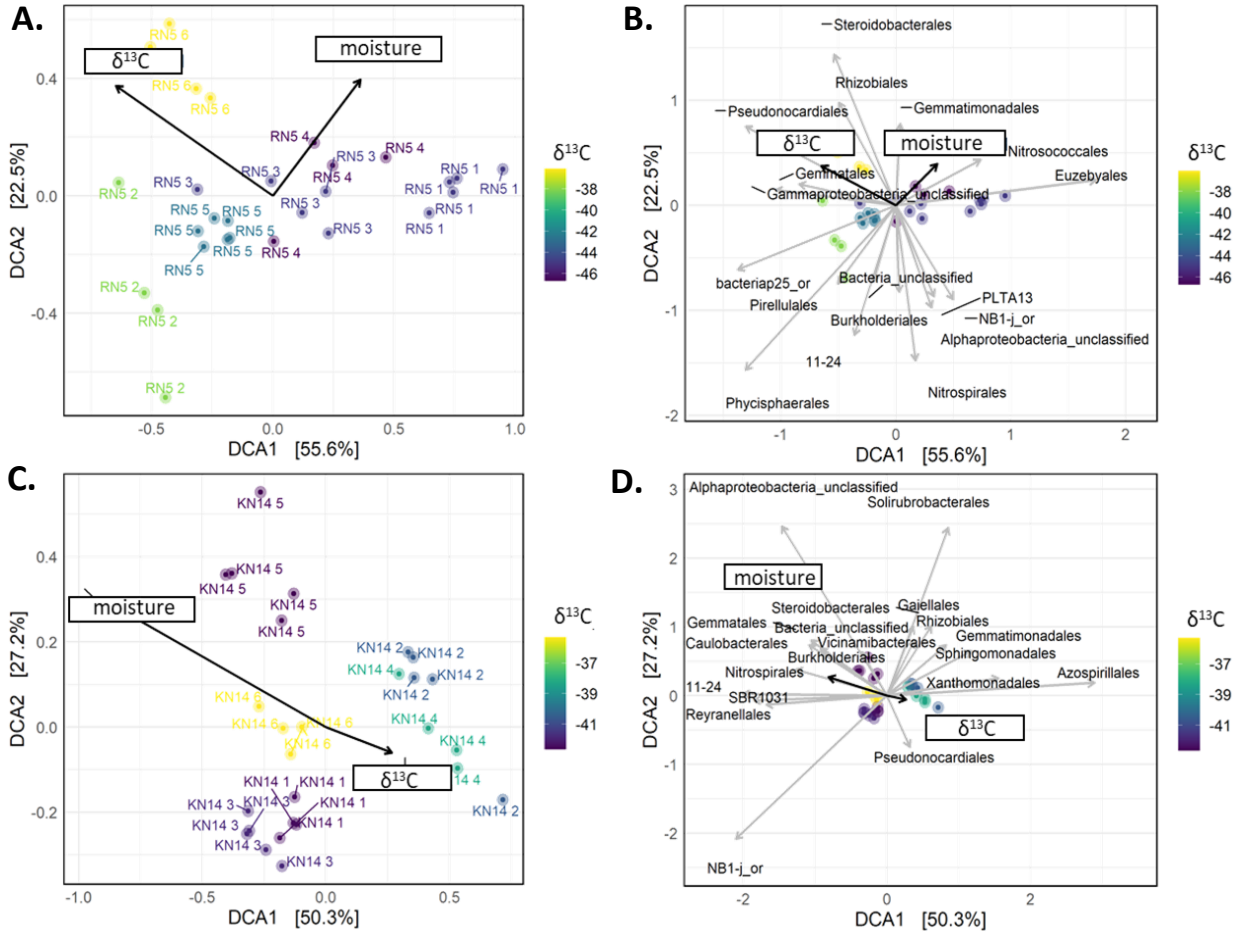


Figure 4.18: DCA plots (panels A and B are the same for RN5; panels C and D are the same for KN14) showing relationships among microbial community structure, $\delta^{13}\text{C}_{\text{SAB}}$, and percent moisture across both cave sites. Panels B and D show order-level correlations among taxa and overall community structure. Color gradients for each set of plots represent differences in $\delta^{13}\text{C}_{\text{SAB}}$ values.

CHAPTER FIVE DISCUSSION

Prevalent Taxonomic Groups in Subaerial Biofilms from Cave Environments

Overall SAB bacterial community compositions for KN14 and RN5 caves agree with findings from earlier cave SAB studies that report SABs are dominated by Actinobacteria and Proteobacteria phyla and have relatively low diversity (e.g., Porca et al., 2012; Tomczyk-Zak & Zeilenkiewicz, 2015; Wu et al., 2015; Gonzalez-Pimentel et al., 2018; Luis-Vargas et al., 2019; Marques et al., 2019). Specifically, Shannon diversity indices from KN14 and RN5 were like those calculated for SABs in lava tubes, with values ranging from 1.0 to 5.68 (e.g., Lavoie et al., 2007; Riquelme et al., 2015; Gonzalez-Pimentel et al., 2018; Luis-Vargas et al., 2019). The relative abundances of actinobacterial orders Pseudonocardiales, which dominated SABs from KN14, and Euzebyales, which were more prevalent in RN5, were also consistent with abundances retrieved from lava tube and carbonate cave SABs (Hathaway et al., 2014; Riquelme et al., 2015; Duan et al., 2017; Gonzalez-Pimentel et al., 2018).

Consequently, it is not surprising that searching for close relatives for KN14 and RN5 genera using the Basic Local Alignment Search Tool (BLASTn) for the NCBI database revealed that the highest sequence similarities were also to uncultured bacteria from the earlier cave studies. For instance, the most similar sequences (with 98% or greater sequence similarity) to sequences from KN14 and RN5 were related to the Pseudonocardiaceae genus *Crossiella* and uncultured bacteria obtained from geographically distinct SAB colonies on the walls of lava tubes (Northup et al., 2011; Riquelme et al., 2015; Luis-Vargas et al., 2019), as well as a Slovenian limestone cave (Pašić et al., 2010). However, the only cultured *Crossiella* representatives are from Japanese soil (Labeda, 2001) and horse placentas (Donahue et al., 2002), which means that the cave representatives are likely new species. In general, members of Pseudonocardiaceae are abundant in desert soils (Lynch et al., 2014) and can potentially withstand extreme conditions (Mohammadipanah & Wink, 2016). Members of this family are also considered metabolically flexible because some possess genes for complete CO₂ fixation via the CBB pathway, although others grow heterotrophically (Lynch et al., 2014). In arid environments, Pseudonocardiaceae are suspected to utilize atmospheric CO₂ as a source of carbon due to extreme nutrient limitation (Lynch et al., 2014).

Similarly, *Euzebya* spp. from KN14 and RN5 had 98% or greater sequence similarity to uncultured bacteria identified from lava tubes, including the Chimalacatepec lava tube system in Mexico (Luis-Vargas et al., 2019; accession number: MK311202), a lava tube in the Azores (Northup et al., 2011; accession number: JF265714), an Hawaiian lava tube (Northup et al., 2011; accession number: KC569846), and a lava tube in the Canary Islands (unpublished data by J. Gonzalez-Pimentel, accession number: LT854958). Gonzalez-Pimentel et al. (2018) found that Euzebyales were the most metabolically active members of lava tube SABs. However, cultured representatives of this genus, which include aerobic chemoorganoheterotrophs, are from marine environments (Kurahashi et al., 2010; Yin et al., 2018), again emphasizing the potential novelty of the cave SAB species.

Sequences from KN14 and RN5 that were affiliated with the unclassified group wb1-P19 from the Nitrosococcales, which is an order within the Gammaproteobacteria, shared 99% or greater sequence with SAB bacteria from a Slovenian carbonate cave (Porca et al., 2012; accession number: HE602817) and tan and yellow SAB colonies in an Azores lava tube (Northup et al., 2011; accession numbers: JF265778, HM749682), as well as to bacteria from a stream in Mammoth Cave, Kentucky (R. Fowler, unpublished data; accession number: GQ500804) and from an Illinois aquifer (Flynn et al., 2013; accession number: KC605633). Members of this order, and specifically Nitrosococcaceae, are putative chemolithoautotrophic AOB (Klotz et al., 2006). Also, members of the Nitrospira phylum (Nitrospirales) have been previously identified from cave SABs (e.g., Pašić et al., 2010 Riquelme et al., 2015), and all are chemolithoautotrophic nitrite-oxidizers (e.g., Ehrich et al., 1995). Both KN14 and RN5 SABs had low relative abundances of Nitrospirales, and specifically *Nitrospira* spp., although all RN5 unflooded sites and site 6 in KN14 (i.e., also not flooded) had higher relative abundances of *Nitrospira* spp. compared to the flooded sites, which may be because some taxonomic groups prefer drier conditions.

Close relatives of an unclassified genus belonging to the Methyloiligellaceae were the most abundant putative methylotrophs in KN14 and RN5, but other putative C1-metabolizing (i.e., methanotrophic) bacterial groups, including the Methyloimabilaceae, Methyloacidiphilaceae, Methylococcales, Methyloimabilia, Rhizobiales, and Verrucomicrobia, were related to unclassified, uncultured representatives from a range of habitats, including caves. Although many methanotrophs require CH₄ concentrations higher than ambient atmospheric levels to grow, some

bacteria possess the ability to grow at atmospheric levels of CH₄ (Tveit et al., 2018). These methanotrophs, referred to as the “upland soil cluster γ ,” have been identified in soils, as well as cave microbial communities (Zhao et al., 2018). Interestingly, evolutionary relatedness between the particulate methane monooxygenase enzyme pathway and ammonia monooxygenase pathway commonly results in co-oxidation of CH₄ by ammonia-oxidizers (Holmes et al., 1995). In fact, members of both Nitrosococcaceae and Nitrosomonadaceae (Gammaproteobacteria), which were represented in the top 20 most abundant taxa in the KN14 and RN5 SAB communities, actively oxidize and incorporate carbon from CH₄ oxidation (Jones & Morita, 1983; Klotz et al., 2006). Nitrifiers are also known to contribute to the uptake of CH₄ in forest soils where they compete with methanotrophs for CH₄ oxidation (Goldman et al., 1995). Therefore, despite low relative abundances of putative methanotrophs in the cave SABs, ammonia-oxidizers could co-oxidize CH₄ as a carbon source.

Although this study was the first to attempt to measure bulk $\delta^{15}\text{N}_{\text{SAB}}$ measurements from cave SABs, low overall nitrogen content and insufficient material resulted in only single measurements from each SAB site. Therefore, interpretation of the results is limited, especially because $\delta^{15}\text{N}$ values of nitrogen sources, including nitrate and ammonium in drip water and streams, would also be needed. Nevertheless, low $\delta^{15}\text{N}_{\text{SAB}}$ values and the corresponding presence of several putative diazotrophic taxa potentially supported the hypothesis that N₂ fixation is likely occurring in SAB communities. However, there were differences in $\delta^{15}\text{N}_{\text{SAB}}$ values between the caves and lower $\delta^{15}\text{N}_{\text{SAB}}$ values were associated with some putative N₂-fixing organisms but not putative nitrifiers (Table 4.14 and Table 4.15). N₂ fixation by free-living diazotrophs fractionates ca. -2.5‰ from N₂ (~0‰), and ammonia produced through diazotrophy or delivered to the SABs could be fractionated even further through assimilation by microbes, which would result in biomass with low $\delta^{15}\text{N}_{\text{SAB}}$ values, such as those observed at sites 2 (-5.98‰) and 5 (-6.25‰) in KN14 and all sites in RN5 (-4.19 to -11.88‰). In addition, oxidation of this ammonia to nitrate via nitrification, or ammonia delivered to the biofilm through percolating meteoric water or streams, would produce nitrate enriched in ¹⁴N, which could then be assimilated by SABs into biomass. The significantly lower $\delta^{15}\text{N}_{\text{SAB}}$ values in RN5 compared to KN14 also coincide with significantly higher overall relative abundance of the AOB Nitrosococcaceae in RN5.

Influence of Moisture on Subaerial Biofilm Diversity

The main goals of measuring cave environmental conditions were to evaluate potential sources for nutrients and to determine which variables could explain variations in bacterial community composition, such as moisture content. One of the research hypotheses predicted that variation in SAB microbial community diversity would be driven by environmental variation within the caves more than geography. This hypothesis has been tested in other studies, including for cave SABs, where examination of physically distant lava tube communities concluded that geographic barriers play the most important role in determining taxa abundances (Hathaway et al., 2014; Gonzalez-Pimentel et al., 2018). Explanation for these geographic rather than environmental controls stems from the idea that individual caves and their overlying epikarstic soils have unique characteristics that are unquantifiable but that also affect variance in taxonomic data (Hathaway et al., 2014). But, multiple other studies for surface (i.e., phototrophic) SABs in soils across geographic distances indicate that moisture content is the most important driver for bacterial biomass production (Serna-Chavez et al., 2013) and that duration of wetness is more important than the amount of precipitation (e.g., Gladis-Schmacka et al., 2014; Prieto et al., 2020).

Most of the environmental variables measured in this study did not explain variation in SAB community composition, but there were statistically significant correlations identified between diversity and moisture content at each SAB site for both caves (Table 4.10 and Figure 4.17). Not only do cave streams or drips provide water to surfaces that SABs can then colonize, but exposure to different water sources by proximity to periodic or frequent flooding and dripping would also affect nutrient availability for SABs. SABs in KN14 were exposed to stream water at least once during the study, with three sites being frequently flooded (sites 1, 2, and 3) (Figure 4.1), and sites 3 and 6 had no active drips (Table 3.1). In contrast, only one site in RN5 (site 1) was frequently flooded by the stream and all other RN5 sites were not flooded (Figure 4.1); sites 2 and 6 had no active drips (Table 3.1). The DOC concentrations in KN14 stream and drip water were higher during the study period than what would be considered oligotrophic conditions (Kaplan & Newbold, 2000), which implies that SABs exposed to stream and/or dripping water have more readily available organic carbon sources for metabolism than SABs away from an active water source. Even the lower, oligotrophic DOC concentrations for RN5 drips would provide some organic carbon to SABs. Moreover, SABs near water sources could also have access to and use nitrate or other nutrients.

These findings differ slightly from previous research of lava tube SABs in the Azores and Hawai`i, where microbial taxa abundances in the different caves are influenced predominately by rock organic carbon, nitrogen, and copper content (Hathaway et al., 2014), although moisture content was not measured in that study. In another cave microbial community study, moisture was not measured from cave walls but water content of cave sediments was found to significantly influence microbial diversity (Zhu et al., 2019). Moisture of weathered rock surfaces was measured in a study on methanotroph abundance in cave microbial communities, but the results of these analyses were not reported (Zhao et al., 2018). As such, measuring this environmental variable for future cave SAB studies will be important.

Another hypothesis that was tested as part of this research predicted that SABs in areas with lower organic carbon availability from flooding stream or percolating water (e.g., growing on relatively dry surfaces) would have higher relative abundances of chemolithoautotrophs compared to SABs growing in areas actively exposed to allochthonous carbon input. Based on comparisons with environmental conditions, proximity of SAB colonies to moisture sources, which could provide access to carbon and other nutrients, may select for certain taxa, with lower moisture selecting for Pseudonocardiaceae but higher moisture selecting for Nitrosococcaceae (Tables 4.13 and 4.14). Specifically, where Pseudonocardiaceae abundances were lower, SABs were dominated by Nitrosococcaceae (Tables 4.8 and 4.9, Figure 4.14). Pseudonocardiaceae have the capacity for CO₂ fixation (e.g., Lynch et al., 2014; Mohammadipanah & Wink, 2016) but Nitrosococcaceae are also chemolithoautotrophs (Klotz et al., 2006). Therefore, the hypothesis is partially supported because under high and low moisture content, the potential for SAB communities to be comprised of chemolithoautotrophs was equally possible.

Chemolithoautotrophic Carbon Fixation in Subaerial Biofilms

Only two other isotope studies for cave SABs are known, both from hypogenic caves with SABs dominated by sulfur-oxidizing and acidophilic microbes (Vlasceanu et al., 2000; Engel et al., 2001), which makes this the first study to evaluate the potential contribution of chemolithoautotrophy to epigenic cave SABs using isotope tracers. This research proposed the hypothesis that $\delta^{13}\text{C}$ values for cave SAB biomass would support the presence of chemolithoautotrophic functions, such as CO₂ fixation and/or CH₄ oxidation, and correspond to relative abundances of those taxonomic groups based on 16S rRNA gene sequence data. From other studies, the primary source of carbon to cave bacterial communities in epigenetic caves and

lava tubes is assumed to be from photosynthetically-derived, allochthonous organic carbon, which could be delivered through streams, percolating meteoric water at drip sites, or animals (Poulson & Lavoie, 2000). However, because nutrient availability and access to DOC or other nutrients for cave-wall SABs can be limited or insufficient to sustain adequate growth, community members may need to supplement their carbon needs by relying on chemolithoautotrophy (e.g., Ortiz et al., 2014), which has been suggested for cave SABs in the literature but not demonstrated.

To test the hypothesis, carbon isotope measurements were completed for the cave SABs and potential carbon sources (e.g., DOC, DIC, and atmospheric CO₂ and CH₄), or estimates from the literature were used for sources whose $\delta^{13}\text{C}$ values could not be measured in this study (i.e. dissolved CH₄). If the microbial communities within cave SABs rely solely on allochthonous organic carbon for biomass production, then the $\delta^{13}\text{C}_{\text{SAB}}$ values would be comparable to the local $\delta^{13}\text{C}_{\text{DOC}}$ values. The $\delta^{13}\text{C}_{\text{DOC}}$ values in KN14 and RN5 averaged $-21.4 \pm 0.56\text{‰}$ ($n = 3$) and $-25.2 \pm 1.02\text{‰}$ ($n = 3$), respectively. In contrast, $\delta^{13}\text{C}_{\text{SAB}}$ values ranged from -46.7‰ to -35.3‰ , with 63% of the $\delta^{13}\text{C}_{\text{SAB}}$ values being lower than -40‰ (Tables 4.5 and 4.6, and Figure 4.11), which is lower than would be expected for exclusively heterotrophic metabolism of DOC. Regarding DIC and atmospheric gases, based on drip water $\delta^{13}\text{C}_{\text{DIC}}$ values in KN14 ($-12.9 \pm 1.8\text{‰}$, $n = 3$) and RN5 ($-13.0 \pm 0.45\text{‰}$, $n = 3$) (Table 4.4), if the chemolithoautotrophic CBB cycle was solely responsible for CO₂ fixation and fractionating the carbon isotopes via the Rubisco enzyme (i.e., by -20 to -35‰) (Preuß et al., 1989), then chemolithoautotrophic biomass $\delta^{13}\text{C}$ values could fall between approx. -33‰ to -48‰ . However, SABs are also potentially able to utilize gaseous CO₂ in the cave. For KN14, $\delta^{13}\text{C}_{\text{CO}_2}$ was similar (-14.4‰) to $\delta^{13}\text{C}_{\text{DIC}}$ (-11.3 to -14.5‰), but $\delta^{13}\text{C}_{\text{CO}_2}$ in RN5 was lower at -19.4‰ compared to $\delta^{13}\text{C}_{\text{DIC}}$ values (-12.6 to -15.1‰), likely due to microbial respiration in the soil and low ventilation rates in RN5. If the inorganic carbon source was cave air CO₂ instead of DIC, then the chemolithoautotrophic biomass $\delta^{13}\text{C}$ values would fall between -34.4 and -49.4‰ for SABs in KN14 and between -39.4 and -54.4‰ for SABs in RN5.

Under the assumption that the CBB pathway alone is responsible for fixing CO₂ (as DIC or gaseous CO₂) and that inorganic carbon fixation is the only process responsible for the low $\delta^{13}\text{C}_{\text{SAB}}$ values, then the expected proportion of carbon derived from DIC can be calculated using a two-member mixing model (Belle et al., 2014) between heterotrophic biomass ($\sim\delta^{13}\text{C}_{\text{DOC}}$) and estimated autotrophic biomass. Autotroph biomass estimates were calculated for each SAB

sampling site depending on the local DIC and CO₂ measurements made at each site and using the expected fractionation range for Rubisco. For instance, RN5 site 1 was very close to the stream and stream $\delta^{13}\text{C}_{\text{DIC}}$ values were used to calculate autotroph biomass, but drip $\delta^{13}\text{C}_{\text{DIC}}$ values were used for this calculation for adjacent biofilm collection sites. Estimated proportions of DIC and CO₂-derived carbon were then calculated using the following isotope mass balance constraint:

$$\text{Equation 5.1} \quad \delta^{13}\text{C}_{\text{SAB}} = x * \delta^{13}\text{C}_{\text{autotroph}} + (1-x) * \delta^{13}\text{C}_{\text{heterotroph}}$$

where x represents the relative proportion of bulk biomass carbon ($\delta^{13}\text{C}_{\text{SAB}}$) derived from the two potential carbon metabolic pathways represented in this model: (i) $\delta^{13}\text{C}_{\text{autotroph}}$, which is the estimated $\delta^{13}\text{C}$ value for chemolithoautotrophic biomass produced through CO₂ fixation and based on carbon sources (i.e., $\delta^{13}\text{C}$ values of DIC and cave air CO₂ measured in this study) and the fractionation factor associated with CO₂ fixation using the Rubisco enzyme and the CBB pathway, and (ii) $\delta^{13}\text{C}_{\text{heterotroph}}$, which is the estimated $\delta^{13}\text{C}$ value for heterotrophic biomass produced through the consumption of organic carbon sources (i.e., $\delta^{13}\text{C}_{\text{DOC}}$ in drip water and streams) and assuming no fractionation of carbon isotopes between source and the produced microbial biomass. Consequently, to explain the measured carbon isotope compositions of cave SABs using only CO₂ fixation through the CBB pathway and heterotrophic consumption of DOC, 46%–100% of the biofilm-supplied carbon would need to be derived from DIC or 31–100% derived from cave air CO₂ (Table 5.1). For SABs with $\delta^{13}\text{C}_{\text{SAB}}$ values that were more negative than -40‰, CO₂-derived carbon would need to make up between 67% and 100% of all biofilm-supplied carbon derived from DIC or 56–100% derived from cave air CO₂. For SABs with the lowest $\delta^{13}\text{C}$ values (i.e., RN5 site 4), this would require between 96 and 100% of all biofilm-supplied carbon to be obtained through chemolithoautotrophic CO₂ fixation starting from DIC or between 71 and 100% starting from cave air CO₂ (Table 5.1).

Alternatively, methanotrophy and/or methylotroph metabolism of isotopically light, C1 compounds, such as CH₄, methanol, and carbon monoxide, fractionates carbon during fixation into biomass and could also be responsible for the low $\delta^{13}\text{C}_{\text{SAB}}$ values. When the source of CH₄ to methanotrophs is biogenic CH₄, which typically has $\delta^{13}\text{C}$ values between -85 to -55‰, methanotrophic biomass $\delta^{13}\text{C}$ values fall between -110 and -85‰ (Vieth & Wilkes, 2010).

However, fractionation of carbon isotopes between CH₄ and microbial biomass can vary greatly between type I and II methanotrophs (Templeton et al., 2006). The fractionation factor for CH₄ oxidation is ~1.015 for type II methanotrophs and 1.006 for type I methanotrophs, which corresponds to carbon isotope fractionations of -15‰ and -6‰ from reactant (i.e., CH₄) to product (i.e., biomass), for type II and type I methanotrophs, respectively (Templeton et al., 2006).

Although type II methanotrophs, which are mainly members of the class Alphaproteobacteria and include the genera *Methylocystis*, *Methylocella*, *Methylocapsa*, and *Methylosinus*, generally thrive in environments with low levels of oxygen and elevated concentrations of CH₄, some type II methanotrophs, including the upland soil cluster γ and some *Methylocapsa* spp., can grow solely on CH₄ oxidation at low concentrations (Deng et al., 2019; Tveit et al., 2019). Some type I methanotrophs, such as those of the family Methylococcaceae, can also grow in CH₄-limited environments (Hanson & Hanson, 1996). Growth at low levels, like those of the caves, contradicts previous indications that CH₄ oxidation was kinetically impossible (e.g., Bender, 1992). Therefore, because the most abundant putative methanotrophic group identified in this study was the family Methylogellaceae (0.3 - 3.1‰), a member of the Alphaproteobacteria class and potentially a type II methanotroph, the fractionation factor for type II methanotrophs were used to estimate the $\delta^{13}\text{C}$ values of methanotrophic biomass and, subsequently, the proportion of biomass needed to explain the observed $\delta^{13}\text{C}_{\text{SAB}}$ values. Based on the $\delta^{13}\text{C}_{\text{CH}_4}$ values, which were -43.4‰ and -42.9‰ in KN14 and RN5, respectively, and a fractionation of -15% between source CH₄ and biomass, methanotroph biomass produced from the consumption of atmospheric CH₄ would produce a $\delta^{13}\text{C}$ value of ~-58‰.

Estimates of heterotrophic biomass $\delta^{13}\text{C}$ values were again derived from local $\delta^{13}\text{C}_{\text{DOC}}$ values relevant to each site. Using the methanotrophy estimate and assuming that the cave SABs were comprised only of carbon derived from DOC and CH₄, a two-member mixing model was used to calculate the proportion of CH₄-derived carbon needed to explain measured $\delta^{13}\text{C}_{\text{SAB}}$ values according to the following formula:

$$\text{Equation 5.2} \quad \delta^{13}\text{C}_{\text{SAB}} = x * \delta^{13}\text{C}_{\text{methanotroph}} + (1-x) * \delta^{13}\text{C}_{\text{heterotroph}}$$

where x represents the relative proportion of bulk biomass carbon ($\delta^{13}\text{C}_{\text{SAB}}$) derived from the two potential carbon metabolic pathways represented in this model: (i) $\delta^{13}\text{C}_{\text{methanotroph}}$, which

is the estimated $\delta^{13}\text{C}$ value for methanotroph biomass, and (ii) $\delta^{13}\text{C}_{\text{heterotroph}}$, which is the estimated $\delta^{13}\text{C}$ value for heterotrophic biomass produced through the consumption of organic carbon sources (i.e., $\delta^{13}\text{C}_{\text{DOC}}$ in drip water and streams) and assuming no fractionation of carbon isotopes between source and the produced microbial biomass. Therefore, assuming only methylotrophic and/or methanotroph and heterotroph metabolisms in the SABs, between 32% and 66% of carbon derived from CH_4 could explain the $\delta^{13}\text{C}_{\text{SAB}}$ values (Table 5.1).

Because the $\delta^{13}\text{C}_{\text{SAB}}$ values are lower than would be expected if heterotrophs were assimilating DOC alone, the end-member mixing models support the hypothesis that chemolithoautotrophy contributes to SAB biomass because chemolithoautotrophy via the CBB pathway can result in the low $\delta^{13}\text{C}_{\text{SAB}}$ values for SAB biomass, with a smaller but no less significant contribution from methanotrophy (Table 5.1). Given the higher relative abundance of putative CO_2 -fixing bacteria compared to putative methanotrophs, specifically members of the orders Pseudonocardiales and Nitrosococcales, with lower abundances of Nitrospirales and Rhizobiales (Table 4.9 and Figure 4.14), CO_2 fixation is likely the most important metabolic function contributing to the observed negative bulk $\delta^{13}\text{C}_{\text{SAB}}$ values. Specifically, the relative abundances of Pseudonocardiaceae, Nitrosococcaceae, Nitrospiraceae, and Nitrosomonadaceae were collectively 25–59% of all the taxa in the SABs, which compares well with the minimum proportions needed to explain $\delta^{13}\text{C}_{\text{SAB}}$ values derived from DIC and or cave air CO_2 , being between 40–96% or 31–71%, respectively (Figure 5.1). When considering the summed relative abundances of putative methylotrophs, including the Methyloligellaceae and Methylomirabilia, unclassified members of the family Rhizobiales, which include methanotrophs, and members of the AOB families Nitrosococcaceae and Nitrosomonadaceae capable of mixotrophic growth on CH_4 , the proportion of putative methanotrophs is 2.2–22% of the overall SAB communities (Figure 5.2). However, the estimated proportion of CH_4 -carbon needed to explain $\delta^{13}\text{C}_{\text{SAB}}$ values ranged from 32–66% (Figure 5.2).

Collectively, these estimates provide a starting point to consider the role of autotrophy to cave SABs. The assumptions necessary to make the two end-member mixing calculations are likely unrealistic, as it is probably more realistic to consider that there are multiple sources of carbon being used by the SAB microbes over a long period of time. A multi-member mixing model may be more accurate to address these complexities. Similarly, recycling of carbon by

heterotrophs, and potential incorporation of localized, isotopically lower CO₂ from respiration, which is known to occur within phototrophic biofilm communities (Staal et al., 2007), could also be considered through modeling. Moreover, it is possible that not all the metabolisms are known well enough for many of the bacterial groups within the SABs, and there is the potential for chemolithoautotrophic contributions from Archaea, which were not investigated in this study but could add to the relative proportions of different autotrophs in the SABs (e.g., Figure 5.1). There is also no knowledge of SAB growth or microbial metabolic rates, succession patterns, live-dead proportions, or SAB ages. These aspects should be addressed with additional research and potentially different experimental methods that could assess metabolic activity using RNA-based approaches or to quantify abundances using quantitative methods, such as quantitative PCR of specific metabolic gene linked to specific taxonomic groups.

Table 5.1: Estimated proportions of carbon derived from CO₂ or CH₄ based on two-member mixing models between putative chemolithoautotrophic or methanotrophic biomass compared with heterotrophic biomass. Upper and lower limits are based on uncertainties of biomass δ¹³C values found in the literature. For example, uncertainty in autotrophic biomass δ¹³C values are based on variability in Rubisco fractionation factors starting from CO₂ to produced biomass, whereas the upper and lower limits of CH₄-derived carbon estimates are based on literature information about fractionation factors for methanotrophic metabolism and biomass production.

Site ID	δ ¹³ C biofilm (‰)	δ ¹³ C DIC (‰)	δ ¹³ C CO ₂ (‰)	δ ¹³ C DOC (‰)	Autotroph biomass max (‰)	Autotroph biomass min (‰)	Proportion autotroph carbon (~DIC)	Proportion autotroph carbon (~CO ₂)	Proportion methanotroph carbon
KN14 1	-42.45	-14.53	-14.0	-22.50	-34.53	-49.53	0.74 - 1.0	0.75-1.0	0.56
KN14 2	-40.56	-14.53	-14.0	-22.50	-34.53	-49.53	0.67 - 1.0	0.68-1.0	0.51
KN14 3	-41.83	-14.53	-14.0	-22.50	-34.53	-49.53	0.71 - 1.0	0.73-1.0	0.54
KN14 4	-38.30	-14.53	-14.0	-22.50	-34.53	-49.53	0.58 - 1.0	0.60-1.0	0.44
KN14 5	-42.65	-11.26	-14.0	-20.75	-31.26	-46.26	0.86 - 1.0	0.78-1.0	0.59
KN14 6	-35.31	-11.26	-14.0	-20.75	-31.26	-46.26	0.57 - 1.0	0.52-1.0	0.39
RN5 1	-44.89	-15.06	-19.4	-24.87	-35.06	-50.06	0.79 - 1.0	0.68-1.0	0.60
RN5 2	-38.07	-12.59	-19.4	-24.92	-32.59	-47.59	0.58 - 1.0	0.45-0.91	0.40
RN5 3	-44.85	-12.59	-19.4	-24.92	-32.59	-47.59	0.88 - 1.0	0.68-1.0	0.60
RN5 4	-46.70	-12.59	-19.4	-24.92	-32.59	-47.59	0.96 - 1.0	0.74-1.0	0.66
RN5 5	-42.68	-12.59	-19.4	-24.92	-32.59	-47.59	0.78 - 1.0	0.60-1.0	0.54
RN5 6	-36.10	-13.40	-19.4	-25.66	-33.40	-48.40	0.46 - 1.0	0.36-0.76	0.32

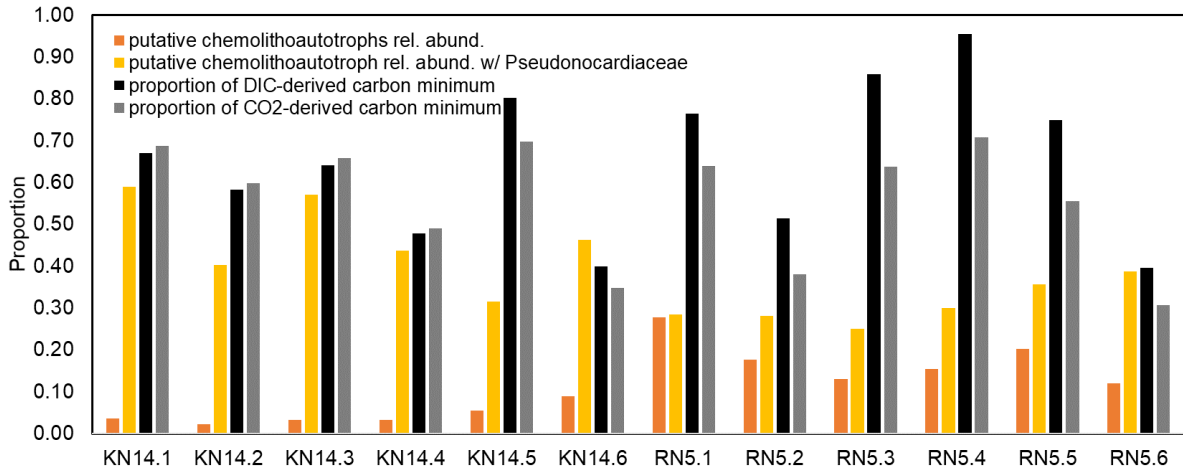


Figure 5.1: Summed relative abundances of putative obligate chemolithoautotrophs at the family level, including Nitrosococcaceae, Nitromonadaceae, and Nitrospiraceae, are shown as orange bars. Relative abundances of obligate chemolithoautotrophic families summed with Pseudonocardiaceae, a potential CO₂-fixer, are shown in yellow. Black bars represent the calculated *minimum* proportion of DIC-derived carbon needed to explain the observed $\delta^{13}\text{C}_{\text{SAB}}$ values for each SAB and grey bars show this proportion based on the $\delta^{13}\text{C}$ of cave-air CO₂ (See Table 5.1).

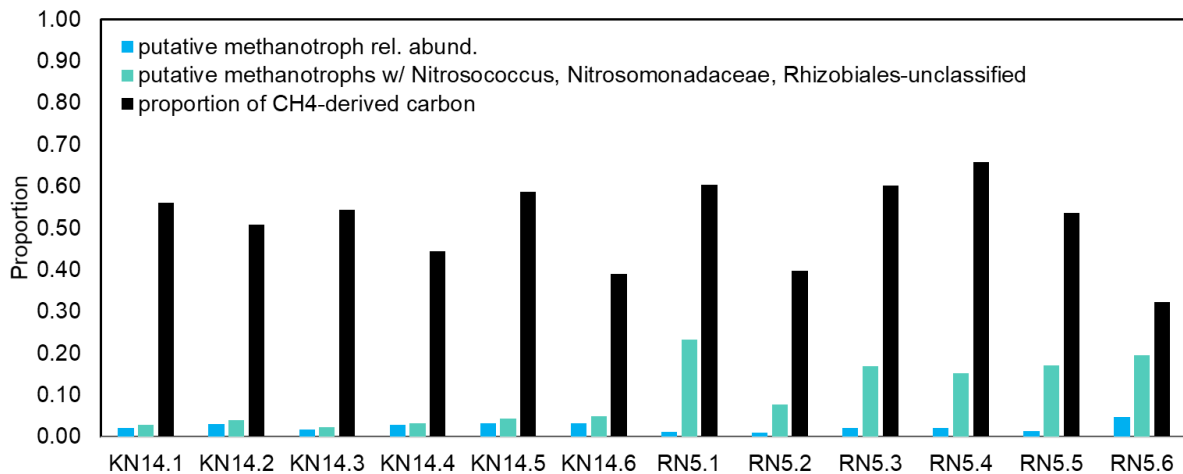


Figure 5.2: Summed relative abundance of putative methanotrophs at the family level, Methyloiligellaceae, Methylomirabilaceae, and Methyloacidiphilaceae, are shown as blue bars. The total abundance of these groups including relative abundance of the AOB Nitrosococcaceae, Nitrosomonadaceae, and unclassified members of Rhizobiales which has the potential to oxidize or co-oxidize CH₄, is shown in green. Black bars represent the calculated proportion of CH₄-derived carbon needed to explain the observed $\delta^{13}\text{C}_{\text{SAB}}$ values for each SAB (See Table 5.1).

CHAPTER SIX CONCLUSIONS AND RECOMMENDATIONS

Cave SAB $\delta^{13}\text{C}$ values in two East Tennessee carbonate caves were low, between -35.3 and -46.7‰, with eight out of twelve SABs having $\delta^{13}\text{C}$ values lower than -40‰. Because heterotrophic consumption of organic matter does not significantly fractionate carbon isotope compositions, cave SABs dominated by heterotrophic metabolism of organic carbon would be expected to display bulk stable isotope values in the same range as measured $\delta^{13}\text{C}_{\text{DOC}}$. However, as shown by consistently lower values across SABs within caves and between two caves, cave SAB $\delta^{13}\text{C}$ values could not be explained solely by consumption of organic matter. The results of $\delta^{13}\text{C}$ analysis of cave SABs instead strongly indicate active microbial incorporation of isotopically light carbon, such as derived from CO_2 or CH_4 via chemolithoautotrophy. Although previous cave SAB research has shown the potential for CO_2 fixation by SABs (e.g., Ortiz et al., 2014; Wiseschart et al., 2019), the results of this study provide evidence for active incorporation of chemolithoautotrophically-fixed carbon into SAB biomass and may indicate a reliance on chemolithoautotrophic carbon fixation to supplement limited carbon resources within the cave ecosystem.

Partially supporting this conclusion, microbial community composition analysis based on relative abundances of 16S rRNA sequences from specific taxonomic groups also revealed an abundance of putative, metabolically flexible, potential CO_2 -fixing group Pseudonocardiaceae and obligate, chemolithoautotrophic nitrifying bacteria (Nitrosococcaceae, Nitrosomonadaceae, and Nitrospiraceae). In addition, microbial communities were strongly influenced by moisture, with Pseudonocardiaceae being most abundant in areas with lower moisture content. Although no direct correlation was identified between Pseudomonadaceae relative abundances and $\delta^{13}\text{C}_{\text{SAB}}$ values, the putative function could partially explain the low $\delta^{13}\text{C}_{\text{SAB}}$ values in some SABs. Preliminary measurement of bulk $\delta^{15}\text{N}_{\text{SAB}}$ values also indicated the potential active involvement of chemolithoautotrophic nitrifiers, such as members of the family Nitrosococcaceae, and potentially N_2 -fixers, such as members of the family Beijerinckiaceae, in the nitrogen cycling of cave SABs. The strong influence of moisture on SAB microbial community composition supported the hypothesis that environmental conditions drive differences in SAB microbial community compositions within caves, but additional environmental factors driving these differences are

possible. Moreover, if Pseudonocardiaceae are involved in CO₂ fixation, then their higher relative abundances in drier areas of the caves could also support the hypothesis that nutrient limitation in areas with limited DOC input, for example from percolating meteoric water, would select for chemolithoautotrophic microbial groups. However, members of this group are known to form spores that are resistant to desiccation (Franco & Labeda, 2014), and are found in abundance in desert soils (Lynch et al., 2014), possibly indicating a general resilience in drier conditions.

Because the microbial community composition of SABs in the caves was consistent with results from earlier cave SAB studies in lava tubes and carbonate caves, at least among the most dominant taxa, it is likely that similar SAB bulk $\delta^{13}\text{C}$ values and metabolic functions, particularly related to chemolithoautotrophy, would exist in other locations. Future directions to study SABs from caves using molecular methods should include (i) comparison of SAB microbial community composition via 16S rRNA sequences between this study and others to determine the phylogenetic relatedness of top taxa between locations, as well as the overall similarity between community structure and composition between these SABs, and (ii) metagenomic analysis of cave SABs to determine the abundance of genes associated with CO₂ fixation and CH₄ oxidation pathways compared to carbon isotope composition and microbial community structure. In addition, although 16S rRNA microbial community composition of cave SABs have been well-characterized, application of methods to investigate active SAB metabolic function are needed, such as the measurement of bulk carbon and nitrogen isotope analysis of SABs from more caves in East Tennessee and elsewhere, and incubation experiments showing (i) CO₂ and CH₄ consumption and production rates, (ii) $\delta^{13}\text{C}$ of CO₂ and CH₄ resulting from isotope fractionation between source carbon and biomass, and (iii) identification of CO₂- and CH₄-fixers using DNA- or RNA-based isotope probing experiments. Finally, the relative abundances and roles of archaea and fungi in cave SABs may provide vital information about carbon fixation, CH₄ cycling, and heterotrophic carbon (re)cycling in the subaerial cave biofilms and should also be investigated.

LIST OF REFERENCES

- Abdulla, H. (2009) Bioweathering and biotransformation of granitic rock minerals by Actinomycetes. *Microbial Ecology*, 58(4):753–761.
- Alfreider, A., Grimus, V., Luger, M., Ekblad, A., Salcher, M. M., & Summerer, M. (2018) Autotrophic carbon fixation strategies used by nitrifying prokaryotes in freshwater lakes. *FEMS Microbiology Ecology*, 94(10): fiy163. doi:10.1093/femsec/fiy163
- Amils R. (2011) Chemolithoautotroph. In: Gargaud M., Amils, R., Cernicharo Quintanilla, J., Cleaves, H.J., Irvine, W.M., Pinti, D., Viso, M. (eds) Encyclopedia of Astrobiology. Springer, Berlin, Heidelberg. doi:10.1007/978-3-642-11274-4
- Barford, C. C., Montoya, J. P., Altabet, M. A., & Mitchell, R. (1999) Steady-state nitrogen isotope effects of N₂ and N₂O production in *Paracoccus denitrificans*. *Applied and Environmental Microbiology*, 65(3), 989-994. doi:10.1128/aem.65.3.989-994.1999
- Barton, H., Taylor, N., Kreate, M., Springer, A., Oehrle, S., & Bertog, J. (2007) The impact of host rock geochemistry on bacterial community structure in oligotrophic cave environments. *International Journal of Speleology*, 36(2):93–104.
- Barton, H. A., Taylor, M. R., & Pace, N. R. (2010). Molecular phylogenetic analysis of a bacterial community in an oligotrophic cave environment. *Geomicrobiology Journal*, 21(1) 11–20. doi:10.1080/01490450490253428
- Belle, S., Parent, C., Frossard, V., Verneaux, V., Millet, L., Chronopoulou, P.-M., Sabatier, P., & Magny, M. (2014) Temporal changes in the contribution of methane-oxidizing bacteria to the biomass of chironomid larvae determined using stable carbon isotopes and ancient DNA. *Journal of Paleolimnology*, 52(3):215–228.
- Bender, M. (1992) Kinetics of CH₄ oxidation in oxic soils exposed to ambient air or high CH₄ mixing ratios. *FEMS Microbiology Reviews*, 101(4):261–269. doi:10.1016/0168-6445(92)90005-g
- Brankovits, D., & Pohlman, J. W. (2020) Methane oxidation dynamics in a karst subterranean estuary. *Geochimica et Cosmochimica Acta*, 277:320–333. doi:10.1016/j.gca.2020.03.007
- Brankovits, D., Pohlman, J. W., Niemann, H., Leigh, M. B., Leewis, M. C., Becker, K. W., Iliffe, T. M., Alvarez, F., Lehmann, M. F., & Phillips, B. (2017) Methane- and dissolved organic carbon-fueled microbial loop supports a tropical subterranean estuary ecosystem. *Nature Communications*, 8(1). doi:10.1038/s41467-017-01776-x
- Casciotti, K. L., & Buchwald, C. (2012). Insights on the marine microbial nitrogen cycle from isotopic approaches to nitrification. *Frontiers in Microbiology*, 3. doi:10.3389/fmicb.2012.00356

- Choe, Y.-H., Kim, M., Woo, J., Lee, M. J., Lee, J. I., Lee, E. J., & Lee, Y. K. (2018) Comparing rock-inhabiting microbial communities in different rock types from a high Arctic polar desert. *FEMS Microbiology Ecology*, 94(6): fiy070. doi:10.1093/femsec/fiy070
- Clayton, R. N., & Degens, E. T. (1959) Use of carbon isotope analyses of carbonates for differentiating fresh-water and marine sediments: *Am. Assoc. Petroleum Geologists Bull.*, 43(4):890–897.
- Craine, J. M., Brookshire, E. N., Cramer, M. D., Hasselquist, N. J., Koba, K., Marin-Spiotta, E., & Wang, L. (2015). Ecological interpretations of nitrogen isotope ratios of terrestrial plants and soils. *Plant and Soil*, 396(1-2):1–26. doi:10.1007/s11104-015-2542-1
- Deng, Y., Che, R., Wang, F., Conrad, R., Dumont, M., Yun, J., Wu, Y., Hu, A., Fang, J., Xu, Z., Cui, X., Wang, Y. (2019) Upland soil cluster gamma dominates methanotrophic communities in upland grassland soils. *Science of The Total Environment*, 670:826–836. doi:10.1016/j.scitotenv.2019.03.299
- Desgarences, D., Garrido, E., Torres-Gomez, M. J., Peña-Cabriales, J. J., & Partida-Martinez, L. P. (2014) Diazotrophic potential among bacterial communities associated with wild and cultivated Agave species. *FEMS Microbiology Ecology*, 90(3):844–857. doi:10.1111/1574-6941.12438
- Dlugokencky, E. J., Nisbet, E. G., Fisher, R., & Lowry, D. (2011) Global atmospheric methane: Budget, changes and dangers. *Philosophical Transactions of the Royal Society A: Mathematical, Physical and Engineering Sciences*, 369(1943):2058–2072. doi:10.1098/rsta.2010.0341
- Donahue, J. M., Williams, N. M., Sells, S. F., & Labeda, D. P. (2002) *Crossiella equi* sp. nov., isolated from equine placentas. *International Journal of Systematic and Evolutionary Microbiology*, 52(Pt 6):2169–2173. doi:10.1099/ijs.0.02257-0
- Dojani, S., Lakatos, M., Rascher, U., Wanek, W., Lüttge, U., & Büdel, B. (2007) Nitrogen input by cyanobacterial biofilms of an inselberg into a tropical rainforest in French Guiana. *Flora - Morphology, Distribution, Functional Ecology of Plants*, 202(7):521–529. doi:10.1016/j.flora.2006.12.001
- Duan, Y., Wu, F., Wang, W., He, D., Gu, J., Feng, H., Chen, T., Liu, G., & An, L. (2017) The microbial community characteristics of ancient painted sculptures in Maijishan Grottoes, China. *PLoS One*, 12(7). doi:10.1371/journal.pone.0179718
- Ehrich, S., Behrens, D., Lebedeva, E., Ludwig, W., & Bock, E. (1995) A new obligately chemolithoautotrophic, nitrite-oxidizing bacterium, *Nitrospira moscoviensis* sp. nov. and its phylogenetic relationship. *Archives of Microbiology*, 164(1):16–23. doi:10.1007/s002030050230

- Engel, A.S., Paterson, A.T., & Niemiller, M.L. (2017) Biogeography of microbes from caves in the Interior Low Plateau and Appalachians karst regions, In Moore, K., White, S. *Proceedings of the 17th International Congress of Speleology*, Sydney, NSW, Australia. July 23-29 2017, Volume 1 (ed. 2), 410.
- Engel, A. S., Porter, M. L., Kinkle, B. K., & Kane, T. C. (2001) Ecological Assessment and Geological Significance of Microbial Communities from Cesspool Cave, Virginia. *Geomicrobiology Journal*, 18(3), 259-274. doi:10.1080/01490450152467787
- Fellman, J. B., D'Amore, D. V., Hood, E., & Boone, R. D. (2008) Fluorescence characteristics and biodegradability of dissolved organic matter in forest and wetland soils from coastal temperate watersheds in southeast Alaska. *Biogeochemistry*, 88(2):169–184. doi:10.1007/s10533-008-9203-x
- Franco C.M.M. & Labeda D.P. (2014) The Order Pseudonocardiales. In: Rosenberg E., DeLong E.F., Lory S., Stackebrandt E., Thompson F. (eds) *The Prokaryotes*. Springer, Berlin, Heidelberg. doi:10.1007/978-3-642-30138-4_190
- Frey, B., Rieder, S. R., Brunner, I., Plotze, M., Koetzsch, S., Lapanje, A., Brandl, H., & Furrer, G. (2010) Weathering-associated bacteria from the Damma Glacier Forefield: Physiological capabilities and impact on granite dissolution. *Applied and Environmental Microbiology*, 76(14):4788–4796.
- Gladis-Schmacka, F., Glatzel, S., Karsten, U., Böttcher, H., & Schumann, R. (2014) Influence of local climate and climate change on aeroterrestrial phototrophic biofilms. *Biofouling*, 30: 401–414. doi:10.1080/08927014.2013.878334.
- Goldman, M. B., Groffman, P. M., Pouyat, R. V., McDonnell, M. J., & Pickett, S. T. (1995) CH₄ uptake and N availability in forest soils along an urban to rural gradient. *Soil Biology and Biochemistry*, 27(3), 281-286. doi:10.1016/0038-0717(94)00185-4
- Gonzalez-Pimentel, J. L., Miller, A. Z., Jurado, V., Laiz, L., Pereira, M. F. C., & Saiz-Jimenez, C. (2018) Yellow coloured mats from lava tubes of La Palma (Canary Islands, Spain) are dominated by metabolically active Actinobacteria. *Scientific Reports*, 8(1944). doi:10.1038/s41598-018-20393-2
- Gorbushina, A. A., & Broughton, W. J. (2009) Microbiology of the atmosphere-rock interface: How biological interactions and physical stresses modulate a sophisticated microbial ecosystem. *Annual Review of Microbiology*, 63(1):431–450.
- Gorbushina, A. A. (2007) Life on the rocks. *Environmental Microbiology*, 9(7):1613–1631.
- Hanson, R. S., & Hanson, T. E. (1996) Methanotrophic bacteria. *Microbiological Reviews*, 60(2):439–471.

- Hardeman, W.D., Miller, R.A., & Swingle, G.D. (1966) Geologic Map of Tennessee: Division of Geology, Tennessee Department of Environment and Conservation, 4 sheets, scale 1:250,000.
- Hathaway, J. J. M., Garcia, M. G., Balasch, M. M., Spilde, M. N., Stone, F. D., Maria De Lurdes N. E. Dapkevicius, Amorim, I. R., Gabriel, R., Borges, P. A., & Northup, D. E. (2014) Comparison of bacterial diversity in Azorean and Hawaiian lava cave microbial mats. *Geomicrobiology Journal*, 31(3):205–220.
- Hajna, N. Z. (2003). Chemical weathering of limestones and dolomites in a cave environment. *Speleogenesis and Evolution of Karst Aquifers*, 1(3):347–356
- Holmes, A. J., Costello, A., Lidstrom, M. E., & Murrell, J. C. (1995) Evidence that participate methane monooxygenase and ammonia monooxygenase may be evolutionarily related. *FEMS Microbiology Letters*, 132(3), 203–208. doi:10.1111/j.1574-6968.1995.tb07834.x
- Holmes, A. J., Tujula, N. A., Holley, M., Contos, A., James, J. M., Rogers, P., & Gillings, M. R. (2001) Phylogenetic structure of unusual aquatic microbial formations in Nullarbor caves, Australia. *Environmental Microbiology*, 3(4):256 –264. doi:10.1046/j.1462-2920.2001.00187.x
- Hügler, M., & Sievert, S. M. (2011) Beyond the Calvin Cycle: Autotrophic carbon fixation in the ocean. *Annual Review of Marine Science*, 3(1), 261–289. doi:10.1146/annurev-marine-120709-142712
- Hutchens, E., Radajewski, S., Dumont, M. G., McDonald, I. R., & Murrell, J. C. (2003) Analysis of methanotrophic bacteria in Movile Cave by stable isotope probing. *Environmental Microbiology*, 6(2):111–120. doi:10.1046/j.1462-2920.2003.00543.x
- Hutchins, B. T., Engel, A. S., Nowlin, W. H., & Schwartz, B. F. (2016) Chemolithoautotrophy supports macroinvertebrate food webs and affects diversity and stability in groundwater communities. *Ecology*, 97(6):1530–1542. doi:10.1890/15-1129.1
- Ji, M., Greening, C., Vanwonderghem, I., Carere, C. R., Bay, S. K., Steen, J. A., Montgomery, K., Lines, T., van Dorst, J., Snape, I., Stott, M. B., Hugenholtz, P., & Ferrari, B. C. (2017) Atmospheric trace gases support primary production in Antarctic desert surface soil. *Nature*, 552:400–403. doi:10.1038/nature25014
- Jones, D. S., Albrecht, H. L., Dawson, K. S., Schaperdoth, I., Freeman, K. H., Pi, Y., Pearson, A., & Macalady, J. L. (2011) Community genomic analysis of an extremely acidophilic sulfur-oxidizing biofilm. *The ISME Journal*, 6(1):158–170. doi:10.1038/ismej.2011.75
- Jones, R. D., & Morita, R. Y. (1983) Methane Oxidation by *Nitrosococcus oceanus* and *Nitrosomonas europaea*. *Applied and Environmental Microbiology*, 45(2), 401–410. doi:10.1128/aem.45.2.401-410.1983

- Kaplan, L. A., & Newbold, J. D. (2000) Surface and subsurface dissolved organic carbon. *Streams and Ground Waters*, 237–258. doi:10.1016/b978-012389845-6/50011-9
- Karwautz, C., Kus, G., Stöckl, M., Neu, T. R., & Lueders, T. (2017) Microbial megacities fueled by methane oxidation in a mineral spring cave. *The ISME Journal*, 12(1), 87–100.
- Klotz, M. G., Arp, D. J., Chain, P. S. G., El-Sheikh, A. F., Hauser, L. J., Hommes, N. G., Larimer, F. W., Malfatti, S. A., Norton, J. M., Poret-Peterson, A. T., Vergez, L. M., & Ward, B. B. (2006) Complete genome sequence of the marine, chemolithoautotrophic, ammonia-oxidizing bacterium *Nitrosococcus oceani* ATCC 19707. *Applied and Environmental Microbiology*, 72(9):6299–6315.
- Kim, B., Shin, J., Guevarra, R. B., Lee, J. H., Kim, D. W., Seol, K., Lee, J., Kim, H. B., & Isaacson, R. E. (2017) Deciphering diversity indices for a better understanding of microbial communities. *Journal of Microbiology and Biotechnology*, 27(12):2089–2093. doi:10.4014/jmb.1709.09027
- Konstantinidis, K. T., & Tiedje, J. M. (2005) Genomic insights that advance the species definition for prokaryotes. *Proceedings of the National Academy of Sciences*, 102(7): 2567–2572. doi:10.1073/pnas.0409727102
- Kozich J.J., Westcott S.L., Baxter N.T., Highlander S.K., & Schloss P.D. (2013) Development of a dual-index sequencing strategy and curation pipeline for analyzing amplicon sequence data on the MiSeq Illumina sequencing platform. *Applied and Environmental Microbiology*. 79(17):5112–20.
- Kussmaul, M., Wilimzig, M., & Bock, E. (1998) Methanotrophs and methanogens in masonry. *Applied and Environmental Microbiology*, 64(11):430–4532.
- Kurahashi M, Fukunaga Y, Sakiyama Y, Harayama S, & Yokota A. (2010). *Euzebya tangerina* gen. nov., sp. nov., a deeply branching marine actinobacterium isolated from the sea cucumber *Holothuria edulis*, and proposal of Euzebyaceae fam. nov., Euzebyales ord. nov. and Nitriliruptoridae subclassis nov. *Int. J. Syst. Evol. Microbiol.*, 60:2314–2319.
- Labeda, D.P. (2001) *Crossiella* gen. nov., a new genus related to *Streptoalloteichus*. *International Journal of Systematic and Evolutionary Microbiology*, 51:1575–1579.
- Lang, S. Q., Bernasconi, S. M., & Früh-Green, G. L. (2011) Stable isotope analysis of organic carbon in small ($\mu\text{g C}$) samples and dissolved organic matter using a GasBench preparation device. *Rapid Communications in Mass Spectrometry*, 26(1): 9–16. doi:10.1002/rcm.5287
- Lavoie, K. H., Winter, A. S., Read, K. J., Hughes, E. M., Spilde, M. N., & Northup, D. E. (2017) Comparison of bacterial communities from lava cave microbial mats to overlying surface soils from Lava Beds National Monument, USA. *PLoS One*, 12(2). doi:10.1371/journal.pone.0169339

- Li, Q., Zhang, B., He, Z., & Yang, X. (2016) Distribution and diversity of bacteria and fungi colonization in stone monuments analyzed by high-throughput sequencing. *PLoS One*, 11(9). doi:10.1371/journal.pone.0163287
- Luis-Vargas, M. N., López-Martínez, R. A., Vilchis-Nestor, A. R., Daza, R., & Alcántara-Hernández, R. J. (2019) Bacterial insights into the formation of opaline stromatolites from the Chimalacatepec lava tube system, Mexico. *Geomicrobiology Journal*, 36:8:694–704, doi: 10.1080/01490451.2019.1607952
- Lynch, R. C., Darcy, J. L., Kane, N. C., Nemergut, D. R., & Schmidt, S. K. (2014) Metagenomic evidence for metabolism of trace atmospheric gases by high-elevation desert Actinobacteria. *Frontiers in Microbiology*, 5:698. doi:10.3389/fmicb.2014.00698
- Macalady, J. L., Jones, D. S., & Lyon, E. H. (2007) Extremely acidic, pendulous cave wall biofilms from the Frasassi cave system, Italy. *Environmental Microbiology*, 9(6):1402–1414. doi:10.1111/j.1462-2920.2007.01256.x
- Macalady, J. L., Lyon, E. H., Koffman, B., Albertson, L. K., Meyer, K., Galdenzi, S., & Mariani, S. (2006) Dominant microbial populations in limestone-corroding stream biofilms, Frasassi Cave System, Italy. *Applied and Environmental Microbiology*, 72(8):5596–5609.
- Mahendra, S., & Alvarez-Cohen, L. (2005) *Pseudonocardia dioxanivorans* sp. nov., a novel actinomycete that grows on 1,4-dioxane. *International Journal of Systematic and Evolutionary Microbiology*, 55(2):593–598. doi:10.1099/ijs.0.63085-0
- Mansch, R., & Bock, E. (1998) Biodeterioration of natural stone with special reference to nitrifying bacteria. *Biodegradation*, 9:47–64. doi: 10.1023/A:1008381525192
- Marín I. & Arahall D.R. (2014) The Family Beijerinckiaceae. In: Rosenberg E., DeLong E.F., Lory S., Stackebrandt E., Thompson F. (eds) *The Prokaryotes*. Springer, Berlin, Heidelberg. doi:10.1007/978-3-642-30197-1_255
- Marques, E., Dias, J., Gross, E., Silva, A., Moura, S. D., & Rezende, R. (2019) Purple sulfur bacteria dominate microbial community in Brazilian limestone cave. *Microorganisms*, 7(2):29. doi:10.3390/microorganisms7020029
- Mattey, D., Atkinson, T., Barker, J., Fisher, R., Latin, J., Durrell, R., & Ainsworth, M. (2016) Carbon dioxide, ground air and carbon cycling in Gibraltar karst. *Geochimica et Cosmochimica Acta*, 184:88–113. doi:10.1016/j.gca.2016.01.041
- McMurdie, P. J., & Holmes, S. (2013) phyloseq: An R package for reproducible interactive analysis and graphics of microbiome census data. *PLoS One*. 8(4):e61217.
- Mohammadipanah, F., & Wink, J. (2016) Actinobacteria from arid and desert habitats: Diversity and biological activity. *Frontiers in Microbiology*, 6. doi:10.3389/fmicb.2015.01541

- Oksanen, J., Blanchet, F. G., Friendly, M., Kindt, R., Legendre, P., McGlinn, D., Minchin, P. R., O'Hara, R. B., Simpson, G. L., Solymos, P., Stevens, M. H., Szoecs, E., & Wagner, H. (2019) *vegan: Community Ecology Package*. R package version 2.5–6. url:<https://CRAN.R-project.org/package=vegan>.
- Opsahl, S. P., & Chanton, J. P. (2006) Isotopic evidence for methane-based chemosynthesis in the Upper Floridan aquifer food web. *Oecologia*, 150(1):89–96.
- Oren A., & Xu, X.W. (2014) The Family Hyphomicrobiaceae. In: Rosenberg E., DeLong E.F., Lory S., Stackebrandt E., Thompson F. (eds) *The Prokaryotes*. Springer, Berlin, Heidelberg. doi:10.1007/978-3-642-30197-1_257
- Ortiz, M., Legatzki, A., Neilson, J. W., Fryslie, B., Nelson, W. M., Wing, R. A., Soderland, C. A., Pryor, B. M., & Maier, R. M. (2014) Making a living while starving in the dark: metagenomic insights into the energy dynamics of a carbonate cave. *The ISME Journal*, 8(2):478–491.
- Pabich, W.J., Valiela, I., & Hemond, H.F. (2001) Relationship between DOC concentration and vadose zone thickness and depth below water table in groundwater of Cape Cod, U.S.A.. *Biogeochemistry*, 55:247–268.
- Paliy, O., & Shankar, V. (2016) Application of multivariate statistical techniques in microbial ecology. *Molecular Ecology*, 25(5):1032–1057. doi:10.1111/mec.13536
- Palmer, S. M., Hope, D., Billett, M. F., Dawson, J. J., & Bryant, C. L. (2001) Sources of organic and inorganic carbon in a headwater stream: Evidence from carbon isotope studies. *Biogeochemistry*, 52:321–338.
- Pašić, L., Kovče, B., Sket, B., & Herzog-Velikonja, B. (2010) Diversity of microbial communities colonizing the walls of a Karstic cave in Slovenia. *FEMS Microbiology Ecology*, 71:50–60. doi: 10.1111/j.1574-6941.2009.00789.x.
- Paul, D., & Skrzypek, G. (2007). Assessment of carbonate-phosphoric acid analytical technique performed using GasBench II in continuous flow isotope ratio mass spectrometry. *International Journal of Mass Spectrometry*, 262(3):180–186. doi:10.1016/j.ijms.2006.11.006
- Porca, E., Jurado, V., Žgur-Bertok, D., Saiz-Jimenez, C., & Pašić, L. (2012) Comparative analysis of yellow microbial communities growing on the walls of geographically distinct caves indicates a common core of microorganisms involved in their formation. *FEMS Microbiology Ecology*, 81(1):255–266.
- Porter M.L., Engel A.S., Kane T.C., & Kinkle B.K. (2009) Productivity-diversity relationships from chemolithoautotrophically based sulfidic karst systems. *Int. J. Speleol.*, 3:27–40.

- Power, J., Schepers, J. (1989) Nitrate contamination of groundwater in North America. *Agriculture, Ecosystems & Environment*, 26(3-4):165187. doi:10.1016/0167-8809(89)90012-1
- Poulson, T. L. & Lavoie, K. H. (2000) The trophic basis of subsurface ecosystems. In Wilkens, H., Culver, D. C., Humphreys, W. F. (Eds.). *Ecosystems of the World: Subterranean Ecosystems*. Amsterdam: Elsevier, 231–249.
- Preuß, A., Schauder, R., Fuchs, G., & Stichler, W. (1989) Carbon isotope fractionation by autotrophic bacteria with three different CO₂ fixation pathways. *Zeitschrift Für Naturforschung C*, 44(5-6):397–402.
- Prieto, B., Vázquez-Nion, D., Fuentes, E., & Durán-Román, A. (2020) Response of subaerial biofilms growing on stone-built cultural heritage to changing water regime and CO₂ conditions. *International Biodeterioration & Biodegradation*, 148:104882. doi:10.1016/j.ibiod.2019.104882
- Prosser J.I., Head I.M., & Stein L.Y. (2014) The Family Nitrosomonadaceae. In: Rosenberg E., DeLong E.F., Lory S., Stackebrandt E., Thompson F. (eds) *The Prokaryotes*. Springer, Berlin, Heidelberg. doi:10.1007/978-3-642-30197-1_372
- Quast C., Pruesse E., Yilmaz P., Gerken J., Schweer T., Yarza P., Peplies J., & Glöckner F.O. (2013) The SILVA ribosomal RNA gene database project: improved data processing and web-based tools. *Nucl. Acids Res.*, 41(D1):D590–D596.
- Quay, P., Stutsman, J., Wilbur, D., Snover, A., Dlugokencky, E., & Brown, T. (1999) The isotopic composition of atmospheric methane. *Global Biogeochemical Cycles*, 13(2):445-461. doi:10.1029/1998gb900006
- Rey-Sanchez, C., Bohrer, G., Slater, J., Li, Y.-F., Grau-Andrés, R., Hao, Y., Rich, V. I., & Davies, G. M. (2019) The ratio of methanogens to methanotrophs and water-level dynamics drive methane transfer velocity in a temperate kettle-hole peat bog. *Biogeosciences*, 16(16):3207–3231.
- Riquelme, C., Rigal, F., Hathaway, J. J., Northup, D. E., Spilde, M. N., Borges, P. A., Gabriel, R., Amorin, I. R., & Dapkevicius, M. N. (2015) Cave microbial community composition in oceanic islands: Disentangling the effect of different colored mats in diversity patterns of Azorean lava caves. *FEMS Microbiology Ecology*, 91(12):fiv141. doi:10.1093/femsec/fiv141
- Ryabenko, E. (2013) Stable Isotope Methods for the Study of the Nitrogen Cycle. *Topics in Oceanography*. Ed. Enrico Zambianchi, IntechOpen, doi:10.5772/56105. Available from: <https://www.intechopen.com/books/topics-in-oceanography/stable-isotope-methods-for-the-study-of-the-nitrogen-cycle>.

- Sampson, A., Ings, N., Shelley, F., Tuffin, S., Grey, J., Trimmer, M., Woodward, G., & Hildrew, A. G. (2019) Geographically widespread ^{13}C -depletion of grazing caddis larvae: A third way of fuelling stream food webs? *Freshwater Biology*, 64(4):787–798. doi:10.1111/fwb.13262
- Sarbu, S. M., Kane, T. C., & Kinkle, B. K. (1996) A chemoautotrophically based cave ecosystem. *Science*, 272(5270):1953–1955.
- Schabereiter-Gurtner, C., Saiz-Jimenez, C., Pinar, G., Lubitz, W., & Rolleke, S. (2002) Phylogenetic 16S rRNA analysis reveals the presence of complex and partly unknown bacterial communities in Tito Bustillo cave, Spain, and on its Palaeolithic paintings. *Environmental Microbiology*, 4(7):392–400.
- Schabereiter-Gurtner, C., Saiz-Jimenez, C., Pinar, G., Lubitz, W., & Rolleke, S. (2004) Phylogenetic diversity of bacteria associated with Paleolithic paintings and surrounding rock walls in two Spanish caves (Llonin and La Garma). *FEMS Microbiology Ecology*, 47(2):235–247.
- Schloss P.D. (2020). Reintroducing mothur: 10 years later. *Applied and Environmental Microbiology*. 86: e02343-19. DOI: 10.1128/AEM.02343-19.
- Schloss, P. D., Westcott, S. L., Ryabin, T., Hall, J. R., Hartmann, M., Hollister, E. B., Lesniewski, R. A., Oakley, B. B., Parks, D. H., Robinson, C. J., Sahl, J. W., Stres, B., Thallinger, G. G., Van Horn, D. J., & Weber, C. F. (2009) Introducing mothur: Open-source, platform-independent, community-supported software for describing and comparing microbial communities. *Applied and Environmental Microbiology*, 75(23):7537–7541. doi:10.1128/aem.01541-09
- Serna-Chavez, H. M., Fierer, N., & Bodegom, P. M. (2013) Global drivers and patterns of microbial abundance in soil. *Global Ecology and Biogeography*, 22(10), 1162–1172. doi:10.1111/geb.12070
- Simon, K. S., Benfield, E. F., & Macko, S. A. (2003) Food web structure and the role of epilithic biofilms in cave streams. *Ecology*, 84(9):2395–2406.
- Spoelstra, J., Schiff, S., Hazlett, P., Jeffries, D., & Semkin, R. (2007). The isotopic composition of nitrate produced from nitrification in a hardwood forest floor. *Geochimica et Cosmochimica Acta*, 71(15):3757–3771. doi:10.1016/j.gca.2007.05.021
- Spötl, C., Fairchild, I. J., & Tooth, A. F. (2005) Cave air control on dripwater geochemistry, Obir Caves (Austria): Implications for speleothem deposition in dynamically ventilated caves. *Geochimica et Cosmochimica Acta*, 69(10):2451–2468. doi:10.1016/j.gca.2004.12.009
- Staal, M., Thar, R., Köhl, M., Loosdrecht, M. C., Wolf, G., Brouwer, J. F., & Rijstenbil, J. W. (2007) Different carbon isotope fractionation patterns during the development of

- phototrophic freshwater and marine biofilms. *Biogeosciences*, 4(4):613–626.
doi:10.5194/bg-4-613-2007
- Steenhoudt, O., & Vanderleyden, J. (2000) Azospirillum, a free-living nitrogen-fixing bacterium closely associated with grasses: Genetic, biochemical and ecological aspects. *FEMS Microbiology Reviews*, 24(4), 487–506. doi:10.1111/j.1574-6976.2000.tb00552.x
- Suzuki, M. T., Taylor, L. T., & Delong, E. F. (2000) Quantitative analysis of small-subunit rRNA genes in mixed microbial populations via 5-nuclease assays. *Applied and Environmental Microbiology*, 66(11):4605–4614.
- Templeton, A. S., Chu, K., Alvarez-Cohen, L., & Conrad, M. E. (2006) Variable carbon isotope fractionation expressed by aerobic CH₄-oxidizing bacteria. *Geochimica Et Cosmochimica Acta*, 70(7), 1739-1752. doi:10.1016/j.gca.2005.12.002
- Tetu, S. G., Breakwell, K., Elbourne, L. D., Holmes, A. J., Gillings, M. R., & Paulsen, I. T. (2013) Life in the dark: Metagenomic evidence that a microbial slime community is driven by inorganic nitrogen metabolism. *The ISME Journal*, 7(6):1227–1236.
doi:10.1038/ismej.2013.14
- Thompson, B., Richardson, D., Vangundy, R., & Cahoon, A. B. (2019) Metabarcoding comparison of prokaryotic microbiomes from Appalachian karst caves to surface soils in southwest Virginia, USA. *Journal of Cave and Karst Studies*, 8(4):244–253.
doi:10.4311/2019mb0112
- Thibodeau, B., Miyajima, T., Tayasu, I., Wyatt, A. S., Watanabe, A., Morimoto, N., Yoshimizu, C., & Nagata, T. (2013) Heterogeneous dissolved organic nitrogen supply over a coral reef: First evidence from nitrogen stable isotope ratios. *Coral Reefs*, 32(4):1103–1110.
doi:10.1007/s00338-013-1070-9
- Tomczyk-Żak, K., & Zielenkiewicz, U. (2015) Microbial diversity in caves. *Geomicrobiology Journal*, 33(1):20–38.
- Tveit, A. T., Hestnes, A. G., Robinson, S. L., Schintlmeister, A., Dedysh, S. N., Jehmlich, N., von Bergen, M., Herbold, C., Wagner, M., Richter, A., & Svenning, M. M. (2019) Widespread soil bacterium that oxidizes atmospheric methane. *Proceedings of the National Academy of Sciences*, 116(17):8515–8524. doi:10.1073/pnas.1817812116
- Vlasceanu, L., Sarbu, S. M., Engel, A. S., & Kinkle, B. K. (2000) Acidic Cave-Wall Biofilms Located in the Frasassi Gorge, Italy. *Geomicrobiology Journal*, 17(2), 125-139.
doi:10.1080/01490450050023809
- Vieth, A. & Wilkes, H. (2010) Stable isotopes in understanding origin and degradation processes of petroleum. *Handbook of Hydrocarbon and Lipid Microbiology*, 97–111.

- Villa, F., Stewart, P. S., Klapper, I., Jacob, J. M., & Cappitelli, F. (2016) Subaerial biofilms on outdoor stone monuments: Changing the perspective toward an ecological framework. *BioScience*, 66(4):285–294.
- Vo, J., Inwood, W., Hayes, J. M., & Kustu, S. (2013) Mechanism for nitrogen isotope fractionation during ammonium assimilation by *Escherichia coli* K12. *Proceedings of the National Academy of Sciences*, 110(21):8696–8701. doi:10.1073/pnas.1216683110
- Waring, C. L., Hankin, S. I., Griffith, D. W. T., Kertesz, M. A., Kobylski, V., Wilson, N. L., Coleman, N. V., Kettlewell, G., Zlot, R., Bosse, M., & Bell, G. (2017) Seasonal total methane depletion in limestone caves. *Scientific Reports*, 7(8314). doi:10.1038/s41598-017-07769-6
- Waser, N. A., Harrison, P. J., Nielsen, B., Calvert, S. E., & Turpin, D. H. (1998) Nitrogen isotope fractionation during the uptake and assimilation of nitrate, nitrite, ammonium, and urea by a marine diatom. *Limnology and Oceanography*, 43(2):215–224. doi:10.4319/lo.1998.43.2.0215
- Webster, K. D., Mirza, A., Deli, J. M., Sauer, P. E., & Schimmelmann, A. (2016) Consumption of atmospheric methane in a limestone cave in Indiana, USA. *Chemical Geology*, 443:1–9.
- Webster, K. D., White, J. R., & Pratt, L. M. (2015) Ground-level concentrations of atmospheric methane in southwest Greenland evaluated using open-path laser spectroscopy and cavity-enhanced absorption spectroscopy. *Arctic, Antarctic, and Alpine Research*, 47(4):599–609. doi:10.1657/aaar0014-051
- White, D. C. & Ringelberg, D. B. (1998) Signature lipid biomarker analysis. In Burlage, R. S., Atlas, R., Stahl, D., Geesey, G., Saylor, G. (Eds.). *Techniques in Microbial Ecology*, New York: Oxford University Press, 255–272.
- Wischart, A., Mhuantong, W., Tangphatsornruang, S., Chantasingh, D., & Pootanakit, K. (2019) Shotgun metagenomic sequencing from Manao-Pee cave, Thailand, reveals insight into the microbial community structure and its metabolic potential. *BMC Microbiology*, 19(1). doi:10.1186/s12866-019-1521-8
- Yarnes, C. (2013) $\delta^{13}\text{C}$ and $\delta^2\text{H}$ measurement of methane from ecological and geological sources by gas chromatography-combustion/pyrolysis-isotope-ratio mass spectrometry. *Rapid Commun. Mass Spectrom.*, 27:1036–1044.
- Yilmaz P., Parfrey L.W., Yarza P., Gerken J., Pruesse E., Quast C., Schweer T., Peplies J., Ludwig W., & Glöckner F.O. (2014) The SILVA and "All-species Living Tree Project (LTP)" taxonomic frameworks. *Nucl. Acids Res.* 42:D643-D648
- Yin, Q., Zhang, L., Song, Z. M., Wu, Y., Hu, Z. L., Zhang, X. H., Zhang, Y., Yu, M., & Xu, Y. (2018) *Euzebya rosea* sp. nov., a rare actinobacterium isolated from the East China Sea and

analysis of two genome sequences in the genus *Euzebya*. *Int J Syst Evol Microbiol.*, 68(9):2900-2905. doi:10.1099/ijsem.0.002917

Yun, Y., Xiang, X., Wang, H., Man, B., Gong, L., Liu, Q., Dong, Q., & Wang, R. (2015) Five-Year monitoring of bacterial communities in dripping water from the Heshang Cave in central China: Implication for paleoclimate reconstruction and ecological functions. *Geomicrobiology Journal*, 33(7):1-11.

Zanardini, E., May, E., Purdy, K. J., & Murrell, J. C. (2019) Nutrient cycling potential within microbial communities on culturally important stoneworks. *Environmental Microbiology Reports*, 11(2):147–154.

Zhao, K., Kong, W., Wang, F., Long, X.-E., Guo, C., Yue, L., Yao, H., & Dong, X. (2018) Desert and steppe soils exhibit lower autotrophic microbial abundance but higher atmospheric CO₂ fixation capacity than meadow soils. *Soil Biology and Biochemistry*, 127:230–238.

Zhao, R., Wang, H., Cheng, X., Yun, Y., & Qiu, X. (2018) Upland soil cluster γ dominates the methanotroph communities in the karst Heshang Cave. *FEMS Microbiology Ecology*, 94(12):fiy192. 10.1093/femsec/fiy192

VITA

Vickie Frazier was born in Florida and grew up sorting through seaweed on the beach to find seahorses and brittle stars and swimming in Florida's springs. As the daughter of two teachers, she had the privilege of being enrolled in both of their classes at some point and having to call her father "Mr. Frazier." Driven by the desire to not be a teacher, as well as an interest in being a forensic pathologist in high school, she pursued a bachelor's degree in, for some reason, Microbiology at the University of South Florida. That choice turned out to be an amazing fit. Microbiology course requirements also made her realize an unexpected love for organic chemistry and she took a job tutoring organic chemistry students, already fulfilling her family legacy. Since she never had the desire to attend medical school, she fell into research at an environmental microbiology lab at USF that studied biofilms growing in the submerged Swiss cheese that is the Florida carbonate platform. Although she had thought she loved microbiology before, the realizations that microbes were more than just pathogens, and that biofilms grew on more interesting things than catheters seemed to perfectly unite Vickie's love of puzzles and her fascination with nature. Through this lab, she became interested in geology, environmental microbiology, and scuba diving, and decided to try to pursue all those things at once. Her newfound interest in geology and caves brought her to Tennessee, where she has had the opportunity to learn geology as well as continue to build on her background in microbiology. She has now written this thesis and gotten certified as a cave diver, but it's the middle of a pandemic so who knows what's next.